DEVELOPMENT AND STUDY OF CONDUCTING MATERIALS FOR H_2O_2 AND GLUCOSE SENSORS

TILAGAM A/P MARIMUTHU

THESIS SUBMITTED IN FULFILMENT OF THE REQUIREMENTS FOR THE DEGREE OF DOCTOR OF PHILOSOPHY

DEPARTMENT OF CHEMISTRY
FACULTY OF SCIENCE
UNIVERSITY OF MALAYA
KUALA LUMPUR

2015

UNIVERSITY OF MALAYA

ORIGINAL LITERARY WORK DECLARATION

Name of Candidate: **TILAGAM A/P MARIMUTHU**
(I.C./Passport No.: **850912-01-5602**)

Registration/Matrix No.: **SHC 110018**

Name of Degree: **DOCTOR OF PHILOSOPHY (EXCEPT MATHEMATICS & SCIENCE PHILOSOPHY)**

Title of Project Paper/Research Report/Dissertation/Thesis ("this Work"): **DEVELOPMENT AND STUDY OF CONDUCTING MATERIALS FOR H_2O_2 AND GLUCOSE SENSORS**

Field of Study: **ANALYTICAL CHEMISTRY AND ELECTROCHEMISTRY**

I do solemnly and sincerely declare that:

1) I am the sole author/writer of this Work;
2) This Work is original;
3) Any use of any work in which copyright exists was done by way of fair dealing and for permitted purposes and any excerpt or extract from, or reference to or reproduction of any copyright work has been disclosed expressly and sufficiently and the title of the Work and its authorship have been acknowledged in this Work;
4) I do not have any actual knowledge nor do I ought reasonably to know that the making of this Work constitutes an infringement of any copyright work;
5) I hereby assign all and every rights in the copyright to this Work to the University of Malaya (UM), who henceforth shall be owner of the copyright in this Work and that any reproduction or use in any form or by any means whatsoever is prohibited without the written consent of UM having been first had and obtained;
6) I am fully aware that if in the course of making this Work I have infringed any copyright whether intentionally or otherwise, I may be subject to legal action or any other action as may be determined by UM.

Candidate's Signature Date

Subscribed and solemnly declared before,

Witness's Signature Date

Name:
Designation:

ABSTRACT

This thesis originated with the development and characterisation of composite materials for sensor applications. This study focused on conducting polymer-metal oxide based composites and silica-titania oxide based composites. The conducting polymer-metal oxide composites were synthesised by chemical polymerisation technique with an aqueous solution of pyrrole monomer in the presence of cobalt and nickel salts. Various analytical techniques were employed to characterise these composites such as field emission scanning electron microscope-energy dispersive x-ray (FESEM-EDX), x-ray powder diffraction (XRPD), Fourier Transform Infrared (FTIR) and thermogravimetric analysis (TGA). These composites were then fabricated into chemical sensor by drop-dry electrodeposition method on glassy carbon electrode (GCE). The electrochemical response towards the modified GCE was examined using both cyclic voltammetry and chronoamperometry. The polypyrrole coated cobalt (PPy-Co)/GCE shows sensitivity towards hydrogen peroxide (H_2O_2). While, the polypyrrole coated nickel oxide (PPy-NiO)/GCE shows its current response towards glucose. Both PPy-Co/GCE and PPy-NiO/GCE give high response towards target analyte at optimum condition of 500 μL pyrrole monomer content. Furthermore, the presence of pyrrole monomer greatly increases the sensitivity of the respective modified electrode. The PPy-Co/GCE could detect H_2O_2 in a linear range of 20 μM to 80 mM with two linear segments (low and high concentration of H_2O_2) and the detection limit for both ranges is 2.05 μM and 19.64 μM, respectively. While, PPy-NiO/GCE exhibited good electrocatalytic oxidation towards glucose in alkaline medium and could detect glucose in linear ranges of 0.01 mM to 0.50 mM and 1 mM to 20 mM with detection limit of 0.33 μM and 5.77 μM, respectively. Besides, the Si-Ti oxide based composite was also synthesised and developed as an enzymatic sensor. This composite was synthesised by

sol-gel method in the presence of 1-butyl-3-methylimidazolium bis(trifluoromethylsulfonyl)imide ([C_4MIm][NTf_2]) ionic liquid and was characterised by FTIR, TGA, XRPD, FESEM-EDX, CHN and N_2 adsorption-desorption analysis. The presence of C-N groups in the FTIR spectrum indicates the presence of the ionic liquid in the Si-Ti matrix, while, the XRPD, FESEM and N_2 adsorption-desorption analysis results show that the composite materials possessed good microporous characteristics. This composite was then fabricated as an enzymatic sensor by layer-by-layer drop-dry electrodeposition method onto the surface of GCE. Ferrocene (Fc) was chosen as mediator and horseradish peroxidase (HRP) was selected to detect H_2O_2. The electrochemical response of H_2O_2 towards the modified GCE was examined by using cyclic voltammetry. But, this modified Si-Ti-[C_4MIm][NTf_2]-HRP/Fc/GCE did not give significant electrocatalytic responses towards H_2O_2.

ABSTRAK

Tesis ini bermula dengan pembangunan dan pencirian bahan komposit bagi aplikasi sensor. Komposit berasaskan polimer pengalir-oksida logam dan silika-titania oksida diberi tumpuan di dalam tesis ini. Komposit polimer pengalir-oksida logam telah disintesis dengan teknik pempolimeran kimia dengan menggunakan larutan akueus monomer pyrrole dengan kehadiran garam kobalt dan nikel. Pelbagai teknik analisis telah digunakan untuk mencirikan komposit ini seperti lapangan pelepasan mikroskop imbasan elektron-tenaga serakan sinar x-ray (FESEM-EDX), x-ray serbuk pembelauan (XRPD), Fourier Transform Infrared (FTIR) dan analisis termogravimetri (TGA). Komposit ini kemudian telah difabrikasi sebagai sensor kimia dengan teknik pengenapan penitisan dan pengeringan pada elektrod karbon berkaca (GCE). Respons elektrokimia terhadap GCE yang diubahsuai telah diperiksa dengan menggunakan kedua-dua kaedah voltammetri berkitar dan kronoamperometri. Polypyrrole bersalut kobalt (PPy-Co)/GCE menunjukkan sensitiviti terhadap hidrogen peroksida (H_2O_2). Manakala, polypyrrole bersalut nikel oksida (PPy-NiO)/GCE menunjukkan respons arus ke arah glukosa. Kedua-dua PPy-Co/GCE dan PPy-NiO/GCE memberikan respons yang tertinggi ke arah analit sasaran pada keadaan optimum 500 μL kandungan monomer pyrrole. Tambahan pula, kehadiran monomer pyrrole meningkatkan sensitiviti elektrod diubahsuai. PPy-Co/GCE boleh mengesan H_2O_2 dalam julat linear dari 20 μM hingga 80 mM dengan dua segmen linear (kepekatan rendah dan tinggi H_2O_2) dan had pengesanan untuk kedua-dua julat ini adalah 2.05 μM dan 19.64 μM. Di samping itu, PPy-NiO/GCE pula menunjukkan aktiviti elektrokatalitik yang baik terhadap pengoksidaan glukosa dalam medium alkali dan boleh mengesan glukosa dalam julat linear dari 0.01 mM hingga 0.50 mM dan dari 1 mM hingga 20 mM dengan had pengesanan 0.33 μM dan 5.77 μM. Di samping itu, komposit berasaskan Si-Ti oksida

juga telah disintesis dan digunakan sebagai sensor enzim. Komposit ini telah disintesis melalui kaedah sol-gel dengan kehadiran cecair ionik 1-butil-3-methylimidazolium bis(trifluoromethylsulfonyl) imide ($[C_4MIm][NTf_2]$) dan dicirikan oleh FTIR, TGA, XRPD, FESEM-EDX, CHN dan N_2 analisis penjerapan-penyahserapan. Kehadiran kumpulan C-N dalam spektrum FTIR menunjukkan kehadiran cecair ionik dalam matriks Si-Ti, manakala, XRPD, FESEM dan N_2 analisis penjerapan-penyahserapan menunjukkan bahan komposit mempunyai ciri mikroporus yang baik. Komposit ini kemudian telah difabrikasikan sebagai sensor enzim dengan teknik pengenapan penitisan dan pengeringan lapisan demi lapisan di atas permukaan GCE. Ferocene (Fc) telah dipilih sebagai penghantara dan peroksidas lobak pedas (HRP) telah dipilih untuk mengesan H_2O_2. Respons elektrokimia H_2O_2 terhadap GCE yang diubahsuai telah diperiksa dengan menggunakan voltammetri berkitar. Tetapi, Si-Ti-$[C_4MIm][NTf_2]$-HRP/Fc/GCE ini tidak memberi aktiviti elektrokatalitik yang ketara terhadap H_2O_2.

ACKNOWLEDGEMENTS

First and foremost, I would like to thank God and His Devine Grace for His grace and blessing. He is the help, the strength and the hope that keeps me on.

I would like to thank my supervisor, Professor Dr. Yatimah Alias and co-supervisor, Associate Professor Dr. Sharifah Mohamad, for their continued support during my PhD. They gave me supports and encouragements and a belief in myself and my accomplishments. Without their support and guidance, I would not have completed my PhD.

I would like to thank Dr. Reza, for always being there to guide and answer any questions. His wealth of knowledge and expertise is inspiring and I am indebted to him for sharing some of that with me. I would like to thank you to all the staffs of the chemistry department who have been there to support me when I needed the assistance on department facilities.

Hemavathy Surikumaran, Muggundha Raoov and Kavirajaa Pandian, we started together and now we are finishing together four years on – thank you for the memories, the chats and for being there for me and being my friends and I wish you all the best in your future; what ever you all decide to do, I'm sure you all will be great at it. To the rest of the lab group, Kumuthini, Zohreh, Dazylah, Maizatul and Rahimah – Thank you for sharing knowledge and creating enjoyable lab atmosphere and I wish you all the success in the future also. To all my friends outside of the labs, a special thanks for the visits and the chats.

The last but not the least, I would like to thank my family. To my dad, Marimuthu, you have always stood by me and believed in me, even when I doubted myself. To my mum, Danaletchumy, thank you for teaching me to stand on my own two feet and aim for the sky. Thank you all for your unconditional love and support.

TABLE OF CONTENTS

LIST OF FIGURES

LIST OF TABLES

LIST OF SCHEMES

LIST OF SYMBOLS AND ABBREVIATIONS

%	Percentage
AA	Ascorbic acid
Au	Gold
Ag	Silver
$AgNO_3$	Silver nitrate
BrO_3^-	Bromate ion
BET	Brunauer-Emmett-Teller
$[C_4MIm][NTf_2]$	1-butyl-3-methylimidazolium bis(trifluoromethylsulfonyl) imide
C	Celsius
cm	centimetre
Cl_2	chlorine gas
ClO_3^-	Chlorate ion
CoO	Cobalt Oxide
CoOOH	Cobalt oxyhydroxide
CoPC	Cobalt phtalocyanine
CuO	Copper oxide
CuO_2	Cuprous Oxide
CV	Cyclic Voltammetry
DA	Dopamine
EtOH/ C_2H_5OH	Ethanol
Fe_2O_3	Iron Oxide
$FeCl_3$	Iron(III) chloride
FESEM-EDX	Field emission scanning electron microscopy and energy dispersive x-ray
Fc	Ferrocene
FTIR	Fourier Transform InfraRed
G	Graphite
GCE	Glassy Carbon Electrode
h	hour
HCl	Hydrochloric acid
H_2O_2	Hydrogen peroxide
H_2S	Hydrogen sulphide
HRP	Horseradish Peroxidase

IO_3^-	Iodate
ITO	Indium Tin Oxide
K	Kelvin
kV	kilo Volt
KBr	Potassium Bromide
$KMnO_4$	Potassium permanganate
$LiClO_4$	Lithium perchlorate
LOD	Limit of Detection
LOQ	Limit of Quantification
mA	milli Ampere
mg	milli gram
mL	milli Litre
µL	micro Litre
µm	micro metre
mm	milli metre
M	Molarity
min	minute
Mn	Manganese
MWCNT	Multi walled carbon nanotube
n	number of measurements
NADH	Nicotinamide adenine dinucleotide
NaOH	Sodium hydroxide
NH_3	Ammonia
nm	nanometre
NiO	Nickel oxide
NO_2	Nitrogen dioxide
ox	oxidation
O	Oxygen
PANi	Polyaniline
PBS	Phosphate Buffer Solution
PEDOT	Poly(3,4-ethylenedioxythiophene)
Pb	Lead
Pd	Palladium
PMT	Poly(3-methylthiophene)
POT	Poly(o-toluidine)

PPy	Polypyrrole
Pt	Platinum
PTh	Polythiophenes
pTs	p-toluenesulfonate
red	reduction
rGO	reduced graphene oxide
rpm	Revolutions per minute
RSD	Relative standard deviation
SCE	Saturated calomel electrode
SD	Standard deviation
Si	Silica
Si-MPC	Silicon microchannel plate
SnO_2	Tin oxide
TEOS	Tetraethylorthosilicate
TGA	Thermogravimetric analysis
Ti	Titania
TTIP	Titanium(IV) isopropoxide
UV-Vis	Ultraviolet-Visible
v/v	volume/volume
x	Result of every measurement
$\bar{x}$	Mean of the measurements
XRPD	X-ray powder diffraction
WO_3	Tungsten oxide
wt	weight
Zn	Zinc
ZnO	Zinc oxide

CHAPTER 1

INTRODUCTION

1.1 Background study

The demand for sensors in a wide range of applications has been recognised since many years ago. As is well known, the scope of sensor technology is truly wide and no simple classification is absolutely adequate. However, the categorisation of sensors can be made by either their chemical composition or their operation principle (Chaparro, 2007). The invention and evolution of sensors require more consideration especially in the choice of the material for sensing, signal amplification issues, relay and measurement of the sensor.

Among different kinds of sensor materials, composite or nanocomposite based sensors are being used for many applications. The following are some of advantages of composite or nanocomposite, which have attracted in great amount of interest for the sensor fabrication (Liu et al., 2013):

1. Production at low cost, generally by chemical synthesis method instead of electrochemical method;
2. Relatively cheap material applied for fabrication of the device;
3. Easy and simple synthesis method;
4. Availability of entirely new material structures and morphologies
5. Vast possibilities for different composition and thus properties of the inorganic and polymer materials can be used as device components.

All the mentioned advantages make composite or nanocomposite based device highly attractive in sensor technology at their present stage of development.

Currently, huge advancement has been accomplished in the synthesis of different types of conducting polymer-metal oxide composite or nanocomposite for sensor applications. The development of such composites based devices discovered the possibility of filling conducting polymer matrices such as polyaniline (PANi), polypyrrole (PPy), polythiophenes (PTh), with metal oxide nanoparticles such as iron oxide (Fe_2O_3), copper oxide (CuO), nickel oxide (NiO) and cobalt oxide (CoO) (Navale et al., 2014b; Poyraz et al., 2014; Das et al., 2013; Kumar et al., 2013; Kumary et al., 2013).

Polypyrrole (PPy) is a conducting polymer broadly used for fabrication of sensors and supporting matrix in electrochemistry due to its good physical and electrical properties (Meng et al., 2013; Safarnavadeh et al., 2013; Li, C. et al., 2012). Moreover, PPy can provide a good dispersion of metal oxide nanoparticle for the essential presence of functional groups within long carbon chains (Li, X. et al., 2012; Ramanavicius et al., 2006). PPy-metal oxide nanocomposites show different properties over their single component, creating them capable for non-enzymatic sensor applications.

The metal oxides are also very significant materials for being used in sensor devices, chemical industries and medical applications. An increasing development for the nanomaterials is the composite structures fabrication and devices with materials that able to improve the properties of the composite material (Devadathan & Raveendran, 2014). Cobalt oxide (CoO) and nickel oxide (NiO) were selected for the present study

due to their distinctive electrochemical properties. Among the metal oxides, CoO and NiO are the subject of significant attention due to their exciting fundamental properties and technological uses particularly in sensor applications. Hence, in this dissertation, a simple, easy and new reaction process is explored for the production of polypyrrole coated cobalt nanocomposites (PPy-Co) and polypyrrole coated nickel composites (PPy-NiO) and these composites are used to fabricate a highly sensitive non-enzymatic hydrogen peroxide (H_2O_2) and glucose sensor, respectively.

Besides, sol-gel has recently become a subject of enthusiasm in electrochemistry since they combine the advantages of the intersection between sol-gel chemistry and electrochemistry. The sol-gel process is familiar in the prior art, simple to implement, occur under mild conditions and facilities the shaping of materials (Brinker & Scherer, 1990). The sol-gel matrix materials have remarkable properties such as physical rigidity, chemical inertness, high thermal and photochemical stability, negligible swelling in aqueous as well as in organic solvent and it is especially alluring for the biosensor fabrications. Sol-gel derived silica-titania (Si-Ti) binary inorganic materials have gained attention from the researchers (Ma, H. et al., 2014; Li, D. et al., 2012; Siwinska-Stefanska et al., 2012). These materials have been extensively utilised as anti-reflecting coating, optical-chemical sensor, glasses, supporting materials and catalysts due to their superior optical and thermal properties. The aim of this study is to prepare Si-Ti composite in the presence of room temperature ionic liquids (RTILs), a new material which has not previously been investigated, in order to obtain materials that are potentially useful as coating for electrodes.

Over the years, RTILs have been used as solvent and solvent additive for the preparation of sol-gel (Klingshirn et al., 2005). RTILs are low-melting point salts from

the combination of heterocyclic cations and a variety of anions, which are in liquid state at temperature close to ambient temperature. They have noticeable properties, for example, zero volatility and a high ionic conductivity as well as catalytic properties (Branco et al., 2002). Because of negligible vapour pressure, the RTILs employed as non-volatile drying control chemical additive during the synthesis of sol-gel, producing reduced shrinkage and ensuing matrix collapse during the formation of the gels (Klingshirn et al., 2005). The use of RTILs as co-solvents for sol-gel process would permit to control the structural properties of the resultant gels, specifically the pore size, structure as well as distribution and also make benefit of the readily modifiable and controllable solvent and physical characteristics of RTILs (Klingshirn et al., 2005).

To our best of knowledge, the Si-Ti composite in the presence of RTIL for sensor application has not been previously reported. Thus, in a part of this dissertation, Si-Ti composite will be investigated with and without RTIL, 1-butyl-3-methylimidazolium bis(trifluoromethylsulfonyl)imide, $[C_4MIm][NTf_2]$ and fabricated as enzymatic sensor. Horseradish peroxidase (HRP) is chosen as an enzyme in sol-gel because it is inexpensive and could catalyse the hydrogen peroxide (H_2O_2)-dependent one electron oxidation.

1.2 Objective of the research

The purpose of this study is to synthesise and characterise a new class of conducting polymer/metal oxide nanocomposites and mixed oxide composites. The results may provide viable functional composite or nanocomposite for new sensing platforms. The following goals are pursued toward the overall objective:

1) To develop composite and nanocomposite materials based on conducting polymer-metal oxide and Si-Ti/[C_4MIm][NTf_2] matrix.
2) To fabricate these composite materials for non-enzymatic and enzymatic sensors at different analyte concentration levels.
3) To validate the sensor performance on target analyte and real sample analysis.

1.3 Scope of the research

Research scope is very important to ensure the objective of the research is accomplished. In general, the scopes are used as a guideline for carrying on the research in a correct pathway. The scopes of this thesis are summarised as follows:

1) Synthesis conducting polymer/metal oxide and mixed oxide composites which include PPy-Co nanocomposites, PPy-NiO composites and Si-Ti/([C_4IMm][NTf_2]) composites.
2) Structural and morphological attributes of these materials are characterised by using field-emission scanning electron microscopy-energy dispersive x-ray (FESEM-EDX), x-ray powder diffraction (XRPD), Fourier Transform Infrared (FTIR) and thermogravimetric analysis (TGA). In addition, Brunauer-Emmett-Teller (BET) desorption analysis is applied for Si-Ti/[C_4MIm][NTf_2] composite to determine the pore size of the matrix.
3) These newly synthesised materials will then be used to fabricate H_2O_2 and glucose sensor, respectively and these sensors will be optimised towards target analyte by using cyclic voltammetry and chronoamperometry techniques.
4) These sensors will finally be tested with real sample.

1.4 Outline of the thesis

This thesis contains five chapters:

Chapter 1: This introductory chapter outlines key themes that are relevant to all the areas of research in this thesis. A brief introduction on research background, research objectives and scope of the study are provided within this chapter.

Chapter 2: A review of previous and current research related to the use of composite and/or nanocomposite, particularly composites composed of conducting polymer, metal oxide and mixed oxide is presented. It describes the techniques used to form the composites and/or nanocomposites, as well as sensors that can be developed using this class of materials.

Chapter 3: The details of the relevant synthesis process, experimental techniques and apparatus employed, along with an overview of the theories and related equations used in this thesis are presented.

Chapter 4: The results and discussions of three main research areas are included in this chapter. In the first research area, the characterisation of polypyrrole coated cobalt nanocomposite and its development towards hydrogen peroxide detection will be discussed. While, in the second research area, the characterisation and development of polypyrrole-nickel composite for glucose detection will be presented. The results of silica-titania/RTIL and its development as enzymatic sensor to detect hydrogen peroxide will be argued in the third research area.

Chapter 5: An overall conclusion together with recommendations to the research is presented.

CHAPTER 2

LITERATURE REVIEW

2.1 Sensor

A sensor can be defined as device which senses a particular analyte or a substance. It is a device that receives a stimulus and responds with a signal that can be read by an observer or instrument (Issac, 2011). Generally, a sensor can be classified into physical sensor and chemical sensor. The physical sensor is sensitive to physical responses such as temperature, pressure, magnetic field, force, etc. and does not have a chemical interface. While, the chemical sensor is depends on particular chemical reaction for their response.

2.1.1 Electrochemical sensor

A chemical sensor is a device that transforms chemical information ranging from the concentration of a specific sample component to total composition analysis into an analytical useful signal (Hulanicki et al., 1991). The chemical information may comes from a chemical reaction of the analyte or from a physical property of the system investigated. Generally, a chemical sensor comprises two basic functional units (as shown in Figure 2.1): a receptor part and a transducer part. The receptor part of a sensor is the chemical information that transformed into a form of energy which is measured by the transducer. While, in the transducer part of a sensor, the device is capable of transforming the energy, carrying the chemical information about the sample into a useful analytical signal.

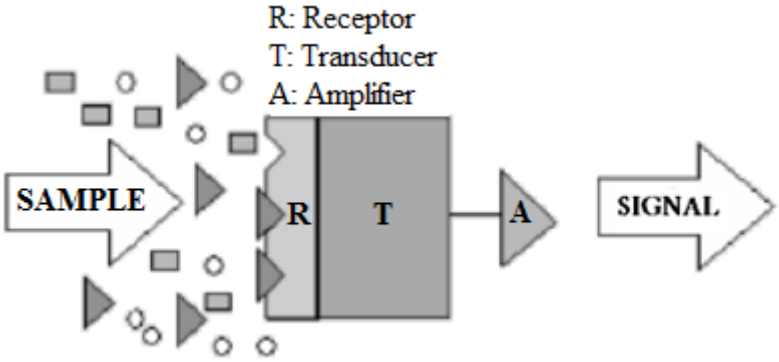

Figure 2.1: Basic elements of a chemical sensor

The chemical sensors categorised into few groups depending on the transducer types are depicted as follows (Hulanicki et al., 1991):

(i) **Electrochemical** sensor that transform the effect of the electrochemical interaction analyte-electrode into useful signal. Such effects may be stimulated electrically or may result in a spontaneous interaction at the zero-current condition.

(ii) **Optical** sensor transforms the changes of optical phenomena which are the results of an interaction of the analyte with the receptor part. Absorbance, reflectance and luminescence measurements are used in various types of optical sensors.

(iii) **Mass sensitive** sensor transforms the mass changes at a specially modified surface into a change of a property of the support material. The mass change is caused by accumulation of the analyte.

(iv) **Heat sensitive** sensor is based on the measurement of the heat effects of a specific chemical reaction or adsorption which involve the analyte. They are often called calorimetric sensors.

Among these devices, the electrochemical sensors are particularly attractive due to their significant detectability, experimental ease and relatively cheap. Electrochemical sensors are well established and use relatively inexpensive equipment to produce unique characterisation information for molecules and chemical systems

including qualitative and quantitative analytical, thermodynamic and kinetic data. Moreover, these types of sensors have high sensitivity which makes them able to detect sub-micro molar concentrations and sub-picomolar amounts of electroactive material. Another point to mention is that these electrochemical sensors are selective which make them able to control the potential of an electrode. Hence, the electrochemical sensors have a main attraction among the currently available commercial sensors and have discovered a limitless scope of significant application in the clinical, industrial, environmental and agricultural investigations.

Besides, electrochemical sensors can be commonly categorised into two such as non-enzymatic and enzymatic electrochemical sensors. The enzyme-based electrochemical sensors are based on the enzymatic catalysis reaction that produce or consume electrons and such enzymes are called as redox enzyme. These electrochemical sensors exploit the selectivity and sensitivity of enzyme as biological recognition element and detect the catalytic biological reaction with a specific substrate/analyte by electrochemical transduction (Ahmadalinezhad, 2011). However, effective immobilisation and electrical contact of redox enzymes with the surface of the electrode is still challenging. This is because the enzyme-based sensors involve complex, multi-step immobilisation techniques and under critical operating conditions, the measurements give poor reproducibility, thermal and chemical instability as well as high cost (Li et al., 2009). Moreover, the conditions such as temperature, pH as well as humidity and the presence of ionic detergents and enzyme-poisoning molecules in the sample can easily affect the performance of sensors (Wang, G. et al., 2013). To solve these drawbacks, many efforts have been made without using enzymes which are known as non-enzymatic electrochemical sensors. The non-enzymatic electrochemical sensors depend on the current response of oxidation or reduction directly at the surface

of the modified electrode. Therefore, the non-enzymatic electrochemical sensors showed higher stability for a long period and the capability to resist the environment aspects compared to the electrochemical sensors using enzymes (Shua et al., 2014). In addition, these non-enzymatic sensors offer a high selectivity, long-term stability, low cost and simple fabrication method which catch the attention of the researchers to extensively develop such sensors.

2.1.2 Classification of electrochemical techniques

Electrochemical techniques comprise quantitative analytical methods that are based on the electrical properties of a solution of the analyte. These techniques can produce vey low detection limits and many characterisation information describing electrochemical addressable systems (Bard & Faulkner, 2000). Electrochemical techniques are superior and adaptable analytical techniques, which offer high sensitivity, accuracy, precision and a large linear dynamic range. Electrochemical measurements offer a numerous benefits such as specificity, selectivity resulting from the choice of electrode material, high sensitivity and low detection limit, possibility of providing results in real time or close to real time and application as miniaturised sensors (Issac, 2011). A wide scope of electrochemical techniques can be utilised for this mentioned reason.

Electrochemical measurements are two-dimensional: the first one which is potential is associated to qualitative properties (with thermodynamic or kinetic control) and the second one is that current is related to quantitative properties (controlled by either mass transport process or reaction rates) (Issac, 2011). Hence, compounds can be selectively detected by electrochemical techniques. The most commonly employed

electrochemical techniques are depicted as follows: (i) voltammetry: in voltammetry technique the current-potential behaviour at an electrode surface is measured. The potential is differed in certain systematic method results in oxidation or reduction of the electroactive chemical species at the electrode. The resultant current is proportional to the concentration of the electrochemical species. It employs two or three electrode in an electrochemical system. The three electrodes namely working, auxiliary/counter and reference, along with the potentiostat allow accurate performance of the potential functions and the measurement of the resultant current; (ii) amperometry: In amperometry, a constant potential is applied and the change in current is observed as function of time. At a chosen potential, the magnitude of current is directly proportional to concentration. This current is the resultant of electrochemical oxidation or reduction of the electroactive compound. Furthermore, if steady state convection is employed as in flowing streams and the concentration of electroactive species is uniform, then a constant current is measured; (iii) potentiometry: based on the measurement of potential under no current flow. In potentiometry the measuring set up consists of two electrode namely measuring/indicator electrode and reference electrode. The measured signal is the potential difference between the indicator electrode and the reference electrode. The potential that develops in the electrochemical cell is the result of the free energy change that would occur if the chemical phenomena were to proceed until the equilibrium condition has been satisfied; (iv) conductometry: the ability of the analyte to conduct an electrical current is observed. From Ohm's law (E = IR), it is obvious that the electric current (I) is inversely proportional to the resistance (R), where E represents potential difference. The inverse of the resistance is the conductance (G = 1/R). In conductometry, a sample's electrical conductivity is determined by the component and their concentration. However, conductivity measurements are difficult because of the

different ionic background of the samples and relatively low conductivity changes that are monitored in such high ionic strength solutions.

The work described in this thesis involves voltammetry and amperometry techniques, specifically cyclic voltammetry and chronoamperometry. Cyclic voltammetry is a comprehensively utilised electrochemical technique in different areas of chemistry. It is usually employed for investigation of redox process, understanding reaction intermediates and gaining reaction products stability. This technique takes into account on changing the applied potential at the working electrode in both forward and reverse directions while observing the current. Besides, chronoamperometry is a potential-controlled technique that measures the current response to an applied potential as a function of time.

2.1.3 Chemically modified electrode

A chemically modified electrode is an electrode surface coated with a thin film of selected conducting materials for the purpose of improving the chemical, electrochemical, optical and electrical and electron transfer properties of the film in a rational and chemically designed manner (Zhi et al., 2009). Thus, the modified electrode can exhibit properties related to those of the modifying substance.

A number of methods have been used to fabricate chemically modified electrodes. Such methods can be carried out by attaching molecules of modifying species on conductive solid substrates (such as gold, carbon paste matrix, glassy carbon) by valence force, covalent bonding, coating by polymer (organic) or inorganic poly-nuclear, mixed films such as composites, hybrid organic-inorganic or by mixing the

modifier with electrode matrix material. Electrodepositions, drop-dry method, spin coating, electropolymerisation and vapour deposition are the examples of fabrication techniques that have drawn the attention of researchers.

Among the mentioned techniques, drop-dry method was employed in the present study. This method involves drop-coating the electrode with small droplets (usually 10 μl) of the desired solution and then to allow drying out. The films prepared in this way are usually non-uniform. However, the morphology of the film depends on different factors including the concentration of the casting solution, rate of evaporation and the roughness of the electrode surface.

2.2 Development of composite and nanocomposite materials for electrochemical sensor applications

Composite and nanocomposite materials

A composite is a multiphase material formed from a combination of materials, which differ in composition or form. While, nanocomposites are materials in which the constituents are mixed on a nanometre length scale (Advani, 2007). They often have properties that are superior to conventional micro scale composites and can display various mechanical, electrical, optical, electrochemical, catalytic and structural properties as compared to individual component (Ajayan et al., 2003).

2.2.1 Conducting polymer-metal oxide composite/nanocomposite

Polymer matrix based nanocomposites is one of the most significant materials in the field of nanotechnology. Particularly, conducting polymer nanocomposites have a appropriate composition of a conducting polymer with one or more insulating materials to produce desirable properties. Conducting polymer nanocomposites are defined as polymers bonded with nanoparticles to produce novel materials with enhanced characteristics which lead to improved properties over regular composites (Mavinakuli, 2010).

Conducting polymer-based composites are increasingly investigated since the end of the 1990s. The composites of conducting polymers with metal or metal oxide nanoparticles (Tai et al., 2007; Vibha et al., 2007; Geng et al., 2006; Tandon et al., 2006; Ram et al., 2005; Torsi et al., 1998), carbon nanotubes (Chen, Y. et al., 2007; Ting et al., 2007; Bavastrello et al., 2004), organic and metal organic compounds (Radhakrishnan & Paul, 2007) and insulating polymers (Bai et al., 2007; Hosseini & Entezami, 2003; Ogura & Shiigi, 1999) provide new analytical systems. Among these composites, conducting polymers with metal oxide composites form a promising class of new materials, due to the beneficial properties of polymer matrix and embedded inorganic particles. The combinations often lead to synergistic effect, which result in improved properties, making these materials applicable in numerous fields.

Conducting polymer-metal oxide nanocomposite could be synthesised by two reaction pathways (Xu et al., 2014). One of the pathways involves the direct reduction of cation by the conducting polymer powder or films as shown in Scheme 2.1 (a) and the other pathway involves the chemical oxidation of monomers by metal salts as shown

in Scheme 2.1 (b). The benefits of this conducting-mediated synthetic platform is cost-effective and environmentally friendly as no organic solvent, reducing agents and polymers capping agents or surfactant are required compared to the conventional solution chemistry pathways. Besides, it permits facile control over the size, morphology and structure of the metal oxide nanoparticles by altering the surface chemistry and redox properties of the conducting polymer. It is a one-step reaction procedure leading to conducting polymer-metal oxide nanocomposites with combined properties related to the two components.

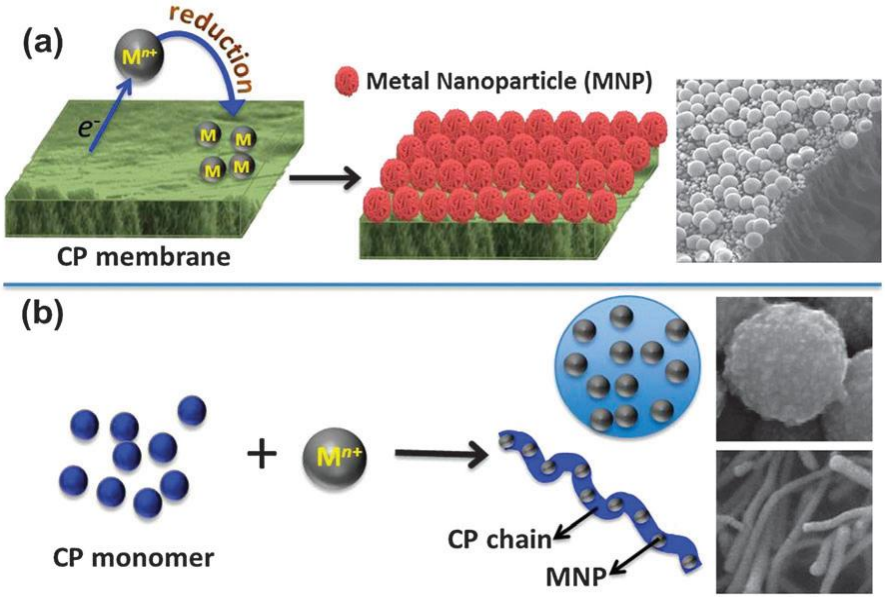

Scheme 2.1: Illustration of the reaction pathways to fabricate conducting polymer nanocomposites via a direct chemical reduction technique: (a) chemical reduction of metal ions by conjugated polymers and (b) chemical oxidation of monomers by metal salts (Xu et al., 2014)

Recently, conducting polymer and their composites developed as a new filed of research, focusing on making of new smart materials for application in modern and forthcoming technologies. Particularly, electrochemistry-related aspects of conducting polymers based nanocomposites have currently attracted with a great interest. Some of the recent mentioned electrochemistry-related applications for these nanocomposites are

listed in Table 2.1. The main expected application of electrochemistry related fields for conducting polymer nanocomposites are electric energy storage systems, chemical-to-electric or vice versa energy conversions, sensors and biosensors and materials for corrosion protection (Malinauskas et al., 2005).

2.2.1.1 Conducting polymers

Conducting polymers, refered as "synthetic metals" and are polymers with a highly π-conjugated polymeric chain (Heeger, 2001b; Macdiarmid, 2001; Shirakawa, 2001). Understanding of the conductivity in polymers was first developed by the trio of Heeger, MacDiarmid and Shirakawa in the 1970s, based on polyacetylene, which is the simplest form of any conducting polymers (Chiang et al., 1977; Shirakawa et al., 1977). Since then the development in the conducting polymers field has continued to rapidly growing. Table 2.2 presents some typical conducting polymers and their chemical structures. Depending on the level of doping and nature of the dopants, these conjugated polymers can be divided into electrical insulators, semiconductors or conductors. The electrical conductivity of these conjugated polymers could be enhance by several orders of magnitude upon treatment with dopants and/or subjecting to chemical or electrochemical redox reactions (Lu et al., 2011).

Conducting polymers are the best choice for chemical and biological sensors due to the interactions with different analytes, which may influence the redox and the doping states of conducting polymers, causing to a change of resistance, current or electrochemical potential. As for electrochemical sensors, the first applications of conducting polymer modified electrodes were demonstrated in potentiometric sensors, predominantly in ion-selective electrodes (Bobacka et al., 2003; Gyurcsanyiet al., 1998).

Table 2.1: Recent electrochemistry-related applications for conducing polymer based nanocomposites

Application	Significant characterisation	Reference
Batteries	ZnO/PPy composites with different morphology synthesised by a facile ultrasound-assisted chemical polymerisation method were used as anode material in order to improve the cycle performance of Zn/Ni rechargeable battery.	(Huang & Yang, 2014)
	Hydrothermal reverse micro emulsion method was developed for the synthesis of tin dioxide/PPy nanocomposites which have potential applications for lithium batteries.	(Sun et al., 2014)
	PPy-Co-O complex was electrochemically fabricated and proved to be a high-performance lithium-storage material.	(Guo et al., 2011)
	NiO-PPy composites for lithium-ion batteries were prepared by a chemical polymerisation method with sodium pTS as the dopant, Triton-X as the surfactant, and $FeCl_3$ as the oxidant. Capacities and cycle lives obtained from the cells constructed from NiO-PPy composite are much better than those from cells constructed using pure NiO.	(Idris, 2011)
Corrosion protection	The effect of the surface area of PPy nanotube and the incorporation of Zn in the PPy nanotube and the anticorrosion performance of the coatings are investigated.	(Mahmoudian et al., 2013b)
	Polyaniline-titanium dioxide nanocomposites in epoxy coating showed better physico-mechanical properties as compared to nano-polyaniline containing coatings and could be useful as an adhesion promoter and corrosion inhibitor	(Mahulikar, 2011)
Electrocatalytic reduction of oxygen	Cobalt precursor plays an essential role on the synthesis process as well as microstructure and performance of the pyrolysed carbon-supported cobalt-polypyrrole catalysts towards oxygen reduction reaction.	(Yuan, 2013)

Table 2.1, continued.

Application	Significant characterisation	Reference
	The PPy and pTS anion doped PPy synthesised using in-situ surfactant mediated chemical oxidative polymerisation approach in a mixed surfactant aqueous solution for its controlled growth and has shown that PPy/pTS-Co can be utilised as a non-precious catalyst material for oxygen reduction reaction.	(Kumar et al., 2013)
	The properties and electrocatalytic activity of candidate cathode catalyst for polymer electrolyte membrane fuel cells based on carbon-supported PPy modified with cobalt and/or platinum were studied.	(Martínez et al., 2010)
	Studied the effect of Co loading and heat treatment on Co-PPy/carbon-black based catalyst materials and the oxygen reduction reaction mechanism that occurs in alkaline media.	(Olson, 2010)
Energy storage devices	Polyaniline/nickel oxide nanocomposites have been successfully prepared by liquid/liquid interfacial polymerisation and an increase in magnitude of the conductivity (1.8 - 3.8 Scm^{-1}) compared with pure polyaniline was observed from the electrical measurements.	(Bora et al., 2014)
Hydrogen evolution reaction	Micro-structured PPy films modified with nickel layers offer a significantly higher electrocatalytic activity in the hydrogen evolution reaction than PPy or nickel electrode.	(Orináková & Filkusová, 2010)
Sensors	PPy-coated Fe_3O_4 nanostrip bundles investigated as sensor without enzyme for the detection of H_2O_2 and lead (II) ions in hazardous materials.	(Mahmoudian et al., 2014)
	PPy-NiO hybrid nanocomposite thin film sensors were used to study room temperature gas-sensing properties for oxidising (NO_2, Cl_2) as well as reducing (NO_2, H_2S, C_2H_5OH, NH_3 and Cl_2) gases.	(Nalage et al., 2014)
	With the help of impedance spectroscopy results, sensing mechanism between PPy, α-Fe_2O_3 and PPy/α-Fe_2O_3 hybrid nanocomposite films and NO_2 gas molecules was studied and explored.	(Navale et al., 2014a)

Table 2.1, continued.

Application	Significant characterisation	Reference
Sensors	One-step synthesis of poly(o-toluidine) nanofiber/metal nanoparticle composite networks as non-enzymatic glucose sensors.	(Poyraz et al., 2014)
	Polyaniline-gold nanocomposite is chemically synthesised and impregnated in a chitosan matrix for immobilisation of cholesterol oxidase on an indium tin oxide-coated glass plate for development of cholesterol biosensors.	(Srivastava et al., 2014)
	Enzyme-less glucose sensor was investigated using core-shell nanocomposite based on chemical oxidative polymerisation of pyrrole on $ZnFe_2O_4$ nanoparticles surface.	(Shahnavaz et al., 2014)
	The polyaniline-SnO_2 nanohybrid based thin films doped with 10 – 50 wt% camphor sulfonic acid were deposited on the glass substrates using spin coating technique and the sensor response was estimated by the change in the electrical resistance of the film in the absence and presence of NH_3 gas.	(Khuspe et al., 2013)
	The investigation about the ability of Mn/PPy nanowires core shell nanocomposites for the H_2O_2 detection.	(Mahmoudian et al., 2013a)
	CuO and Cu_2O composite nanoparticles modified PPy nanowires were fabricated as a biosensor for glucose detection.	(Meng et al., 2013)
	The electrochemical incorporation of a sulfonated cobalt phthalocyanine in conducting PPy was done, in the presence or absence of $LiClO_4$, in order to use the resulting hybrid material for the sensing of ammonia.	(Patois et al., 2013)
	The ammonia gas sensing behaviour of the zinc oxide/polyaniline nanocomposite films is studied and the results show that it is a promising candidate for ammonia sensing with response time of 15 s and recovery time 45 s.	(Shuklaa et al., 2013)

Table 2.1, continued.

Application	Significant characterisation	Reference
Sensors	A new enzyme-less and mediator-less composite electrode consisting tetrakis(6-hydroxyhexylthio) cobalt phthalocyanine incorporated into a polyaniline film for electrochemical H_2O_2 sensor were investigated.	(Çeken et al., 2012)
	PPy-ZnO nanocomposites were prepared by spin coating method and PPy-ZnO nanocomposites with different ZnO weight ratios (10%, 20%, 30%, 40% and 50%) could detect NO_2 at low concentration with very higher selectivity and sensitivity at room temperature than the reported PPy.	(Chougule et al., 2012a)
	Development of a xanthine biosensor based on ZnO nanoparticles-PPy composite by immobilisation of commercial xanthine oxidase on ZnO nanoparticle-PPy composite film electrodeposited onto Pt electrode.	(Devi et al., 2011)
	Poly(o-anisidine)-SnO_2 nanocomposites were synthesised by using an in-situ chemical polymerisation route and their LPG sensing properties were investigated, particularly focused on the low temperature detection (25 – 100 ºC).	(Patil et al., 2011)
	The Ag nanoparticles decorated PPy colloids were prepared by heating a $AgNO_3$ aqueous solution and pre-formed PPy colloids solution in the absence of any external reducing agent. It is found that such Ag nanoparticle-PPy colloids exhibit remarkable catalytic performance toward the reduction of H_2O_2.	(Qin et al., 2011)
	A modified electrode was fabricated by the electrodeposition of Pt or Pd nanoparticles into poly(3-methylthiophene) film over the surface of Pt electrode and was applied to the simultaneous determination of ascorbic acid and dopamine in physiological.	(Atta & El-Kady, 2010)

Table 2.1, continued.

Application	Significant characterisation	Reference
Sensors	Pt/PPy hybrid hollow microspheres were successfully prepared by wet chemical method via Fe_3O_4 template and evaluated as electro-catalysts for the reduction of H_2O_2.	(Bian, X. et al., 2010)
	Poly(o-anisidine)-SnO_2 nanocomposites have been synthesized through an in-situ chemical polymerisation of o-anisidine in the presence of SnO_2 nanoparticles of 25 – 40 nm in diameters and used it as new humidity sensitive material.	(Patil et al., 2010)
Supercapacitors	One-step synthesis of polypyrrole-silver nanocomposites that were directly deposited on nickel foam by in situ polymerization to achieve supercapacitor electrodes.	(Wei et al., 2013)
	The electrochemical deposited nickel hydroxide film was investigated in the effects of adding the PPy on the electrochemical capacitive behaviour of nickel hydroxide electrodes by means of cyclic voltammetry and cycle stability.	(Kim et al., 2012)

Besides, conducting polymers have also attracted huge interest for voltammetric or amperometric detection of analyte. This interest is due to the factors such as sensitivity, selectivity and homogeneity, strong adherence to the electrode surface and the chemical stability of the film. Such polymers can be used in sensor applications either as the sensitive components or as matrices for immobilisation of specific substrates. Moreover, as an alternative approach, they can be regarded as semi-permeable membranes, which can retain analyte by hindering their diffusion toward the supporting electrode (Janáky & Visy, 2013).

Although the conducting polymers are substantial materials for chemical and biological sensing, their poor selectivity and low sensitivity are their limitations and need to be improved. Addition of second component such as metal and metal oxide particles, carbon nanotubes, insulating polymers, metal salts and biological materials into conducting polymer matrix is one of the ways to overcome the mentioned difficulties since the second component may increase the chain mobility of conducting polymers or alter the affinity of the composite or even act as a catalyst (Lu et al., 2011).

Among the conducting polymers, polyaniline and polypyrrole are the most extensively investigated polymers for the application of chemical sensor. However, this thesis focuses its investigation only on polypyrrole in the composite form. Polypyrrole is a unique polymer among the family of conducting polymers because of its simple synthesis and environmental stability (BaytekİN, 2009).

Table 2.2: Typical conducting polymers and its structures

Name	Structure
Polyaniline	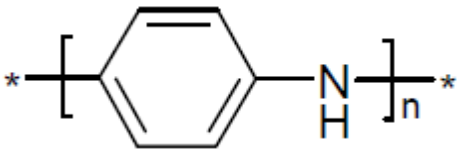
Polypyrrole	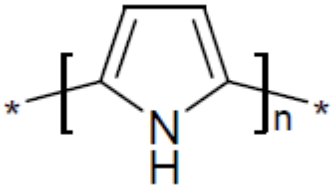
Polythiophene	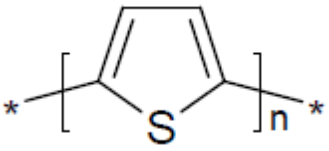
Poly(para-phenylene)	
Poly(phenylene ethylene)	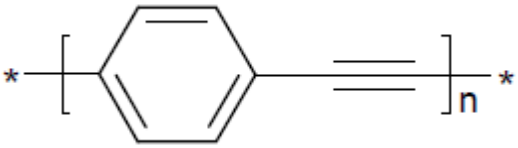
Poly(phenylenesulfide)	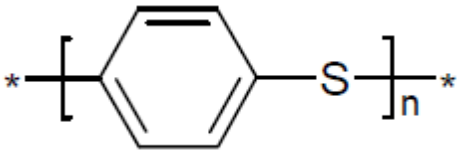
Poly(phenylene-vinylene)	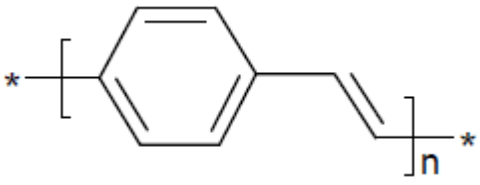

Polypyrrole (PPy)

Polypyrrole (PPy) (Figure 2.2) has drawn a huge and specific interest, due to their high conductivity, stability in oxidised state and redox properties. The ease of the synthetic methods and the readiness of the initial monomers are also attractive characteristics of PPy. As compared with other organic molecules, pyrrole polymerisation is carried out by oxidation of the monomer, which forms a conjugated polymer chain with overlapping π-orbitals and a positive charge along the polymer backbone (Heeger, 2001a). PPy can be synthesised in the form of powders, coatings or films. It is inherently conductive, stable and can be quite easily produced continuously by electrochemical reaction (Aldissi, 1992). PPy with exciting electrical properties was first exploited and reported in early 1960s (Bolto et al., 1963).

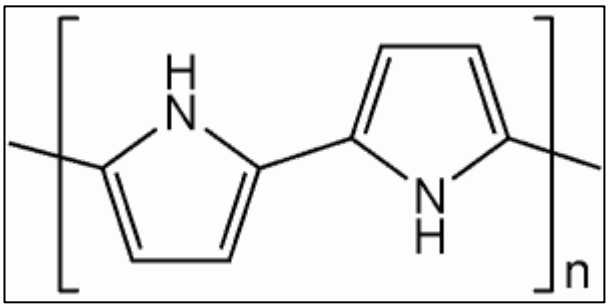

Figure 2.2: The chemical structure of polypyrrole

PPy is extensively synthesised through the oxidation of pyrrole by electro polymerisation at a conductive substrate through the application of an external potential by producing the films deposited on the working electrode or by chemical polymerisation in solution by the use of a chemical oxidant leads to powders (Pionteck et al., 1999). However, chemical oxidative polymerisation methods have drawn huge interest because it can be used to synthesise bulk quantities of PPy in a fast and easy way (Kricheldorf et al., 2005) and it may be easier to scale up the batch process

(Skotheim & Az, 2006). PPy is very attractive for numerous applications particularly sensor applications due to the ease of processing as the pyrrole monomer is soluble in water and the polymer has good conductivity and environment stability. PPy is stable in a wide range of potentials in thousands of charge-discharge cycles and moreover, its response is fast under properly selected conditions. Compared to polyaniline, it can operate both in acidic and neutral solutions, which makes the PPy electrode attractive for use as sensors material in electroanalytical chemistry.

There is a growing interest to combine both PPy and inorganic materials for applications in electrochemical sensors. The combination of metal oxides and PPy has the potential to increase the sensitivity of the conducting polymer. Such composites can operate at room temperature and the sensitivity towards different analytes can be optimised by the volume ratio of metal oxides. In addition, the composite may have better long-term stability. There are number of researches which have already developed PPy-metal oxide nanocomposite for electrochemical sensors. The detailed description is presented in section 2.2.1.3.

2.2.1.2 Metal oxides

Metal oxides play a very important role in many areas of chemistry, physics and material science. Generally metal elements form very large diversity of compounds with various stoichiometries and can form a number of structural geometries with electronic structure displaying metallic, insulator or semiconductor characters (Faleni & Moloto, 2013).

As is by now well known, nanostructured metal oxides have become an area of growing interest and importance in a wide range of fundamental studies and technological applications, due to their unique size and shape-dependent activities, optical, electronic, magnetic, chemical, electrochemical and mechanical properties when compared to their bulk counter parts (Helia & Yadegari, 2010). These characteristics of nanostructured metal oxides provide an ideal platform for electroanalysis, electrocatalysis and bio-catalysis applications, especially in sensor and biosensor fabrications (Tian et al., 2015; Butwong et al., 2014; Ci et al., 2014).

A number of metal oxides such as ruthenium oxides, iron oxides, titanium oxides, manganese oxides, vanadium pentoxide, nickel oxides and cobalt oxides have been investigated as the electrode materials for chemical sensor applications (Bai & Zhou, 2014; Zhang et al., 2014; Pang et al., 2012; Shim et al., 2012; Chauhan & Pundir, 2011; Lenz et al., 2011; Li et al., 2010). Although, a wide variety of oxides exhibits sensitivity towards oxidising and reducing target analyte by a variation of their electrical properties, the oxides of cobalt and nickel were chosen for this study since they are found more effective as compared to other metal oxides and they are the first considered and still are the most frequently used materials for chemical sensor applications.

Cobalt oxide

Cobalt oxide is p-type semiconducting material with a direct band gap of ~ 2.4 eV (Ali et al., 2014). The nanoparticles of cobalt oxide exhibit excellent properties and are widely used in ceramics, drug delivery, adsorbent, rechargeable lithium ion batteries, sensors and electrochromic devices (Bhattacharyya & Snehesh, 2015; Chattopadhyay et al., 2013; Costa et al., 2013; Li et al., 2005; Kadam & Pati, 2001).

Among metal oxides, cobalt oxide has received much attention due to its electro-catalytic properties, chemical stability and low cost.

Furthermore, nanostructured cobalt oxide with high specific surface area and enhanced electrochemical activity is particularly attractive for applying its electrocatalytic properties. For example, Lee et al. (2013) prepared CoOOH nanosheet array on a cobalt substrate via a simple alkaline treatment at room temperature and this simple growth of nanostructures on a conducting substrate allows their direct use as non-enzymatic glucose electrochemical sensor at higher potential. While, Li et al. (2014) reported a graphene-based hybrid nanomaterial by electrochemical deposition of cobalt oxide nanoparticles on the surface of electrochemically reduced graphene oxide deposited on a GCE and successfully applied to the determination of H_2O_2 in samples. Whereas, Salimi et al. (2008) reported a micromolar and/or nanomolar concentration range detection of arsenic(III) on cobalt oxide nanoparticles modified GCE using voltammetry and hydrodynamic amperometric techniques. Meng et al. (2011) described a sensor for determination of nitrite in water samples which was based on cobalt oxide nanoparticles deposited on the surface of MWCNTs/GCE. Hou et al. (2009) synthesised ordered mesoporous carbon/cobalt oxide nanocomposite by thermolysis and utilised it for glutathione detection. Kung et al. (2011) fabricated cobalt oxide acicular nanorods with high sensitivity for glucose detection. Excellent electrocatalytic properties and a relatively cheap, make cobalt a good choice for the development of enzyme-free sensors.

Besides, a few recent studies have shown that conducting polymers can be modified in different ways with cobalt oxide nanostructures. Yu et al. (2013) proposed a method for the fabrication of nanostructure cobalt oxide/over-oxidised PPy composite

film electrochemical sensing interface by two-step electrochemical techniques. They carefully studied the electrochemical properties, electrocatalytic activity; as well as the surface morphology (as shown in Figure 2.3 A) and revealed that this modified electrode exhibited good stability, good anti-interference ability, along with a high electrocatalytic activity to the oxidation of glucose. Whereas, Kumar et al. (2013) studied the structure and electrocatalytic activity of polypyrrole p-toluenesulfonate (PPy/pTS) supported cobalt catalysts for oxygen reduction reaction activity. Such PPy/pTS-Co catalyst, (Figure 2.3 B) were synthesised by in-situ surfactant mediated chemical oxidative polymerisation. Moreover, Olson (2010) synthesised Co-PPy based catalyst material with a commercially available 20 wt% polypyrrole supported on a carbon black in the presence of Co(II) and then studied the effects of Co loading and heat treatment on it. While, Guo et al. (2011) chemically synthesised polypyrrole-cobalt-oxygen (PPy-Co-O) coordination complex (Figure 2.3 C) and then used as high-performance lithium-storage materials. There is a number of conducting polymer-cobalt oxide nanostructures studies as earlier mentioned which were mostly related to the development of electro catalyst towards oxygen reduction reaction and there are only limited numbers of studies on its application in sensors. Therefore, the development of new conducting polymer-cobalt oxide based material for accurately detecting target analyte is still significant.

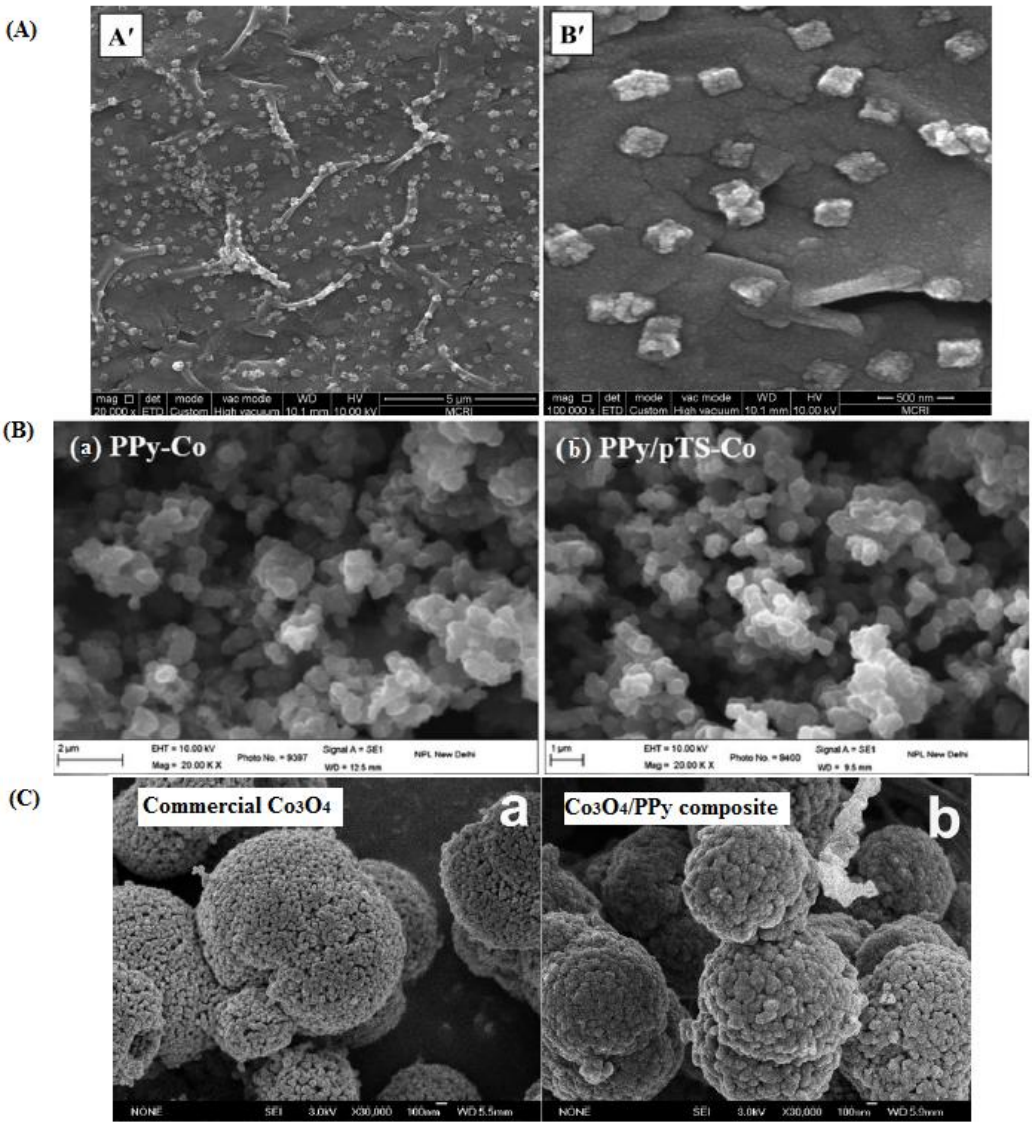

Figure 2.3: (A) SEM images of CoO_x/OPyox/CCE (Yu et al., 2013); (B) SEM images of (a) PPy-Co and (b) PPy/pTS-Co (Kumar et al., 2013); (C) SEM images of the PPy-coated Co_3O_4 composite before and after PPy coating (Guo et al., 2011)

Nickel oxide

Among various metal oxides, nickel oxide is the most promising material, which is extensively used as catalyst, battery cathodes, gas sensors, electro chromic films and magnetic materials (Wang, L. et al., 2012; Makhlouf et al., 1997), due to the advantage of natural abundance, low toxicity, good electrochemical stability and catalytic properties. It is considered as the p-type semi-conductor because of its wide band-gap energy range, which is from 3.6 to 4.0 eV (Das et al., 2013).

Moreover, nickel oxide based composites have been extensively explored for the fundamental scientific and technological interests in accessing new classes of functional materials with unique properties and applications in energy storage devices, supercapacitors, electrochemical sensors and etc. (Nancy & Kumary, 2014; Nandapure et al., 2013; Kim et al., 2012; Idris, 2011). Composites of nickel oxide with various additives were prepared to improve their electrochemical performance including electrocatalysis, conductivity and stability (Aleahmada et al., 2011; Jia et al., 2011; Sonavane et al., 2010).

In recent years, a few studies on conducting polymer-nickel oxide composite materials have been investigated. For example, polyaniline/NiO nanocomposites via liquid/liquid interfacial polymerisation were prepared to evaluate electrical, electrochemical and magnetic properties (Bora et al., 2014). PPy-NiO composites have been synthesised by in situ polymerization method for dielectric spectroscopy (Seema & Prasad, 2014), polyaniline-supported Ni films for methanol oxidation (Nagashree & Ahmed, 2010) and PPy/Ni layers with enhanced cathodic activity for hydrogen evolution by electrodeposition (Orináková & Filkusová, 2010). Besides, Nalage et al. (2014) prepared PPy-NiO hybrid nanocomposite thin-film sensor by spin-coating method on glass substrate. The PPy-NiO hybrid nanocomposite thin film sensors were used to study room temperature gas-sensing properties for oxidizing (NO_2, Cl_2) as well as reducing (NO_2, H_2S, C_2H_5OH, NH_3 and Cl_2) gases. However, there are only few studies on conducting polymer-nickel oxide composite materials in sensor applications. Thus, the formation of conducting polymer-nickel oxide based material for sensor application is still considered.

2.2.1.3 Conducting polymer-metal oxide nanocomposite as electrochemical sensor

Recent research has shown that there is a growing interest to combine both conducting polymers and metal oxide materials for electrochemical sensor applications. In order to investigate the sensing properties of the conducting polymer-metal oxide nanocomposite towards chemical and the possible interaction involved, conducting polymer-metal oxide are typically fabricated with modified graphite or glassy carbon to form the electrodes to study their electrocatalytic capability. It is generally accepted that the sensing ability of a modified electrode is affected by several factors including, electrocatalytic activity, surface area, conductivity, chemical and electrochemical stability and surface properties, which are directly related to the physical and/or chemical properties of the electrode material. The idea of using composite/nanocomposite material as modified electrodes has been introduced to undertake the mentioned factors. The conducting polymer-metal oxide composites/nanocomposites lead to the possibility of enhancing one or more of the properties as mentioned earlier, either by improving the behaviour of the conducting polymer matrix or due to their intrinsic characteristics. In addition, loading metal oxide nanoparticles on conductive polymers produces nanocomposites with high active surface areas and enhanced electron transport, making the nanocomposites suitable materials for the fabrication of electrochemical sensors. The attractiveness of this approach can be seen from the rapidly increasing number of researches reporting successful sensing applications.

There are numbers of researches have been developed for conducting polymer-metal oxide nanocomposite based electrochemical sensors. The most recent fabrications

of such electrochemical sensors are listed in Table 2.3. Some of them particularly PPy-metal oxide based sensors are described in details as follows.

In a study conducted by Mahmoudian et al. (2014), the nanocomposite networks of polypyrrole-coated Fe_3O_4 nanostrip bundles were facilely prepared in one-step (Figure 2.4). The synthesised nanocomposite then fabricated as an electrochemical interface sensing for H_2O_2 and Pb(II) ions in hazardous materials. Figure 2.5 showed that PPy-Fe_3O_4 nanostrip bundles/GCE has a good catalytic performance of H_2O_2 and Pb(II), compared to PPy/GCE. The enhancement of catalytic performance of PPy-Fe_3O_4 nanostrip bundles can be explained by two reasons: (i) a larger surface area for the interaction of Fe_3O_4 can be provided by the morphology of the PPy during the deposition of the Fe_3O_4, (ii) large amount of deposited Fe_3O_4 onto the surface enhances the large catalytic current.

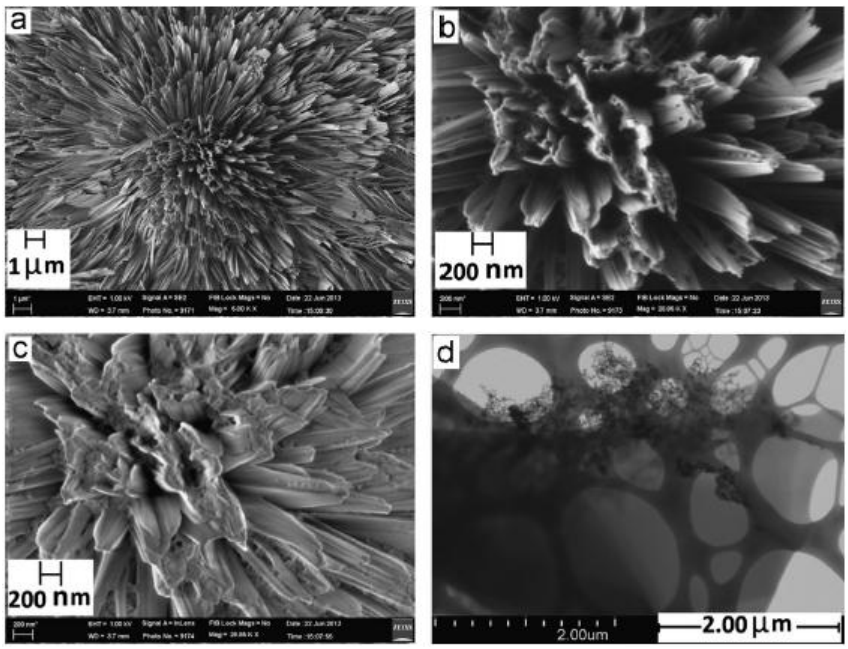

Figure 2.4: (a) FESEM of the PPy/Fe_3O_4 nanostrip bundles, (b) and (c) higher magnifications of (a), and (d) TEM of the PPy/Fe_3O_4 nanostrip bundles (Mahmoudian et al., 2014)

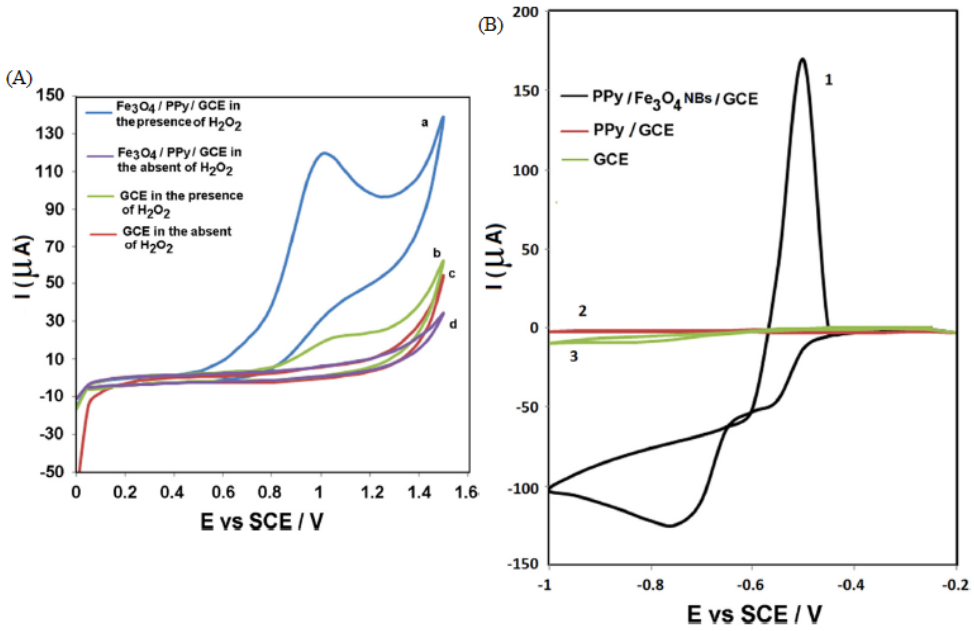

Figure 2.5: (A) The cyclic voltammetric behaviour of the PPy/Fe_3O_4 NBs/GCE (a and d) and bare GCE (b and c) with and without of 2.5 mM H_2O_2 in PBS (Na_2HPO_4 and NaH_2PO_4) with a pH of 7.5 at a scan rate of 50.0 mV s^{-1}; (B) CVs of 10 μM Pb(II) on (1) PPy/Fe_3O_4 NBs/GCE (2), PPy/GCE and (3) bare GCE in 0.1 M PBS (Na_2HPO_4 and NaH_2PO_4) (pH 6.0). Scan rate: 100 mV s^{-1} (Mahmoudian et al., 2014)

Furthermore, Meng et al. (2013) studied an efficient non-enzymatic glucose biosensor, with Cu_xO/PPy nanocomposite modified Au as electrodes configuration. As shown in Figure 2.6, the current as a function of time was monitored at different glucose concentrations. The anodic peak becomes more apparent and the peak current gradually increases upon the addition of glucose to the electrolytic solution. It is found that Cu_xO/PPy/Au has excellent electrocatalytic activity towards the oxidation of glucose and the PPy nanowires finely dispersed Cu_xO nanoparticles and also the nanostructures Cu_xO nanoparticles significantly increased the electrocatalytic active areas and enhanced the electron transfer. Furthermore, the large pores in PPy nanowires provide high surface area for glucose molecules to be adsorbed, effectively transfer electrons between the Au and Cu_xO active sites and high mass transportation rate, which decrease the amount of oxidation products accumulated on the catalytic sites and avoid the electrode from fouling.

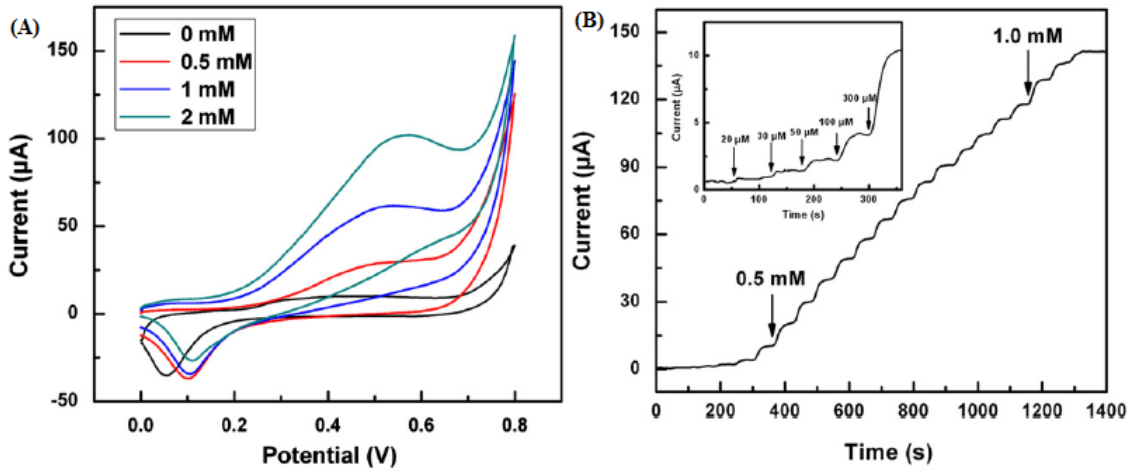

Figure 2.6: (A) CV scans of Cu_xO/PPy/Au in 0.1 M NaOH with and without of 0.5, 1.0, 2.0 mM glucose at 50 mVs^{-1} scanning from 0 to 0.80 V; (B) Current-time responses of Cu_xO/PPy/Au with successive increasing glucose concentration at 0.6 V. The inset displays the enlarged diagram of the current-time response at low concentrations of glucose (Meng et al., 2013)

Liu et al. (2012) carried out a study on metal/conducting polymer composite for H_2O_2 detection, including cyclic voltammetric and amperometric response as shown in Figure 2.7. A continuous increase in the cathodic current density of the cyclic voltammogram can be evidently observed with the increasing H_2O_2 concentration, indicating strong electrocatalytic activities of the composite on reduction of H_2O_2. This can be justified due to the fact that the amplification effect of the metal-support interaction along with the electrocatalytic properties of the Ag NPs towards H_2O_2 is superior. In addition, the rapid response of the PPy/Ag/G electrode respective to each addition of H_2O_2 is shown in (Figure 2.7 B). The enhancement in amperometric current reaches the steady state within 5 s. The electrode displays a linear response and the sensitivity is sufficiently high. Moreover, vanadium pentoxide as a seeding template and microwave assisted nanocarbonisation both play an important role during the reaction process which result in PPy/Ag nanocomposites being an outstanding material for fabricating non-enzymatic H_2O_2 sensors.

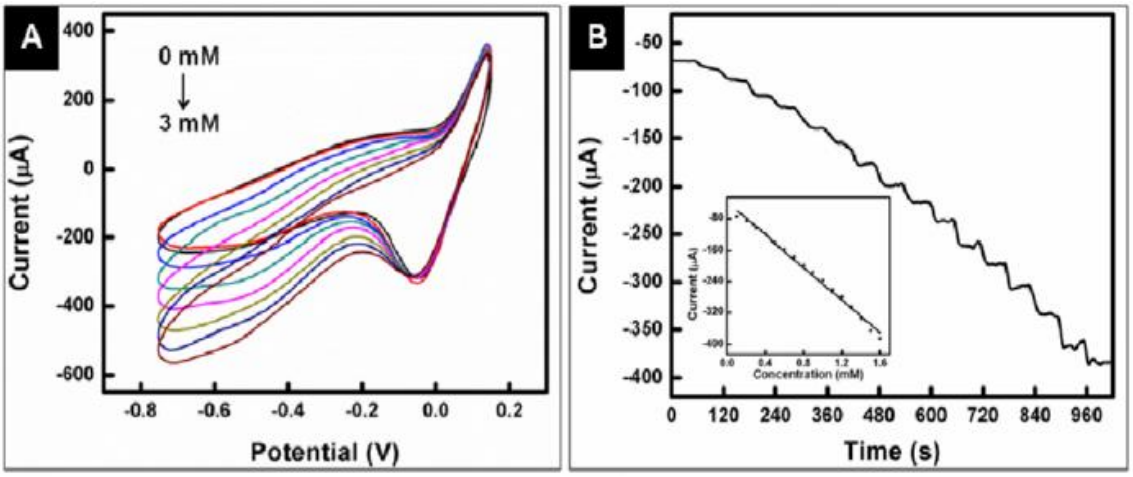

Figure 2.7: (A) CVs of PPy-Ag nanocomposite modified graphite (PPy-Ag/G) electrodes in a 10 mM PBS solution with and without H_2O_2 at different concentrations (from top to bottom: 0, 0.1, 0.5, 1, 1.5, 2, 2.5, 3 mM). Scan rate: 20 mV s^{-1}. (B) Amperometric responses of PPy–Ag/G electrodes upon successive addition of 0.1 mM (0.1-1.6 mM) in a stirred 10 mM PBS solution. Applied potential: -0.45 V. The inset displays the corresponding calibration curves of the electrodes in the measured H_2O_2 concentration range (Liu et al., 2012)

As mentioned, conducting polymer/metal oxide nanocomposites have been synthesised in different techniques and developed for various electrochemical sensors. However, the conducting polymer/metal oxide based sensors are still developing and new techniques are continuously investigated around the world.

Table 2.3: The most recent fabrication of conducting polymer-metal oxides for electrochemical sensor

Conducting polymer	Inorganic particles	Method	Analyte	Electrode	Linear range	Detection limit	Reference
PPy	Fe_3O_4 nanostrip bundles	Chemical polymerisation of pyrrole in the presence of Fe(III)	H_2O_2 Pb(II)	GCE	0.1-60 mM 10-50 nM	0.47 µM	(Mahmoudian et al., 2014)
POT	Au/Cu nanoparticles	Synthesised through a one-step seeding polymerization reaction	Glucose	G	1-30 mM	-	(Poyraz et al., 2014)
PPy	$ZnFe_2O_4$	Chemical oxidative polymerisation of pyrrole on $ZnFe_2O_4$ nanoparticles	Glucose	GCE	0.1-8.0 mM	0.10 mM	(Shahnavaz et al., 2014)
PPy	Mn nanowire	Chemical polymerisation of pyrrole in the presence of Mn(III)	H_2O_2	GCE	0.005- 0.09 mM 0.1-8 mM	2.12 mM 22.3 mM	(Mahmoudian et al., 2013a)
PPy	Cu_xO nanoparticle	Cu_xO nanoparticles deposited on PPy nanowires by electrodeposition and electrochemical oxidation in situ	Glucose	Au	0-8 mM	6.20 µM	(Meng et al., 2013)
PEDOT	Au	Electrodeposition of Au on PEDOT coated carbon paper electrode	Glucose	C	0.03-10 µM	0.03 µM	(Dash & Munichandraiah , 2013)
Over-oxidised PPy	Co	Prepared by two step electrochemical procedure	Glucose	CCE	0.2-0.024 µM 0.24-1.4 mM	0.05 µM 0.05 µM	(Yu et al., 2013)

Table 2.3, continued.

Conducting polymer	Inorganic particles	Method	Analyte	Electrode	Linear range	Detection limit	Reference
PPy	Fe_3O_4	Incorporation of surface-modified magnetite nanoparticles during electropolymerisation	H_2O_2	GCE	10-400 μM	-	(Bencsik et al., 2012)
Polianiline	CoPC	Electrochemical incorporation of non-ionic CoPc into polyaniline film	H_2O_2	GCE	2-18 μM	-	(Çeken et al., 2012)
PPy	Microwave Ag Ag	Chemical polymerisation of PPy nanofibril network with a high-loading of Ag particles	H_2O_2	G	0.1-1.6 mM	-	(Liu et al., 2012)
Conducting polymer	**Inorganic particles**	**Method**	**Analyte**	**Electrode**	**Linear range**	**Detection limit**	**Reference**
PPy	ZnO	A mixture of ZnO nanoparticles and PPy was eletropolymerised on Pt electrode	Xanthine	Pt	0.8-40 μM	0.8 μM	(Devi et al., 2011)
PPy hollow nanocapsules	Pt Nanoparticles	Prepared by using beta-akaganeite nanospindles as templates and methanoic acid as a reducing agent	NADH	GCE	0.04-0.8 mM	0.7 μM	(Mao et al., 2011)

Table 2.3, continued.

Conducting polymer	Inorganic particles	Method	Analyte	Electrode	Linear range	Detection limit	Reference
PPy	Ag nanoparticles	Prepared by heating a $AgNO_3$ aqueous solution and pre-formed PPy colloids solution in the absence of any external reducing agent	H_2O_2	GCE	0.1-90 mM	1.05 μM	(Qin et al., 2011)
Over-oxidised PPy	Pd/Si microchannel	Electrodeposition of OPPy was performed on modified Pd/Si-MCP	Glucose	Pd/Si-MPC	1-24 mM	2.06 μM	(Shi et al., 2011)
PMT	Pd, Pt nanoparticles	Electrodeposition of Pt or Pd nanoparticles into PMT film over the surface of Pt electrode	AA DA	Pt disc	0.02-0.12 mM 0.05-1 μM	6 μM 9 nM	(Atta & El-Kady, 2010)
Polyaniline	WO_3	Electrochemical co-deposition of the composite on to carbon cloth	BrO_3^- ClO_3^- NO_2^-	C cloth	40 μM-1.2 mM 0.12-20 mM 40 μM-2.5 mM	4.8 μM	(Zou et al., 2011)
PPy	Pt hybrid hollow microspheres	Prepared by wet chemical method via Fe_3O_4 template	H_2O_2	GCE	1-8 mM	1.2 μM	(Bian, X. et al., 2010)
Polyaniline	MoO_3	Electrochemical co-deposition of the composite on to carbon cloth	ClO_3^-	C	25 μM- 4.5 mM	17 μM	(Bian, L.-J. et al., 2010)

Table 2.3, continued.

Conducting polymer	Inorganic particles	Method	Analyte	Electrode	Linear range	Detection limit	Reference
Polyaniline	WO_3	Electrochemical co-deposition of the composite, starting from aniline and H_2WO_4-containing solution	IO_3^-	C cloth	10-500 μM	2.7 μM	(Zou et al., 2010)
PEDOT, polyazulene	Prussian blue	Composites were prepared in different configurations by electrochemical methods	DA 4-Nitro-phenol	Pt disk	30- 90 μM 2-100 μM	8.23 μM 0.12 μM	(Lupu et al., 2009)
Polyaniline	Fe_3O_4	Chemical polymerisation of aniline in the presence of magnetite nanoparticles	DA	C	1-50 μM	-	(Radhakrishnan et al., 2009)
PPy	Cu	Electropolymerised Cu nanoparticles on the electrode modified with PPy nanowires	H_2O_2	Au	0.007-4.3 mM	2.3 μM	(Zhang et al., 2008)

2.2.2 Silica-titania oxide composites

Silica-titania oxide composites are very important developed materials and catalysts. They have attracted great interest in academic and research laboratories as well as to be used in several applications (Hou et al., 2008; Mikushina et al., 2008; Shu et al., 2007; Husing et al., 2002).

There has been a great bulk of research on the different preparation methods for creating a solid Si-Ti oxide material. Several characteristics such as, pore size, surface charge, mechanical strength and adsorption sites of the final product are dependent on the synthesis conditions and the type of interaction between Si and Ti oxides. There are two forms of interaction: physical forces of attraction (such as Van der Waals forces) and chemical bonding (creation of a Ti – O – Si bond). The physically supported TiO_2 on SiO_2 preparation methods have been the least researched, while the chemically bonded TiO_2 on SiO_2 methods (also called mixed oxides) have been thoroughly investigated (Londeree, 2002).

The Si-Ti oxides materials properties are intensely relied on the preparation pathway. The approaches employed for the synthesis of binary oxide nanomaterials include conventional solid state mixing, co-precipitation, hydrothermal and sol-gel processes (Mahyar et al., 2010; Chen et al., 2009; Huang et al., 2009; Jin et al., 2009; Colon et al., 2002). Amongst these methods, the most widely and effectively used methods of preparation for creating mixed oxides are sol-gel hydrolysis and co-precipitation. The use of the sol-gel route to prepare raw Si-Ti oxides solids lets us to obtain materials with high homogeneity and good titanium dispersion and to control their composition and properties (Ren et al., 2008).

The alkoxide sol-gel route was found to be the most frequently used method for the preparation of the Si-Ti materials. Tetraethylorthosilicate (TEOS) and titanium (IV) isopropoxide (TTIP) precursors are mostly used to produce mixed Si-Ti oxide materials. Table 2.4 shows their chemical and physical properties. The main challenge faced for success in the preparation of materials in which silica and titanium are mixed in the atomic or molecular level is the difference in the reactivity of TEOS and TIP towards hydrolysis and condensation reactions (Vives & Meunier, 2008). TEOS is identified to be less sensitive to hydrolysis compared to other transition metal alkoxides, in other words, Si is less electropositive and it has no coordination under saturation in $Si(O(C_2H_5))_4$ (Brinker & Scherer, 1990). In the case of silicon alkoxides, acid or basic catalysts are suggested to be used to improve the hydrolysis and condensation reactions. On the other hand, TIP is a common precursor for being used in titania-based sol-gel and is very sensitive to hydrolysis due partially to its monomeric form in organic solution (Babonneau et al., 1988) leading to a rapid precipitation of a poly-disperse product (Brinker & Scherer, 1990). In order to reduce the reactivity of TIP, it is probable to modify this precursor using in acidic medium.

Table 2.4: Chemical and physical properties of alkoxide precursors

Properties	**TEOS**	**TTIP**
Chemical structure	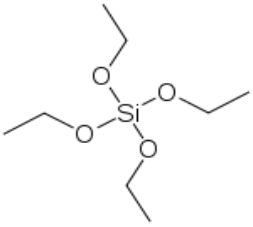	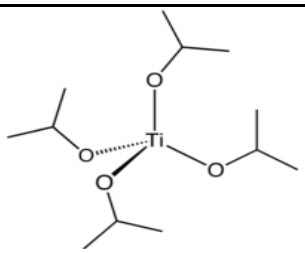
Molecular formula	$SiC_8H_{20}O_4$	$C_{12}H_{28}O_4Ti$
Molar mass	208.33 $gmol^{-1}$	284.215 $gmol^{-1}$
Appearance	colourless liquid	colourless to light-yellow liquid
Density	0.933 gmL^{-1}	0.96 gmL^{-1}
Melting point	-77 °C	17 °C
Boiling point	166 to 169 °C	232 °C
Solubility in water	miscible, but readily decomposes	reacts to form TiO_2

2.2.2.1 Sol-gel chemistry

Sol-gel chemistry offers an effective methodology for the synthesis of macromolecular materials under extraordinarily mild thermal conditions, typically at room temperature. The room temperature operation, inherent in sol-gel chemistry, enables the material synthesis process by easing the operational requirements on equipment specification and laboratory safety. A sol is a colloidal suspension of particles, while the term gel refers to the semi-rigid material formed when the colloidal particles link together in a liquid to form a network. Sol-gel precursors consist of metals or metalloids surrounded by various ligands, of which the most widely used is metal alkoxide (Londeree, 2002). Aluminates, titanates, borates and silicates are the examples of the alkoxides that can be used to create a sol-gel. The classical sol-gel process can be divided into four characteristic steps (Figure 2.8):

1. Generation of a stable solution of molecular metal precursors (the sol).
2. Formation of a bridged network by condensation reactions, gelation with increasing viscosity (the gel).
3. Ageing of the gel with on-going condensation: Formation of a solid mass and expulsion of solvents.
4. Drying of the gel, removal of water and solvents by thermal treatment (xerogel) or by extraction at super-critical conditions (aerogel).

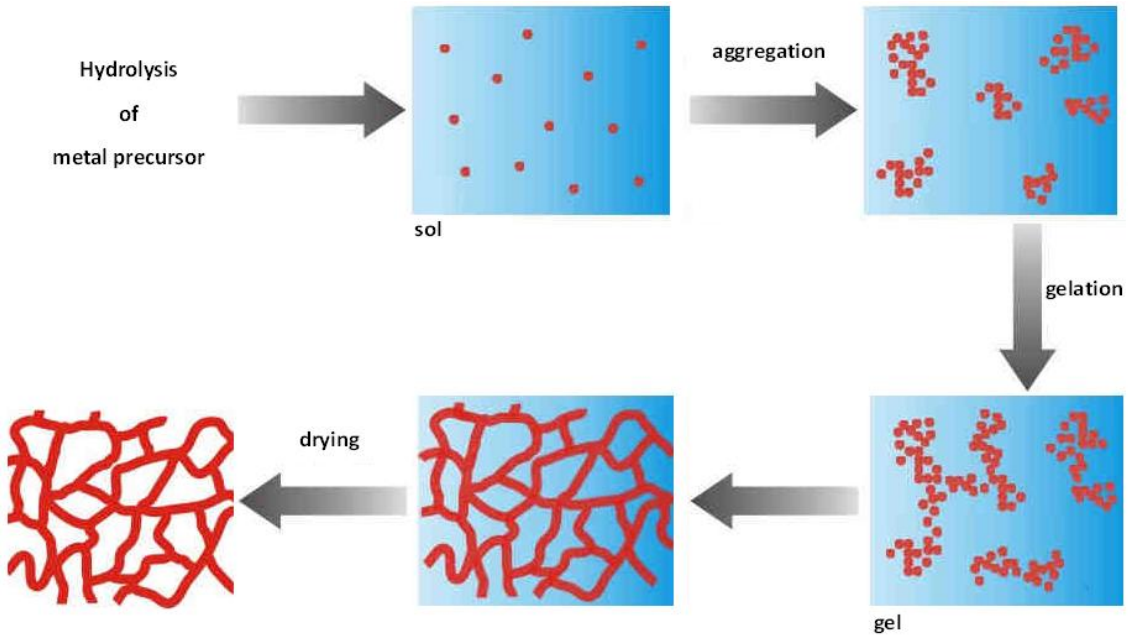

Figure 2.8: Reaction steps of the sol-gel process leading to a condensed inorganic network (Szeifert, 2011)

The simplicity and versatility of the sol-gel process allows it to be used more efficiently for sensing application especially biosensors. Compared to chemical methods to immobilise enzymes, sol-gel encapsulation is a powerful tool for improving the properties of biomolecules immobilised for use as biosensors or biocatalysts (Hernandez & Fernandez-Lafuente, 2011). A great amount of biomolecules have been immobilised by sol-gel techniques and they show better enzymatic activity and stability (Pastor et al., 2010). However, there are also some disadvantages in the process of sol-gel immobilisation, such as shrinkage of the gel during the process of condensation and drying, which can cause denaturation of the enzyme (Souza et al., 2013).

One way to solve these problems is to use additives to stabilise enzymes and support in gel formation within arrays. Currently, the use of room temperature ionic liquids as additives in the immobilisation process has been stated, which increases the activity and stability of immobilised enzymes by modifying the hydration shell of the enzyme and decreasing the shrinkage of the gel (Souza et al., 2013).

2.2.2.2 Room temperature ionic liquid

Ionic liquids can be described as compounds composed entirely of ions that are liquid at a temperature less than 100 ºC. Those salts with very low melting points, so called room-temperature ionic liquids (RTILs), are most desirable solvents for reactions and processes. The mostly used cations are those containing imidazolium, pyridinium, phosphonium, pyrrolidinium, tetraalkylphosphonium, tetraalkylammonium and rialkylsulfonium, normally combine with anions such as tetrafluoroborate hexafluorophosphate, tri-fluorotris(pentafluoroethyl)phosphate, thiocyanate, dicyanamide, ethyl sulfate and bis(trifluoromethylsulfonyl)amid (Shiddiky & Torriero, 2011). Compared to conventional organic solvents, RTILs have several favourable properties including extremely low vapour pressure, low flammability, a wide liquid range, high thermal conductivity, high ionic conductivity and good dissolution power towards many substrates, high chemical and thermal stability and a wide electrochemical potential window (Zhao, 2010).

Another important application of RTILs is to include them into conventional matrixes (such as biopolymers, cellulose, carbon nanotube, metal nanoparticles and sol-gel based silica matrixes) to form stable composite materials, which have drawn huge attraction due to their unique properties (Liu et al., 2005c; Turner et al., 2004; Zhao et al., 2004; Han et al., 2010). These composite materials merge multifunctional properties of materials involved in preparing the composites. In electrochemical biosensors, these composite materials can also be used as immobilising matrix to entrap proteins and enzymes, which offer a favourable microenvironment for redox proteins and enzymes to maintain their bioactivity and perform direct electrochemistry and electrocatalysis. For examples, Liu et al. (2005c) improved activity and thermal stability of HRP after

immobilising in [C_4MIm][BF_4] based sol-gel, Lee and his co-researchers (Lee et al., 2007a; Lee et al., 2007b) studied a variety of RTILs and their mixtures as additives during the sol-gel immobilisation of Candida rugosa lipase and achieved greater hydrolytic and esterification activities of sol-gel encapsulated lipase coated with RTILs as compared to that without RTILs. Furthermore, Hara et al. (2009) immobilised lipase PS from Burkholderia cepacia in a sol-gel and obtained higher enzyme stability in [C_2MIm][BF_4], [C_2MIm][NTf_2] and [C_4MIm][PF_6].

2.2.2.3 Silica-titania composite as enzyme-based electrochemical sensor

The design of sol-gel sensing materials, depend on the careful choice of the starting alkoxide, encapsulated reagents and preparation conditions, allows altering of material properties in a broad range and provides great promise for the development of electrochemical biosensors. The interesting properties of sol-gel materials including the simplicity of preparation, low-temperature encapsulation, tuneable porosity, chemical inertness, negligible swelling, optical transparency and mechanical stability, make them promising materials in the development of chemical sensors and biosensors. Early activities in sol-gel based sensors have been focused towards optical devices because the favourable optical properties of silica. However, the versatility of sol-gel processes and materials are also found to be very useful in the electrochemical devices.

Sol-gel derived composite electrodes have increasingly become advantageous for the design of electrochemical sensors. Nowadays, the sol-gel derived silica and titania materials in the presence of ionic liquids have attracted considerable interests. In spite of some studies on sol-gel derived titania with ionic liquids (Kaper et al., 2010; Chen, S. Y. et al., 2007; Ding et al., 2007), still the researches related to the enzymatic

sensor need to be improved. There are several studies related to sol-gel derived silica with ionic liquid that have been used in enzymatic electrochemical sensors and a few are depicted below. This study may open a new scope in sol-gel field for fabricating enzyme-based electrochemical sensor.

Liu et al. (2005b) developed a H_2O_2 biosensor based on $[C_4MIm][BF_4]$ sol-gel hybrid material, in which the cyclic voltammogram (Figure 2.9) displayed a well-defined oxidation and reduction peaks for Fc. After addition of H_2O_2, a typical voltammogram exhibited a sharp increase of the reduction current and a simultaneous decrease of the oxidation current. These phenomena showed that Fc could effectively transfer electrons from the surface of the GC electrode to the redox centre of HRP immobilised in the IL-silica gel.

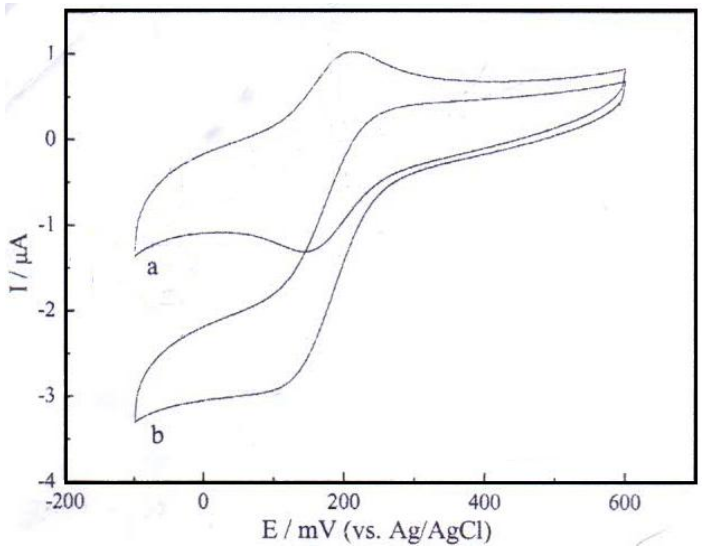

Figure 2.9: Cyclic voltammograms of the $[C_4MIm][BF_4]$ enzyme electrode at a scan rate of 50 mVs^{-1} in 0.05 M PBS (pH 7.0) containing (a) 0, (b) 0.02 mM H_2O_2 (Liu et al., 2005b)

Yang et al. (2007) have firstly incorporated a polyelectrolyte-functionalised ionic liquid (PFIL) into a sol-gel organic-inorganic hybrid material to immobilise glucose oxidase (GO_x) for glucose detection. As shown in Figure 2.10, the current as a

function of time was monitored at different glucose concentrations. The results showed that the current response at the GO_x/PFIL/sol-gel/GCE with the increase of glucose concentration is much higher compared to that at the GO_x/sol-gel/GCE. It seems that the PFIL enhanced the electrochemical glucose response because of its high ion conductivity, biocompatibility and fast substrate diffusion.

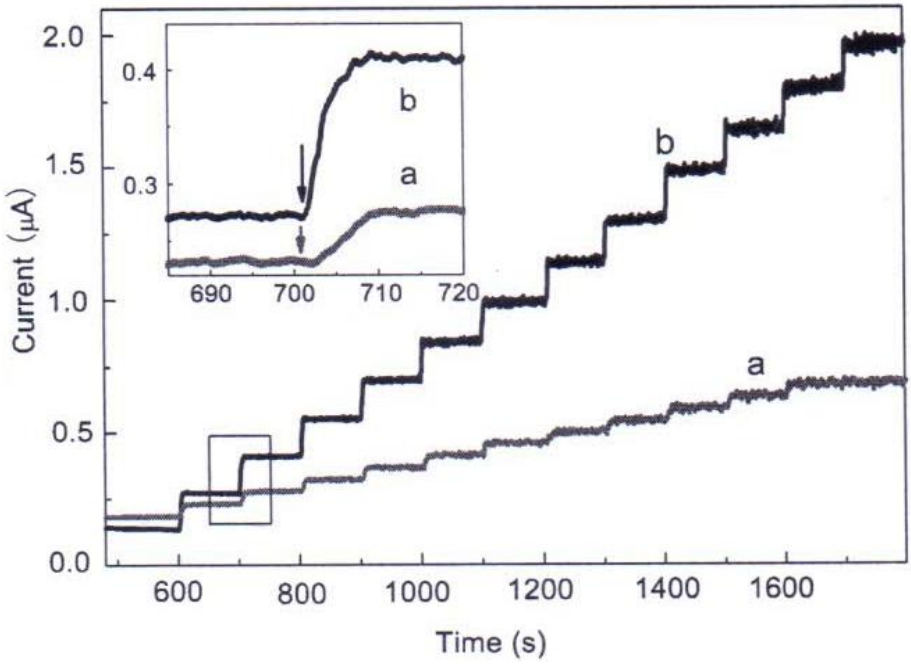

Figure 2.10: Steady-state response of (a) GOx/sol-gel/GCE and (b) GOx/PFIL/sol-gel/GCE with successive addition of glucose concentration (0.4 mmol/L each step). Applied potential: 1.05 V vs. Ag/AgCl (in saturated KCl). Insert displays a magnification of the second addition of glucose (Yang et al., 2007)

2.3 Analyte of interest

Hydrogen peroxide and glucose are two species, which have been targeted in this research. In this section, the introduction to this species, as well as the major applications for sensing them is going to be well described.

2.3.1 Hydrogen peroxide

Louis Jacque Thenard discovered hydrogen peroxide (H_2O_2) in 1818 (Campos-Martin et al., 2006). Each H_2O_2 molecule contains two bonded oxygen atoms, each with one hydrogen molecule attached (H-O-O-H). Due to intermolecular repulsion, H_2O_2 molecule has a skew chain structure as shown in Figure 2.11. H_2O_2 is a colourless liquid which is miscible with water and glycerine in all proportions. Pure H_2O_2 boils at 150.2 ^oC, freezes at -0.43 ^oC and has a density 1.44 gml^{-1} at 25 ^oC.

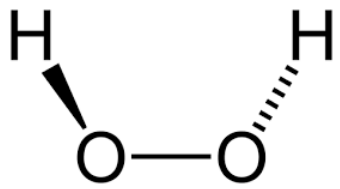

Figure 2.11: Skew chain structure of H_2O_2 molecule

H_2O_2 has wide applications in industrial process and plays a fundamental role as an intermediate in many biological reactions. The applications of H_2O_2 include food processes, textile industry, pulp and paper bleaching, pharmaceutical research, clinical laboratory, medical diagnostics, environmental analysis, antiseptic and disinfecting agents, beverage packages, cleaning product, minerals processes and biochemistry (Chen, S. et al., 2013). Moreover, H_2O_2 is involved in several biological events and intracellular pathways and is the by-product of some classic biochemical reactions catalysed by enzymes such as glucose oxidase, cholesterol oxidase, glutamate oxidase, lactate oxidase, alcohol oxidase, D-amino acid oxidase, lysine oxidase and oxalate oxidase (Chen et al., 2012).

In contrast, the biological researches showed that H_2O_2 has a close relationship with human metabolism and accumulation of H_2O_2 can cause serious injury to cells

through base modifications and strand breakage in genomic DNA (Roninson, 2003), damage to lysosomal membranes (Antunes et al., 2001) and induction of apoptosis (Geiser et al., 2004). Furthermore, H_2O_2 can play a damaging role in tumour occurrence (Valko et al., 2004). Hence, the development of simple, sensitive, selective and accurate determination methods of H_2O_2 is significant in environmental, industrial, clinical, pharmaceutical and biomedical analyses.

There are a number of determination techniques for H_2O_2, such as chemiluminescence (Xu et al., 2010), fluorescence (Abo et al., 2011), chromatography (Toyo'oka et al., 2003) and spectrophotometry (Nogueira et al., 2005). However, most of them exhibit their own technical drawbacks such as low sensitivity and selectivity, time consuming, susceptibility to interferences and complicated or expensive instrumentation (Chen, S. et al., 2013). With high sensitivity and selectivity, fast response, practicality, simplicity, low-cost and convenient operation, electrochemical sensors have been an optimal choice to actualise the accurate and sensitive detection of H_2O_2.

To date, different electrochemical methods have been studied for quantitation of H_2O_2 based on oxidation or reduction on modified electrode surfaces. Several electrochemical sensors have been prepared based on catalysis of immobilised bio-macromolecules, such as horseradish peroxidase (Wang & Wang, 2004), haemoglobin (Chen, S. et al., 2007) and myosin (Yang et al., 2006), towards H_2O_2 reduction. However, their uses have been limited due to some disadvantages of those biomaterials including high cost, instability and critical demand on the environmental condition. In order to attain the disadvantages of enzyme sensors, the development of non-enzyme H_2O_2 sensors has become a trend.

Non-enzyme H_2O_2 sensors have the advantage of simplicity, low cost, high sensitivity, fast response time and convenient operation. Recent advancement in fabrication of nanomaterials has offered new platforms for the non-enzymatic H_2O_2 sensing applications. The performances of these sensors are heavily dependent on the modified nanomaterials. Therefore, exploring new nanomaterials for the accurate and rapid detection of H_2O_2 is highly demanding. Herein, a non-enzymatic and an enzymatic based electrochemical sensor were developed for H_2O_2 detection.

2.3.2 Glucose

Glucose is a monosaccharide or simple sugar with formula $C_6H_{12}O_6$ or H-(C=O)-$(CHOH)_5$-H, as shown in Figure 2.12, whose five hydroxyl (OH) groups are arranged in a specific way along its six-carbon back. It is also known as dextrose or grape sugar. All forms of glucose are colourless and easily soluble in water, acetic acid, and only sparingly soluble in methanol and ethanol.

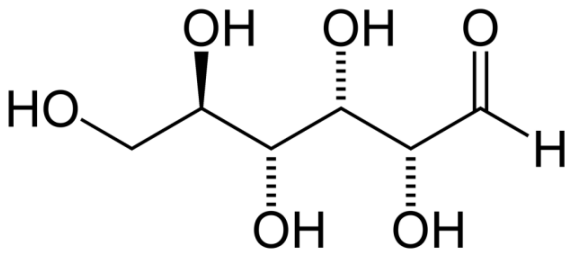

Figure 2.12: The chemical structure of glucose

Glucose is widely distributed in nature. The plants mainly obtain it through the photosynthesis and animals primarily through the diet. Glucose can also be obtained by decomposition through the hydrolysis of other carbohydrates such as starch, cellulose, maltose or glycogen. Industrially, it is obtained from starch with use of acids or by hydrolysis. It is used as a sweetener in food industry and also in leather and dyes

industries. In medicine, the glucose is given intravenously to treat dehydration or intravenous feeding.

Moreover, glucose is widely distributed in human blood and the increasing amount of glucose concentration in blood could lead to diabetes mellitus. The diabetes mellitus has become one of the major health concerns worldwide. This metabolic disorder caused from insulin deficiency and hyperglycaemia is reflected by blood glucose concentrations higher than the normal range of about 3.9 – 6.2 mM (empty stomach) or 3.9 – 7.8 mM (2 h after food) (Chen, C. et al., 2013). Therefore, it is vital to develop fast, stable and accurate technologies to detect glucose levels, not only in blood but also in other sources such as foods and pharmaceuticals.

To date, various technologies for glucose detection have been reported including high performance liquid chromatography method (Ma, C. et al., 2014), fluorophotometry (Jin et al., 2011), spectrophotometric assay (Kanchana et al., 2007), electro-chemiluminescence (Liu et al., 2008), electrochemical sensors or biosensors (Ciftci et al., 2014; Shua et al., 2014) and etc. Among them, the electrochemical methods were proven as effective approaches for the detection of glucose due to the simplicity of the instrumentation and operation.

Electrochemical methods, especially amperometric methods, have been widely utilised in glucose sensing. The enzymatic and the non-enzymatic sensing of glucose are the two main categories of electrochemical glucose sensing which have been extensively investigated and utilised. Although, commercially available glucose sensing devices are controlled by enzymatic systems, there has been growing research interest in enzyme-less glucose sensors since last decade, especially those based on nanomaterials.

The developing nanotechnology has brought new opportunities and ideas for the development of creative enzyme-less glucose sensors. The nanostructured electro-catalysts promise to solve the problems associated with enzyme-less electrode such as poor selectivity and surface fouling and nanomaterials based enzyme-less biosensors demonstrated higher sensitivity compared enzymatic systems (Si et al., 2013). In this regard, herein conducting polymer-metal oxide composite was developed for non-enzymatic glucose sensor.

CHAPTER 3

METHODOLOGY

In this chapter the experimental techniques and apparatus employed during the course of this research are outlined. The procedure for the experiments undertaken also detailed.

3.1 Reagents and apparatus

The chemicals and reagents used in this research together with the purities and sources are listed in Table 3.1. They all were used in the form they were received. The general apparatus for materials preparation and electrochemical measurements are given in Table 3.2.

Table 3.1: Reagents used for materials synthesis and sensor development

Chemicals	Grade	Supplier
1-butyl-3-methylimidazolium bis(trifluoromethylsulfonyl)imide	98%	Sigma-Aldrich
Acetone	99%	Sigma-Aldrich
Cobalt(II) chloride hexahydrate	97%	Sigma-Aldrich
D(+)-glucose	99.5%	Sigma-Aldrich
Ethanol, absolute	99%	J.Kollin Chemical
Fructose	99%	Sigma-Aldrich
Glycine	98%	Friendemann Schmidt
Horseradish peroxidase	-	Sigma-Aldrich
Hydrazine	51%	Acros Organic
Hydrochloric acid	98%	Sigma-Aldrich
Hydrogen peroxide	30%	Friendemann Schmidt
Hydrogen phosphate disodium	99%	Friendemann Schmidt

Table 3.1, continued.

Chemicals	Grade	Supplier
L(+)-ascorbic acid	99%	Sigma-Aldrich
Nafion 117 solution	~5% in a mixture of lower aliphatic alcohol and water	Fluka
Nickel(II) chloride hexahydrate	97%	Sigma-Aldrich
Potassium permanganate	99%	Acros Organic
Pyrrole	98%	Alfa Aesar
Sodium dihydrogen phosphate	99%	Friendemann Schmidt
Sodium hydroxide	99%	Sigma-Aldrich
Sucrose	99%	Sigma-Aldrich
Sulphuric acid	95.9%	R&M Chemicals
Tetraethylorthosilicate	98%	Sigma-Aldrich
Titanium(IV) isopropoxide	97%	Sigma-Aldrich
Uric acid	95.9%	Sigma-Aldrich

Table 3.2: Apparatus

Apparatus	Model or Specification	Manufacturer
Centrifuge	2420	KUBOTA
Electronic balance	AX224	Sartorius
Hot plate and magnetic stirrer	D-91126	Heidolph
Oven	FAC-100	PROTECH
Ultrasonicator	LUC-405	LabTech

3.2 Instrumentations

3.2.1 Field emission scanning electron microscopy and energy dispersive x-ray analysis

Field emission scanning microscopy (FESEM) is generally used in order to generate high-resolution images to visualise very small topographic details on the surface, entire or fractioned objects. The FESEM is usually equipped with an energy

dispersive x-ray analysis (EDX) system enable it to perform compositional analysis on specimens. FESEM Quanta FEG 450 (FEI, Hillsboro, OR, USA) is used to examine, document and analyse the surface morphology or near surface structure of materials and components. The PPy-Co and PPy-Ni samples for FESEM and EDX were prepared by dropping the suspension onto the Indium Tin Oxide (ITO) glass slide surface and then dried overnight at room temperature prior to analysis. Whereas, the Si-Ti/[C_4MIm][NTf_2] for FESEM and EDX were prepared by placing the samples over sticky conducting tape attaching to the FESEM sample holder prior to measurement.

3.2.2 X-ray powder diffraction

X-ray powder diffraction (XRPD) takes advantage of the coherent scattering of x-ray by crystalline materials to obtain a wide range of crystallographic information including orientation, composition, phase, crystallinity and particle size. The samples were characterised by using Cu-Kα irradiation with a PAN analytical EMPYREAN X-ray diffractometer operated at 40 kV and 100 mA. The samples were mounted on a sample holder and scanned from 10 º to 90 º at a speed of 3 º per minute.

3.2.3 Fourier Transform InfraRed

Fourier Transform InfraRed (FTIR) spectroscopy records the interaction of a single beam of undispersed IR radiation with a sample, measuring the frequencies at which the sample absorbs the radiation and the intensities of the absorptions. Chemical functional groups are known to absorb light at specific frequencies. Thus, the chemical structure can be determined from the frequencies recorded. FTIR spectra for synthesised materials were recorded on a Perkin-Elmer RX1 FTIR spectrometer using potassium

bromide (KBr) pellets at a weight ratio of sample: KBr = 1:10. All the samples were run in the spectral region range of 400 – 4000 cm^{-1}.

3.2.4 Thermogravimetric analysis

Thermogravimetric analysis (TGA) is effective for quantitative analysis of thermal reactions that are accompanied by mass changes such as dehydration, evaporation, decomposition and desorption. In this technique, the change in the weight of the sample is measured while the sample is heated at a constant rate. TGA was conducted on a thermal analysis instrument (Pyris TGA 400) with a heating rate of 10 ^{o}C/min under a nitrogen atmosphere at flow rate of 20 mL/min.

3.2.5 Brunauer-Emmett-Teller

Brunauer-Emmett-Teller (BET) analysis offers specific surface area evaluation of materials by nitrogen multilayer adsorption measured as a function of relative pressure using a fully automated analyser. The technique includes external area and pore area evaluations to determine the total specific surface area providing information of surface porosity and particle size. The surface area and porous properties of the synthesised composites were measured through the nitrogen adsorption-desorption analysis at 77 K on the surface area analyser (Quantachrome, Boynton Beach, FL, USA). The samples were previously degassed at 393 K overnight.

3.2.6 Carbon, Hydrogen and Nitrogen analysis

Carbon, Hydrogen and Nitrogen (CHN) analysis was performed on the Perkin Elmer CHNS/O 2400 Series II analyser. The samples were weighted between the ranges of 1.5 – 2.0 mg.

3.2.7 Electrochemical analysis

Electrochemical measurements were performed with an Autolab model PGSTAT-302N controlled by USB_IF030 (Metrohm Autolab) interface and card connected to a computer. Cyclic voltammetry (CV) and chronoamperometry measurements were performed in aqueous solutions of phosphate buffer solution (PBS, pH 7.0) and sodium hydroxide (NaOH, 0.1 M) for hydrogen peroxide and glucose detection, respectively. Chronoamperometry measurements were performed under N_2-saturated steady state and stirring condition, by applying a constant potential to the working electrode. After the background current became stable (about 100 s), a subsequent addition of prepared target analyte solution was applied and the current was measured.

A standard three-electrode electrochemical cell configuration was employed for all electrochemical experiments. This consists of a working electrode, a reference electrode and a counter/auxiliary electrode as shown in Figure 3.1. The working electrode used was a highly polished glassy carbon disk supported into a solvent-resistant CTFE plastic body (7.5 cm length x 6 mm OD) and the electrode disk diameter is 3.0 mm, called glassy carbon electrode (GCE). Prior to each experiment, the GCE was carefully polished with 1.0 μm, 0.3 μm and 0.05 μm alumina powder on polishing

cloth and rinsed thoroughly with distilled water. Then the electrode was sonicated in acetone/ethanol (1:1, v/v) mixture for 3 minutes and finally rinsed with distilled water. The counter electrode consisted of high surface area platinum (Pt) wire with 7.5 cm in length and regularly burnished with silicon carbide based abrasive paper, smoothed, cleaned and sonicated in distilled water. The reference electrode was a saturated calomel electrode (SCE).

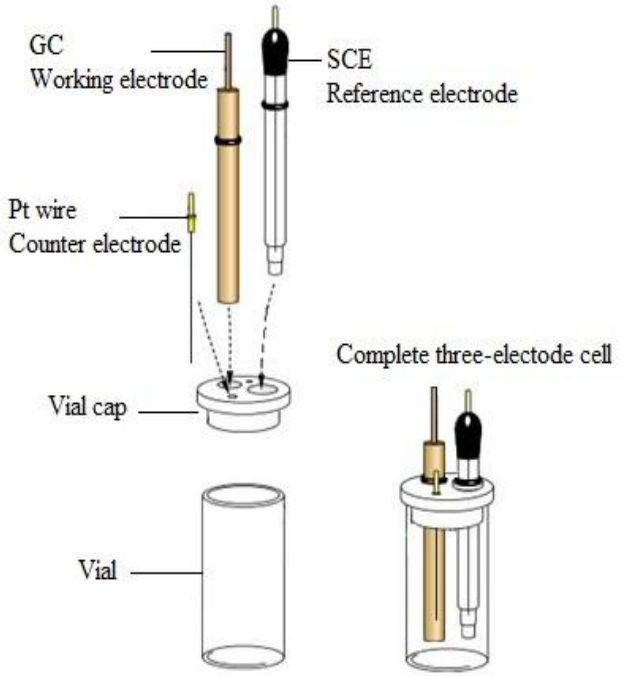

Figure 3.1: A schematic of the three-electrode cell used for electrochemical measurements

3.3 Conducting polymer/metal oxide composite/nanocomposite

3.3.1 Synthesis of PPy-metal oxide composite/nanocomposite

1 mL of 0.1 M metal-hexahydrate solution was added into 30 mL of 7 M NaOH solution and the reaction was continuously stirred at 500 rpm with a mechanical stirrer at room temperature to obtain a homogenous solution. Then, 0.5 mL of pyrrole

monomer was added. After 30 min, the solution colour turned from light to dark, which indicates the completion of polymerisation. Then, 0.01 mL hydrazine monohydrate was injected into the reaction mixture to accomplish the solvothermal reduction and the reaction temperature increased to 60 ºC at 1.5 $^{o}Cmin^{-1}$ and was continued for another 60 min. Finally, the reaction mixture was centrifuged at 4000 rpm for 10 min to separate the PPy-metal oxide composites from the solution, followed by drying in a vacuum oven at 60 ºC for 24 h. Besides, the whole procedure was repeated in the absence and with different content of pyrrole monomer to understand the effect of PPy.

3.3.2 Preparation of modified GCE with synthesised composite materials

1 mg of the synthesised PPy-metal oxide composites were dispersed into 1 mL of distilled water and 10 μL of Nafion using ultra-sonication until a homogenous suspension was obtained. Then, 10 μL of the homogenous suspension was dropped on to the surface of a polished GCE and dried at room temperature.

3.4 Si-Ti/$[C_4MIm][NTf_2]$ composites

3.4.1 Synthesis of Si-Ti mixed oxide with $[C_4MIm][NTf_2]$

In order to obtain the desired composition of the product, since the hydrolysis rate of the tetraethylorthosilicate (TEOS) is smaller than titanium(IV) isopropoxide (TTIP), TEOS was partially hydrolysed in absolute ethanol (EtOH) being stirred in the presence of 0.1 M aqueous hydrochloric acid (HCl). The molar ratio for TEOS: EtOH: HCl was 1: 8: 0.05. After 1 h stirring at room temperature, the solution of TTIP (TEOS: TTIP = 1:1 molar ratio) in absolute EtOH (TTIP: EtOH = 1:20 molar ratio) was added

and a clear aqueous sol was obtained under vigorous stirring. The $[C_4MIm][NTf_2]$ was then added into the sol and stirred until a homogenous solution was obtained. Various weight percentages (wt%) of $[C_4MIm][NTf_2]$ to TEOS were selected to investigate the effect of ionic liquid content on the gel. Then, the sols were left for 24 h at room temperature. After that, the samples were placed in an oven at 80 ºC to remove water and solvent. For nitrogen adsorption-desorption analysis, the entrapped $[C_4MIm][NTf_2]$ was extracted by refluxing the products in ethanol and acetone for 6 h. The subsequent products were then dried at 80 ºC. The final products were white monoliths.

3.4.2 Preparation of the mediated enzyme modified GCE

The mediated horseradish peroxidase (HRP) electrode was prepared as follows: 10 μL of ferrocene (Fc) dissolved in ethanol solution (7.5 mg/1 mL) was dropped on the cleaned surface of GCE and allowed to dry at room temperature. Then, 1 mg of HRP was dissolved in 50 μL of 0.05 M phosphate buffer solution (PBS) (pH 7.0) and 20 μL of the mixture was added to 20 μL of the silica-titania/$[C_4MIm][NTf_2]$ sol. The above mixture was hand-mixed thoroughly and a homogenous solution was obtained. Then, 10 μL of the new mixture was dropped on the surface of Fc/GCE and allowed to dry at 4 ºC for 24 h. Before the electrochemical measurement, the mediated enzyme electrodes were washed with 0.05 M PBS (pH 7.0). All the enzyme electrodes were washed thoroughly with 0.05 M PBS (pH 7.0) and stored at 4 ºC in a dry state unless otherwise specified.

3.5 Method Validation

3.5.1 Linearity

Linear range calibration curves were plotted in certain concentration ranges of target analyte. After the preparation of different working solutions containing standards of target analyte, the calibration curve was obtained by plotting the current on y-axis against concentration of target analyte on x-axis. The concentrations of calibration standards were analysed and the linearity was evaluated by the correlation coefficient (R^2).

3.5.2 Limit of Detection and Limit of Quantification

There are number of terms that have been used to define Limit of Detection (LOD) and Limit of Quantification (LOQ). In general, the LOD described as the lowest concentration of an analyte is a sample that can be detected but not necessarily quantified under the stated conditions of the test (Shrivastava & Gupta, 2011). The LOQ is the lowest concentration of an analyte in a sample that can be determined with acceptable precision and accuracy under the stated conditions of the test (Shrivastava & Gupta, 2011). The LOD and LOQ in this thesis were estimated by using the following Eq. 3.1 (Shrivastava & Gupta, 2011).

$$\mathrm{LOD/LOQ} = \mathrm{F} \times \mathrm{SD/b} \quad \textbf{(3.1)}$$

Where,

F: signal-to-noise ratio of 3 and 10 for LOD and LOQ, respectively

SD: Standard deviation of blank solution

b: Slope of the regression line

3.5.3 Precision

The precision of the sensor was evaluated by replicate analysis of the real sample containing target analyte. It was evaluated at different concentration levels and the precision was estimated by relative standard deviation (RSD) using formula Eq. 3.2, where SD is standard deviation (Eq. 3.3), x is the result of every measurement and $\bar{x}$ is mean of the measurements.

$$\text{Relative standard deviation (RSD)} = \frac{\text{SD}}{\bar{x}} \times 100\% \quad \textbf{(3.2)}$$

$$\text{Standard deviation (SD)} = \sqrt{\frac{\sum(x-\bar{x})^2}{n-1}} \quad \textbf{(3.3)}$$

3.5.4 Recovery

The average recoveries for target analyte were evaluated at different concentration levels with each repeating four times. Recoveries were evaluated using the formula Eq. 3.4. Thus, the concentration of measured samples compared to the one of reference standards prepared, % recovery could be calculated.

$$\text{Recovery, \%} = \frac{\text{Calculated concentration of target analyte in sample}}{\text{Calculated concentration of standard added}} \times 100 \quad \textbf{(3.4)}$$

3.6 Real sample analysis

The determination target analyte in real samples was performed on the modified sensor using standard addition method (Kelley et al., 1992). Moreover, the standard potassium permanganate titration procedure (Kenkel, 2003) and UV-Vis spectroscopy technique were used as a reference for checking the hydrogen peroxide and glucose sensors accuracy, respectively.

3.6.1 Standard addition method

The procedure for standard addition is to add 1 mL of the sample into six separate volumetric flasks. The first flask is then diluted to volume with the aqueous solution up to 5 mL. Standard analyte solution is then added to increasing volumes to the subsequent flasks (except first flask) and each flask is then diluted to volume with the aqueous solution up to 5 mL. The instrument response is then measured for all of the diluted solutions and the data is plotted with volume standard added in the x-axis and current response in the y-axis. These steps are repeated four times for different concentrations of standard solution of target analyte. Linear regression as shown in Figure 3.2, is performed and the slope (m) and y-intercept (b) of the calibration curve are used to calculate the concentration of target in the sample. From the linear regression:

$$\text{Current (A)} = \text{m}(\text{V}_{\text{SD}}) + \text{b} \qquad \textbf{(3.5)}$$

Conceptually, if the curve starts where the current response is zero, the volume of analyte standard solution (V_{SD}) from that point to the point of the first solution on the curve (x = 0) contains the same amount of target as the sample. So,

$$V_S \times C_S = V_{SD} \times C_{SD} \quad \textbf{(3.6)}$$

Where,

V_S: Volume of the sample

V_{SD}: Volume of the analyte standard solution

C_S: Concentration of the sample

C_{SD}: concentration of analyte standard solution

Combining Eq. 3.5 and Eq. 3.6 and solving for concentration of sample results in:

$$C_S = \frac{bC_{SD}}{mV_S} \quad \textbf{(3.7)}$$

And one can then calculate the concentration of analyte in the sample from the slope (m) and intercept (b) of the standard addition calibration curve.

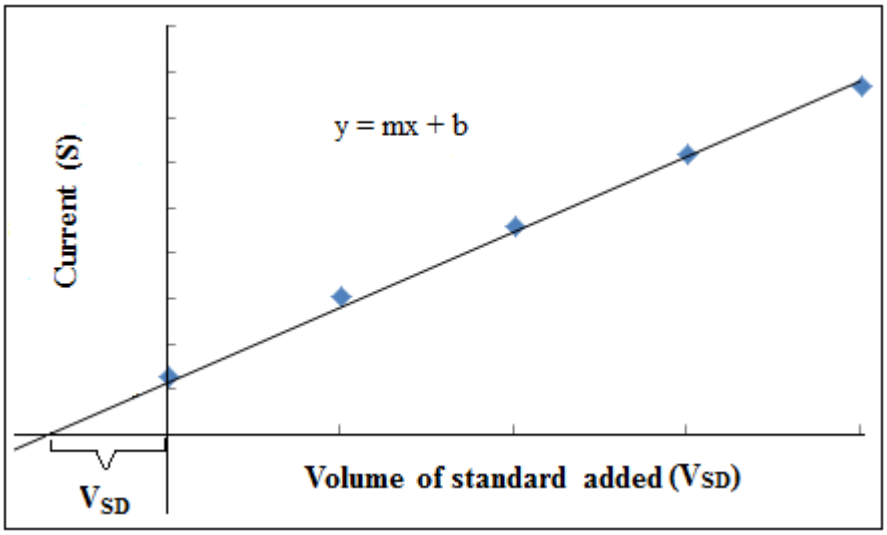

Figure 3.2: Linear regression

3.6.2 Titrimetric determination of H_2O_2 in real sample

A burette was filled with 0.025 M potassium permanganate ($KMnO_4$) solution until the liquid level is just above the zero mark. The stopcock on the burette was open to allow air bubbles to escape from the tip and then closed. The precise level of the solution was recorded (initial volume of $KMnO_4$ solution). 1 mL of real sample (contact lens cleaning solution purchased from market) was added into 25 mL of deionised water in an Erlenmeyer flask. Then, 5 mL of 6 M sulphuric acid was added into the solution. Gently, the flask was swirled to mix the solution. After that, this solution was titrated drop-by-drop with $KMnO_4$ solution while swirling the flask until a light pink colour persists. The final volume of the $KMnO_4$ solution was recorded. The Eq. 3.8 below represents the chemical equation for titration of $KMnO_4$. This procedure was repeated four times by adding standard stock solution of H_2O_2 (0.05, 0.5, 5 and 50 mM) into the real sample solution in the flask, respectively.

$$2KMnO_4(aq)+5H_2O_2(aq)+3H_2SO_4(aq)\rightarrow 2MnSO_4(aq)+K_2SO_4(aq)+5O_2(g)+8H_2O(l) \quad \textbf{(3.8)}$$

3.6.3 Ultraviolet-visible (UV-Vis) spectroscopy

Ultraviolet-visible (UV-Vis) spectroscopy is a very useful analytical technique as it can be used to determine the amount of substance present in a sample and also to identify some chemical species. For the purpose of this study, UV-Vis spectroscopy was employed using a UV-Vis spectrophotometer (Shimadzu, Japan) to investigate the concentration of glucose in solution. For each measurement, a quartz crystal cuvette with a length of 1 cm, containing 1.0 mL of the sample solution, was used. The wavelength was scanned from 190 to 400 nm to determine the presence of glucose.

CHAPTER 4

RESULTS AND DISCUSSION

In this chapter, the development and study of composite and nanocomposite materials for non-enzymatic and enzymatic based sensor were carried out. In the first section of this chapter, the results related to the characterisations of polypyrrole coated cobalt nanocomposite and its development towards non-enzymatic H_2O_2 detection have been discussed. Moreover, in the second section, the characterisation of polypyrrole-nickel composite and fabrication for the non-enzymatic glucose detection were investigated. The results of Si-Ti/RTIL and its development as enzymatic sensor to detect hydrogen peroxide were presented in the third section of this chapter.

4.1 Polypyrrole coated cobalt (PPy-Co) nanocomposite for hydrogen peroxide detection

The conducting polymer-metal oxide nanocomposite formed by metal oxide salts dispersed in electrically conducting polymers has received much attention for sensor applications in recent years. PPy is one of the conducting polymers that have been widely used to make nanocomposite with metal oxide due to its good environmental stability, facile synthesis and higher conductivity. Moreover, these nanocomposites are expected to display new properties over their single component making them more potential for non-enzymatic sensor applications. On the other hand, cobalt oxide was selected for this study, because of its unique fundamental and electrochemical properties. There are few studies on cobalt oxide nanostructure with conducting polymer. However, most of them are related to the enhancement of

electrocatalyst towards oxygen reduction reaction (Kumar et al., 2013; Yuan, 2013; Martínez et al., 2010; Olson, 2010) and only some of these studies were focused on sensor applications (Patois et al., 2013; Yu et al., 2013).

Therefore, in this section, the development and study of a new nanocomposite comprising of polypyrrole and cobalt oxide for the enhanced detection of H_2O_2 are presented. After synthesis, the structure and morphology of PPy-Co nanocomposites and H_2CoO_2 particles in the absence of pyrrole monomer were characterised by using various analytical techniques. Then, these synthesised nanocomposites were fabricated onto GCE in order to examine the sensing properties towards H_2O_2. Several factors influencing the electrocatalytic performances of the proposed non-enzymatic sensor were further improved. Besides, the linear range, detection limit, anti-interference performance, stability and reproducibility of the developed non-enzymatic H_2O_2 sensor also were evaluated. Finally, the PPy-Co nanocomposite modified GCE was successfully applied to a contact lens cleaning solution real sample.

4.1.1 Fourier Transform InfraRed

The Fourier Transform InfraRed (FTIR) spectra of the PPy-Co nanocomposite, PPy and H_2CoO_2 nanoparticles are shown in Figure 4.1. The main FTIR bands detected in the 400 – 4000 cm^{-1} region with assignments are summarised in Table 4.1. The PPy-Co nanocomposite spectrum (Figure 4.1 A) shows the characteristic peaks of PPy, but these peaks have a shift compared to the pure PPy which indicates that an interaction between the polymer backbone and the cobalt nanocomposites has occurred (Zhao et al., 2011) and similar characteristics of FTIR were recently obtained by Wang et al. (2015). In the PPy-Co nanocomposites spectrum, a large and descending baseline appears in the

spectral region of 1600 – 2500 cm^{-1} attributed to the free-electron conduction in conducting polymers (Gnanakan et al., 2009). Besides, the peaks at 3011.78 cm^{-1} and 1684.99 cm^{-1} can be attributed to the N-H bond and N=C bond, respectively, and the characteristic of a typical PPy ring vibration peak at 1376.26 cm^{-1} further supported the occurrence of PPy. Besides, in the FTIR spectrum of PPy-Co nanocomposite, the presence of cobalt nanoparticle was confirmed with the peak at 561.07 cm^{-1} which was related to the vibration of the Co-O bond (Estepa & Daudon, 1997). Therefore, it has been concluded that the polymerisation between pyrrole monomers was completed and nanocomposites of PPy-Co were formed.

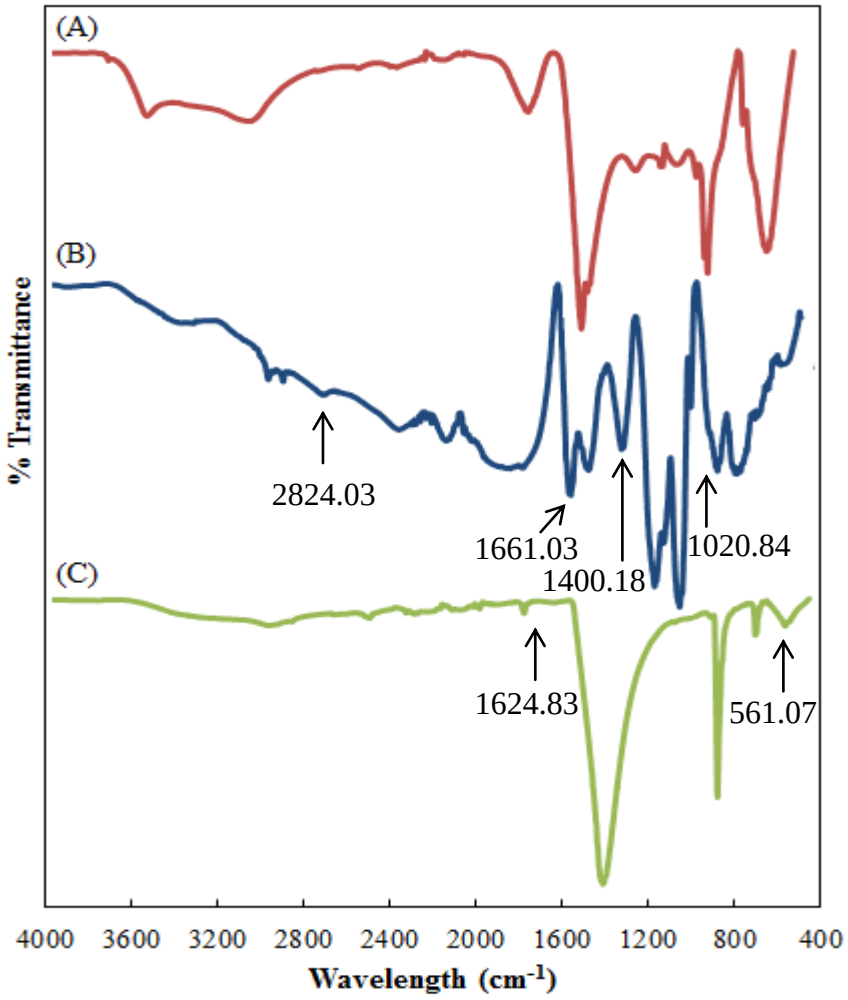

Figure 4.1: FTIR spectra of the (A) PPy-Co nanocomposites; (B) synthesised PPy in the absence of Co^{2+} and (C) H_2CoO_2 particles synthesised in the absence of pyrrole monomers

Table 4.1: The maximum wavenumber of PPy-Co nanocomposites, PPy and H_2CoO_2 particles

Mode	Wavenumber (cm^{-1})		
	PPy-Co nanocomposites	PPy	H_2CoO_2 particles
(C-H)	2811.78	2824.03	-
(C-N=C)	1684.99	1661.03	-
PPy ring	1376.16	1400.18	-
=C-N	1018.40	1020.84	-
Co-O	560.19	-	561.07
C=O	-	-	1624.83

4.1.2 Thermogravimetric analysis

A good thermal stability of the conducting polymer-metal oxide nanocomposites is essential for many practical applications. Therefore, the thermal stability of synthesised PPy-Co nanocomposites was investigated by the thermogravimetric analysis (TGA) in nitrogen atmosphere. Figure 4.2 shows the TGA spectra of the PPy-Co nanocomposites, PPy and H_2CoO_2 particles in the absence of pyrrole monomer. The thermal behaviour of the PPy-Co nanocomposite involved only a two-steps process. In the first step, thermal changes can be observed due to the water loss and the second step decomposition is might account for the content of PPy in the composite. The second degradation step of the PPy-Co nanocomposites took place at temperature between 200 ºC and 300 ºC with low weight loss about 0.36%. These results indicated that PPy-Co nanocomposite possesses a good thermal stability as compared to pristine PPy with weight loss of 87.94%. Apart from that, the high stability of PPy-Co nanocomposite could be due to the addition of H_2CoO_2 particles to the PPy, which was induced the relatively compact structure of PPy (Das et al., 2013).

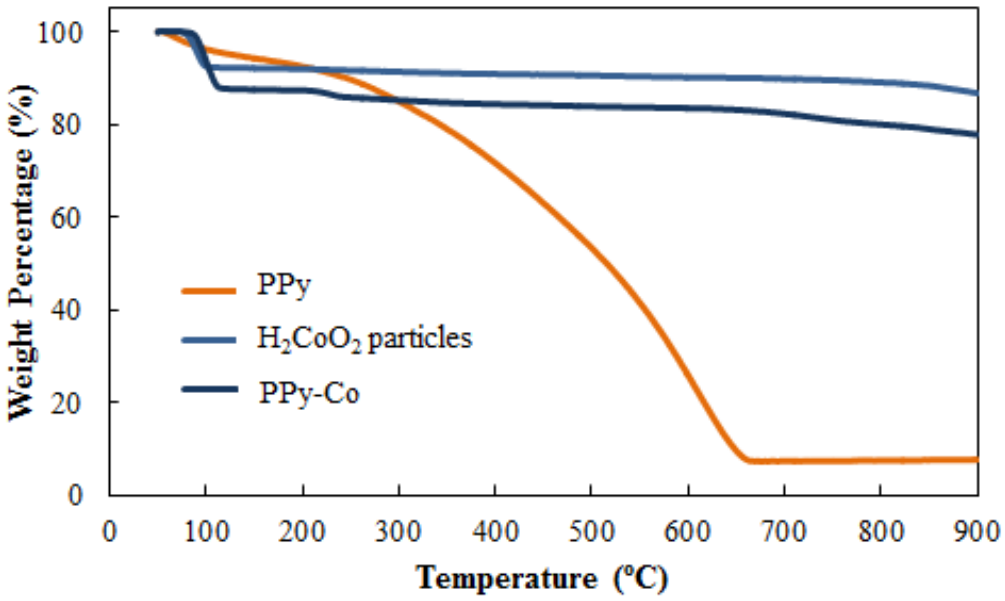

Figure 4.2: TGA spectra of the H_2CoO_2 particles synthesised in the absence of pyrrole monomer, synthesised PPy in the absence of Co^{2+} and PPy-Co nanocomposites

4.1.3 Field emission scanning electron microscopy and energy dispersive x-ray analysis

The surface morphology of PPy-Co nanocomposites and H_2CoO_2 particles in the absence of pyrrole monomer was investigated using field emission scanning electron microscopy (FESEM). The obtained FESEM results are presented in Figure 4.3. The H_2CoO_2 particles synthesised in the absence of pyrrole monomer led to a morphology with a flake-like structure as shown in Figure 4.3 (C) and (D) with low (15 000 x) and high (80 000 x) magnification, respectively. Nevertheless, this surface morphology structure did not remain any longer after forming nanocomposite with PPy. The FESEM images obtained for PPy-Co nanocomposites as shown in Figure 4.3 (A) and (B) with low (8 000 x) and high (60 000 x) magnification respectively indicated a clear difference in the surface morphology structures compared to H_2CoO_2 particles. These images showed that a layer of PPy was covered with cobalt nanocomposites, which can be called ‘a bouquet of cobalt flower cover with a bunch of grassy polypyrrole’. The

effect of pyrrole monomers on the morphology of nanocomposites can be confirmed by these results.

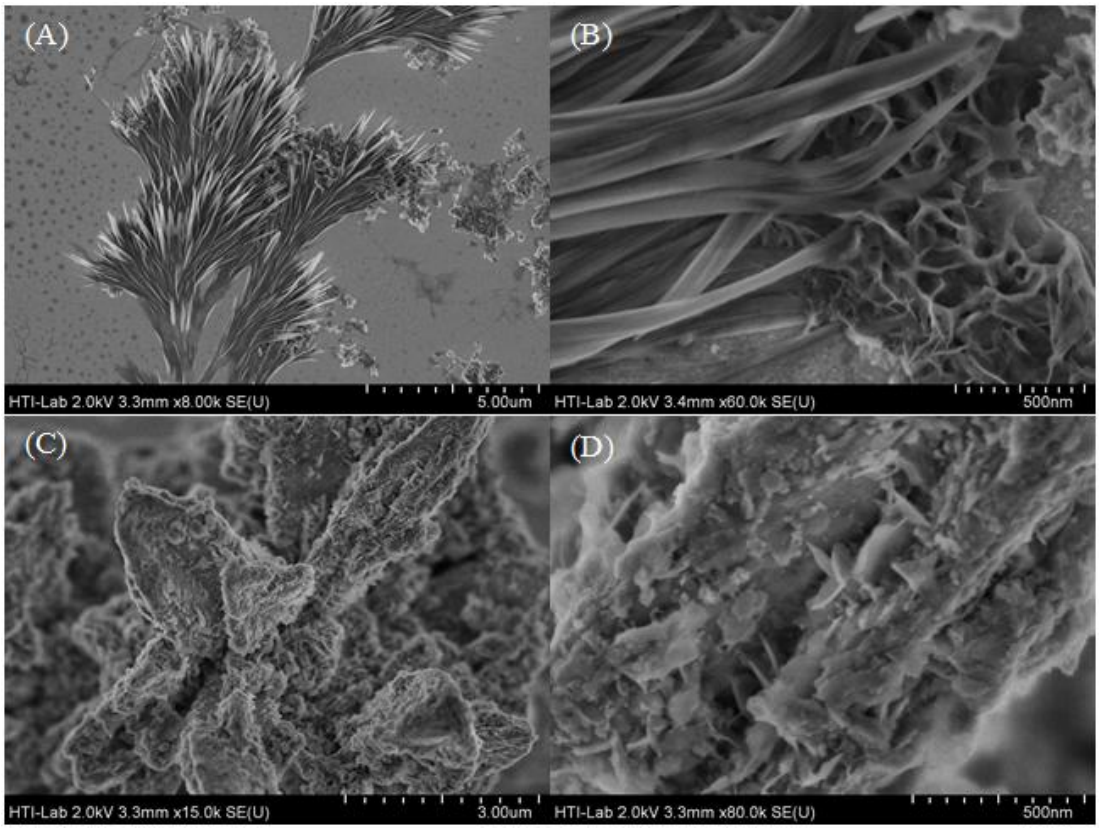

Figure 4.3: FESEM images of the PPy-Co nanocomposites (A and B) and H_2CoO_2 particles in the absence of pyrrole monomer at lower and higher magnification

It has been seen that the surface morphology of micro/nanostructure is strongly influenced by the preparation conditions including the concentration of dopant, oxidant, monomer and molar ratio of the dopant and oxidant to monomer as well as the reaction temperature, time and stirring (Varshney et al., 2012). For example, Chougule et al. (2013) showed that the surface morphology of PPy-ZnO nanohybrid film can be changed by varying the molar ratio of camphor sulfonic acid into PPy. Whereas, Ohlan et al. (2010) indicated that in the case of PEDOT-$BaFe_{12}O_{19}$, core-shell structure can be designed by the dodecyl benzene sulfonic acid. In the present study, the PPy-Co nanocomposites were synthesised at different pyrrole monomer contents in order to

investigate the effect of PPy on the structure and surface morphology of the nanocomposites. Figure 4.4 shows the FESEM images of the PPy-Co nanocomposites with different contents of pyrrole monomer. A thick coating of PPy onto cobalt was observed for the 0.7 ml of pyrrole monomer content as presented in Figure 4.4 (A). This may be due to the presence of higher amount of pyrrole monomer during the polymerisation reaction which gives rise to clusters of pure PPy domains. When the content of pyrrole monomer decreased to 0.3 ml, the morphology of PPy-Co nanocomposites was rough and some of the cobalt surfaces remained uncovered as shown in Figure 4.4 (C). This can be justified as the lesser availability of pyrrole monomer in the reaction mixture during polymerisation. However, for 0.5 ml of pyrrole monomer, the PPy-Co nanocomposites gave a clear and well-structured morphology (Figure 4.4 B). Moreover, it indicated larger surface area of PPy-Co nanocomposites which is added advantage for sensor fabrication. It is also believed that PPy with different contents presented surface property and reduction potential differences which leading to changes in the size and morphology of cobalt nanoparticles.

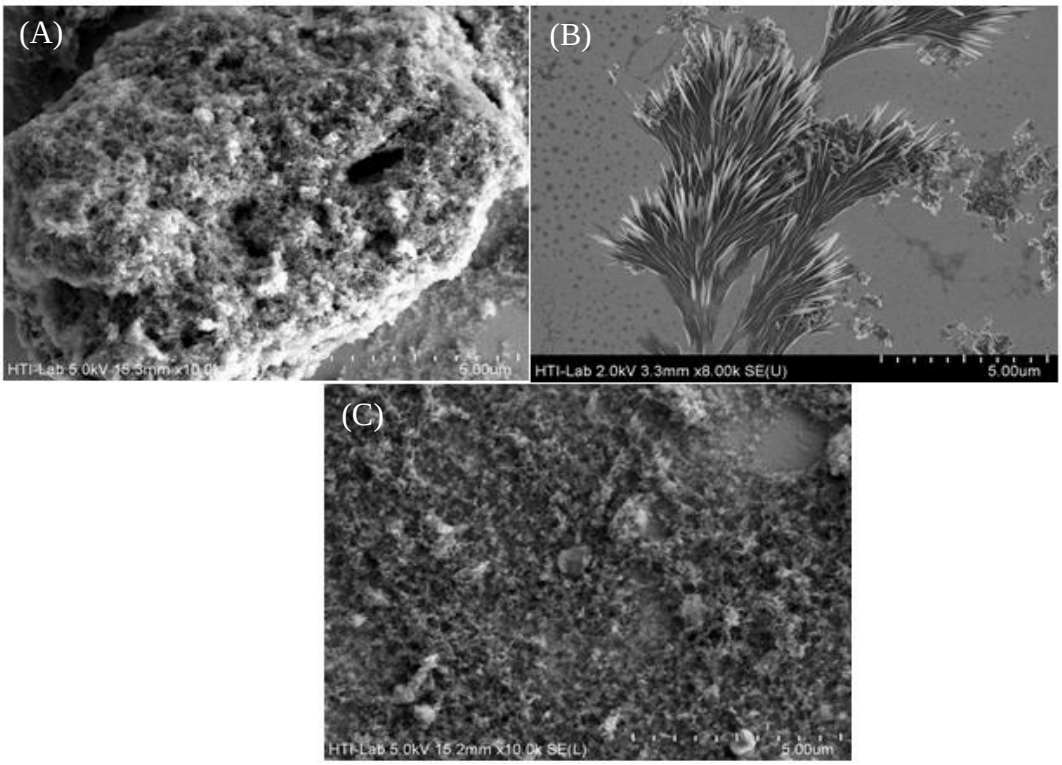

Figure 4.4: FESEM images of the PPy-Co nanocomposites with different content of PPy: 0.7 ml (A) with 10 kx; 0.5 ml (B) with 8 kx; and 0.3 ml (C) with 10 kx

On the other hand, the energy dispersive x-ray (EDX) measurements were also carried out on the PPy-Co nanocomposites, as shown in Figure 4.5. EDX area mapping results confirmed the nanocomposites composition of N, C, Co and O. The spot 1 in the Figure 4.5 showed the signal of Carbon (C) at ~ 0.45 keV, Nitrogen (N) at ~ 0.35 keV, Oxygen (O) at ~ 1.50 keV and Cobalt (Co) at ~ 2.75 keV as the characteristic peaks of PPy-Co nanocomposites. The signal of Indium (In) at ~ 0.30 keV and ~ 0.65 keV which can be found in the spot 2 indicated the ITO glass slide surface. These results further confirmed the formation of PPy-Co nanocomposites.

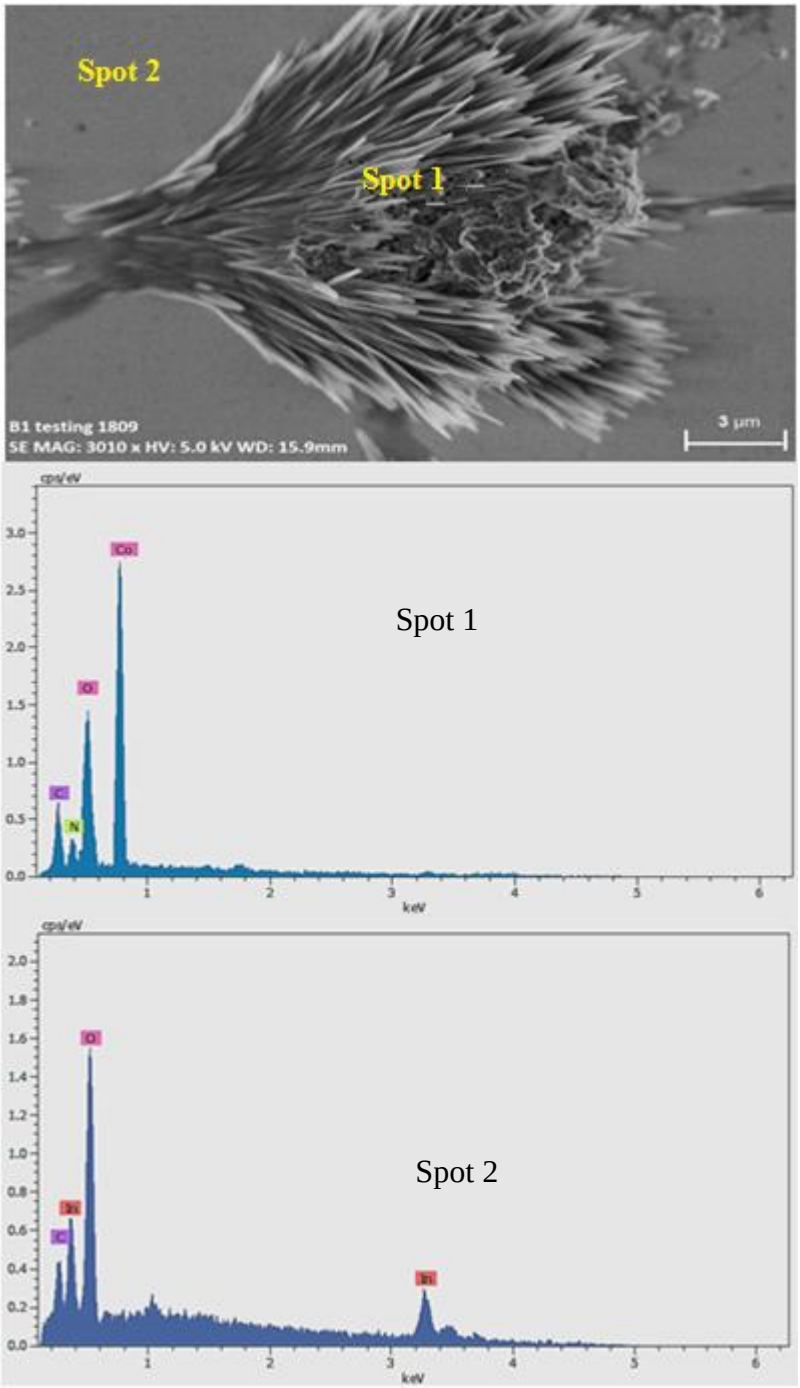

Figure 4.5: FESEM-EDX images of the PPy-Co nanocomposites

4.1.4 X-ray powder diffraction

Figure 4.6 shows the x-ray powder diffraction (XRPD) patterns of the PPy-Co nanocomposites and H_2CoO_2 particles synthesised in the absence of the pyrrole monomers. As seen, the sharp diffraction peaks of H_2CoO_2 particles (19.9 º, 36.5 º, 38.9 º, 50.7 º, 58.1 º, 61.6 º, 69.2 º) indicate that the presence of CoO particles with good

crystallinity and broad diffraction peaks indicate the nano size nature of the particles (Kundu et al., 2013). Hence, it is believed that in the absence of the pyrrole monomer, the product reaction between $CoCl_2.H_2O$ and NaOH is H_2CoO_2. While, for the PPy-Co nanocomposites, three major peaks at 43.5 º, 50.5 º and 74.5 º in the range of 40 º- 80 º can be assigned to the diffraction from the {111}, {200} and {220} planes of cobalt metal, respectively. A broad, amorphous diffraction peak, which appears in the range of 10 º- 30 º in the XRPD pattern of PPy-Co nanocomposites can be attributed to the scattering of the interplanar spacing between the bare polymer chains (Seo et al., 2002). The XRPD results confirmed that Co^{2+} (cobalt(II) chloride) is reduced to Co in the presence of pyrrole monomers and is protected by the PPy. The reduction of some Co^{2+} cation and the growth of CoO are related to the oxidation of pyrrole monomers and the protection of synthesised CoO by polymerised PPy, respectively. These XRPD results further confirmed the obtained FESEM results of PPy-Co nanocomposites. It can be concluded that nanocomposites of PPy-Co were successfully synthesised.

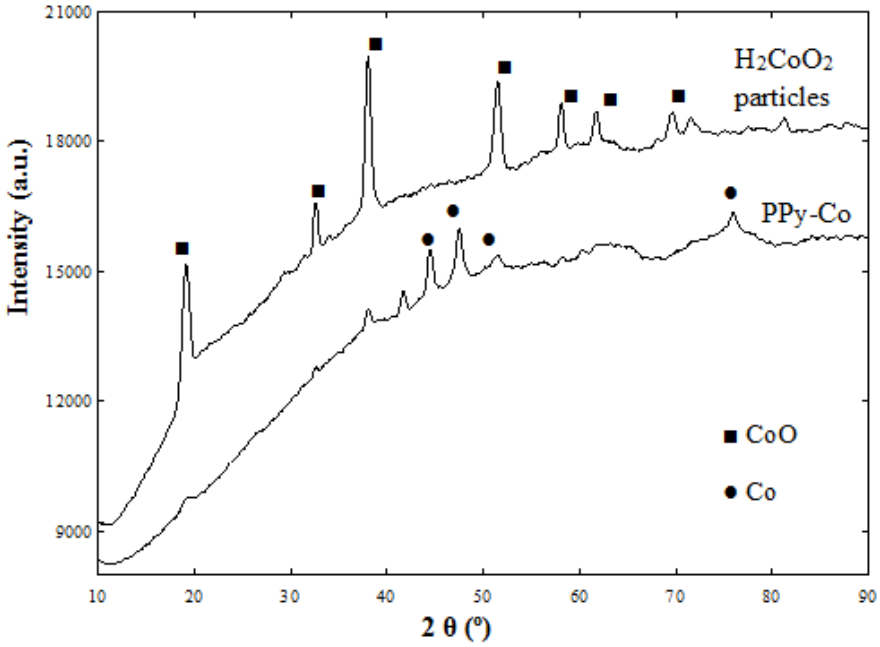

Figure 4.6: XRPD patterns of the PPy-Co nanocomposites and H_2CoO_2 particles synthesised in the absence of pyrrole monomers

4.1.5 Electrochemical studies of the PPy-Co nanocomposites for H_2O_2 detection

The electrocatalytic oxidation of the PPy-Co nanocomposites was investigated with the cyclic voltammetry and the results are shown in Figure 4.7 in 0.2 M PBS (pH 7.0). The bare GCE exhibited no electrochemical response in the absence of H_2O_2 (Figure 4.7 red-lined curve), while a typical oxidation peak was observed for PPy-Co nanocomposites coated GCE in the potential range from 0.4 V to 1.15 V (Figure 4.7 blue-lined curve). On the other hand, after adding 3 mM H_2O_2, the oxidation current of PPy-Co nanocomposites coated GCE greatly increased due to the catalytic oxidation of H_2O_2, while the reduction peak largely disappeared (Figure 4.7 purple-lined curve). The decrease of overvoltage and increased peak current of H_2O_2 confirmed that PPy-Co nanocomposites have high catalytic ability for H_2O_2 oxidation (Salimi et al., 2007). For bare GCE, it yet remains the same condition with no electrochemical response (Figure 4.7 green-lined curve). This shows that PPy-Co nanocomposites are suitable as a mediator to shuttle the electron between the H_2O_2 and working electrode and facilitate electrochemical regeneration following the electron exchange with H_2O_2. The following catalytic reactions (Eq. 4.1) and (Eq. 4.2) describe the reaction sequence for the oxidation of H_2O_2 by the PPy-Co nanocomposites.

$$\mathrm{PPy-Co} \rightarrow \mathrm{PPy-CoO} + 2e^- \text{ (under applied positive potential)} \quad \textbf{(4.1)}$$

$$\mathrm{PPy-CoO} + \mathrm{H_2O_2} \rightarrow \mathrm{PPy-Co} + \mathrm{O_2} + \mathrm{H_2O} \quad \textbf{(4.2)}$$

In a possible catalytic mechanism, Co is electrochemically oxidised to Co^{2+} under positive potential and the formed Co^{2+} can catalyse H_2O_2 oxidation to form O_2 and H_2O.

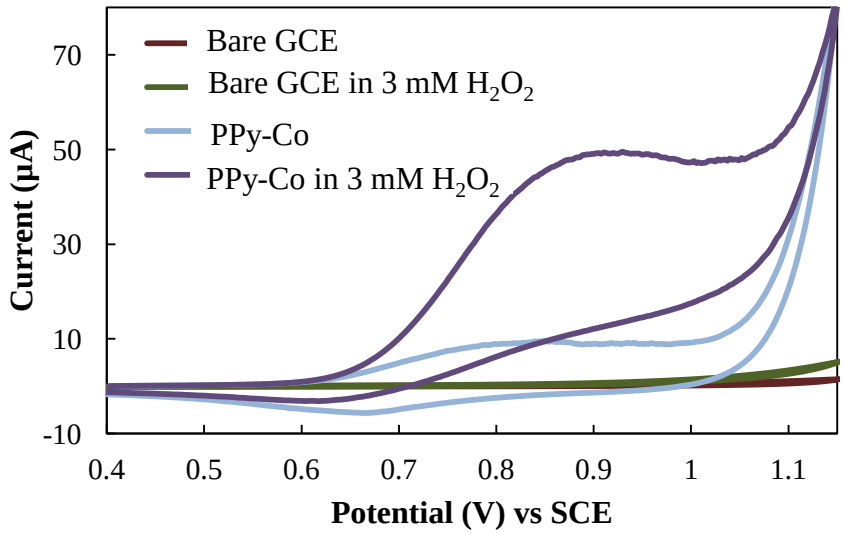

Figure 4.7: Cyclic voltammograms of the bare GCE and PPy-Co nanocomposites coated GCE in the absence and presence of 3 mM H_2O_2 in PBS (pH 7.0) at scan rate 50 mVs^{-1}

Influence of the supporting materials

The electrocatalytic oxidation of each supporting material including H_2CoO_2 particles, nafion and polypyrrole towards 3 mM H_2O_2 in PBS (pH 7.0) was investigated with the cyclic voltammetry and the results are shown in Figure 4.8. It was noticeable that, no electrocatalytic oxidation current towards H_2O_2 was observed on polypyrrole coated GCE without Co^{2+} (Figure 4.8 orange-lined curve), which emphasises the importance of CoO. Whereas, H_2CoO_2 particles coated GCE produced an obvious oxidation peak (Figure 4.8 red-lined curve) suggesting an excellent catalytic activity of H_2CoO_2 particles for oxidation of H_2O_2. One can notice that the oxidation peak current of H_2O_2 on PPy-Co nanocomposites coated GCE was significantly higher than that of H_2CoO_2 particles coated GCE. The effect of nafion on the electrochemical response (Figure 4.8 green-lined curve) could be ignored since nafion was only employed as an adhesive to immobilise the nanocomposite on the surface of GCE. Thus, the increased current on PPy-Co nanocomposites coated GCE obviously benefited from the high

specific area and good conductivity of PPy that could facilitate electrochemical deposition of H_2CoO_2 particles.

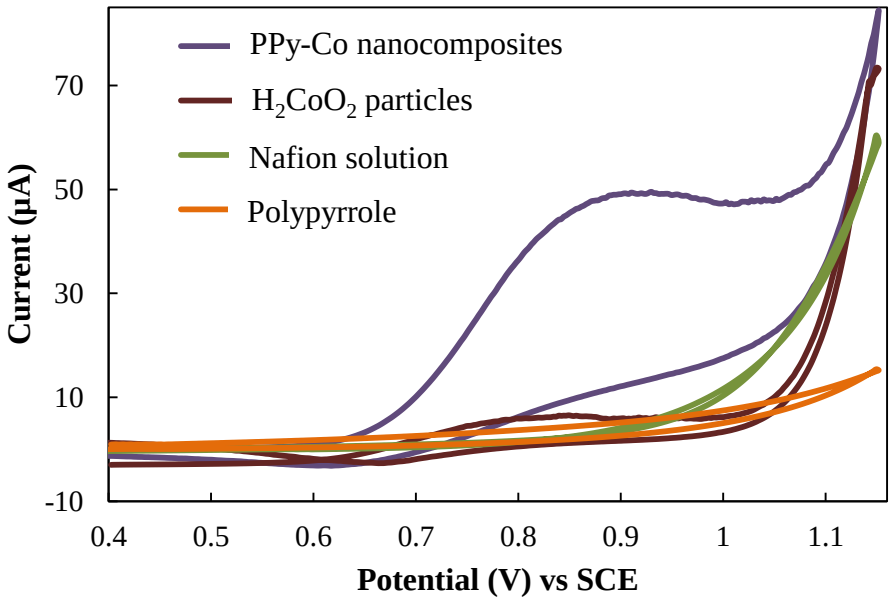

Figure 4.8: Cyclic voltammograms of the PPy-Co nanocomposites, H_2CoO_2 particles, nafion and polypyrrole coated GCE in the presence of 3 mM H_2O_2 in PBS (pH7.0) at scan rate of 50 mVs^{-1}

Influence of scan rate

Apart from that, the effect of the potential scan rates on the electrochemical performance was also studied by cyclic voltammetry as shown in Figure 4.9. Performing the voltammograms under different scan rates demonstrates that the catalytic peak current of the H_2O_2 oxidation is linearly proportional to the scan rate within the range (10 – 100 mVs^{-1}) indicating that the H_2O_2 oxidation follows a diffusion-controlled process at the modified GCE (Yan et al., 2013). Moreover, the peak potential shifts positively when the scan rate increases (shown in Figure 4.9 A) suggesting that the electrochemical reaction is irreversible. However, the charging current is too large when the scan rate increases and likely to cause instability in the

baseline. Therefore, in order to avoid such effect on the determination of H_2O_2, the 50 mVs^{-1} was chosen as the scan rate.

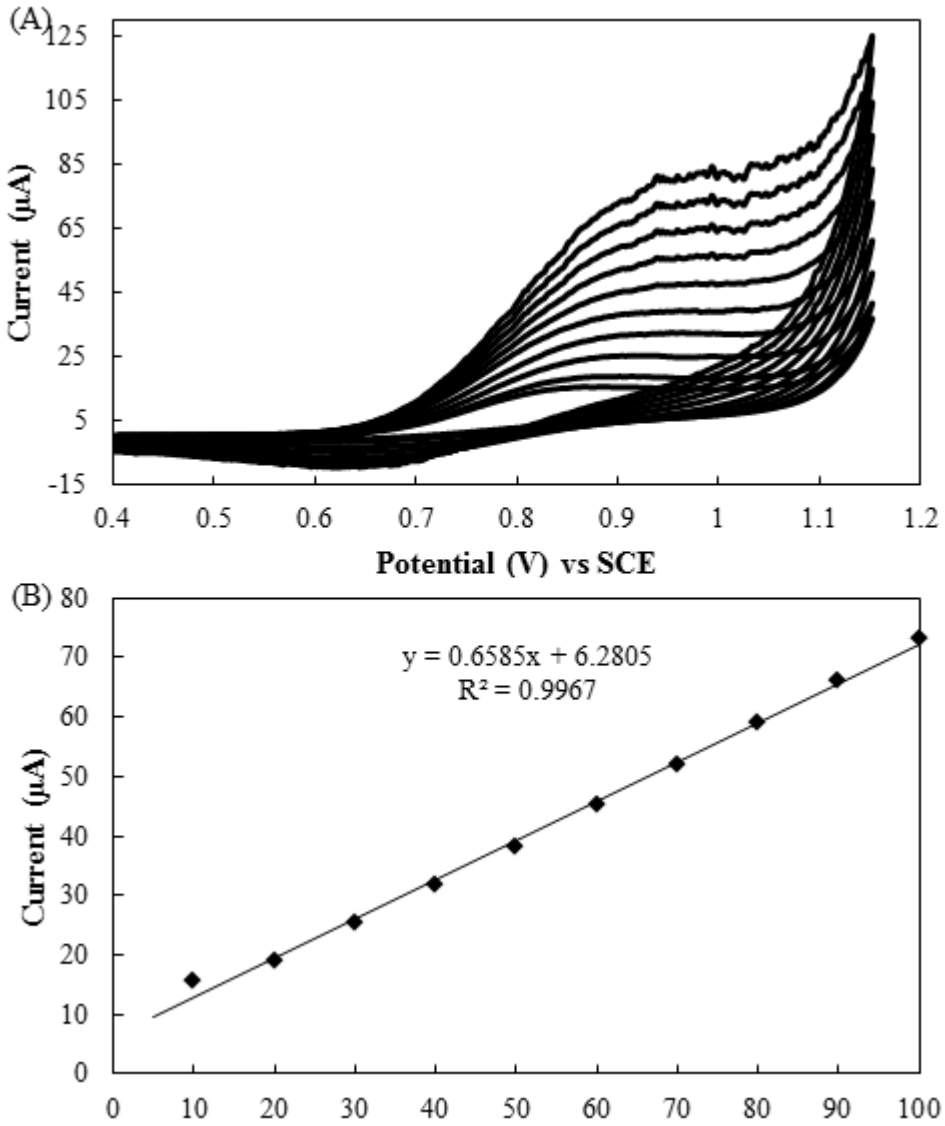

Figure 4.9: (A) Cyclic voltammograms of the PPy-Co nanocomposites coated GCE in the presence of 3 mM H_2O_2 in PBS (pH 7.0) at different scan rates from inner to outer: 10, 20, 30, 40, 50, 60, 70, 80, 90 and 100 mVs^{-1} and (B) A linear plot of oxidation current vs. different scan rate

4.1.6 Optimisation of the sensor

The above electrochemical studies showed that the electrochemical oxidation of H_2O_2 could be achieved in the presence of PPy-Co nanocomposites on the GCE surface.

In order to improve the performance of the sensor, the factors which may influence the response of the sensor such as applied potential, pyrrole monomer content in the nanocomposites and pH were studied and discussed as follow:

Influence of applied potential

The relationship between the applied potential in chronoamperometry and the oxidation current of H_2O_2 was studied and the results are shown in Figure 4.10. The dependency of the amperometric response on the applied potential of the PPy-Co nanocomposites coated GCE under the batch conditions were evaluated over the range of 0.7 V to 1.0 V. The current response gradually increased when the applied potential increased from 0.7 V to 0.9 V suggesting that the oxidation of H_2O_2 was easily achieved at low potential. However, when the potential was more positive than 0.9 V, the response current then slightly decreased. A suitable working potential should be chosen based on the least negative potential to achieve good selectivity, along with a potential value that shows a high analyte-dependent current. Thus, 0.9 V was finally selected as the optimised condition.

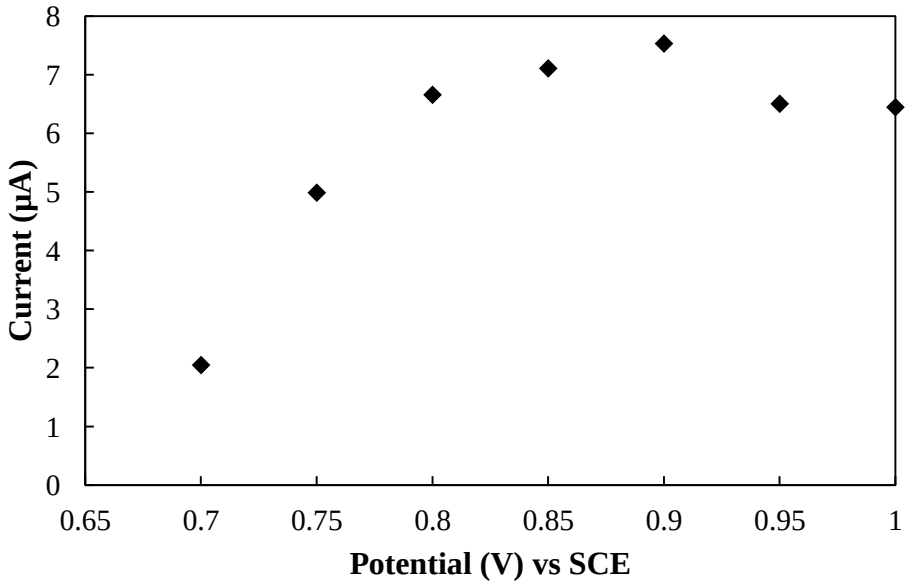

Figure 4.10: Effect of the applied potential on the current response of 3 mM H_2O_2 on the PPy-Co nanocomposites coated GCE in 0.2 M PBS (pH 7.0)

Influence of the pyrrole monomer content

The effect of the pyrrole monomer content in PPy-Co nanocomposites was investigated and the obtained results are shown in Figure 4.11. It can be seen that the catalytic oxidation of H_2O_2 has been significantly influenced by the content of pyrrole monomer in the nanocomposites. The current response rapidly increased with the increase of the pyrrole content from 100 μl to 500 μl. Then, the current response gradually decreased after 500 μl. These results were supported by the obtained FESEM results (shown in Figure 4.4), which suggests that at the higher content of pyrrole monomer, the polymer is rapidly formed and may contain multiple detects or deformities, leading to a loss in the sensing ability towards H_2O_2 (Ramanavicius et al., 2006; Sadki et al., 2000).

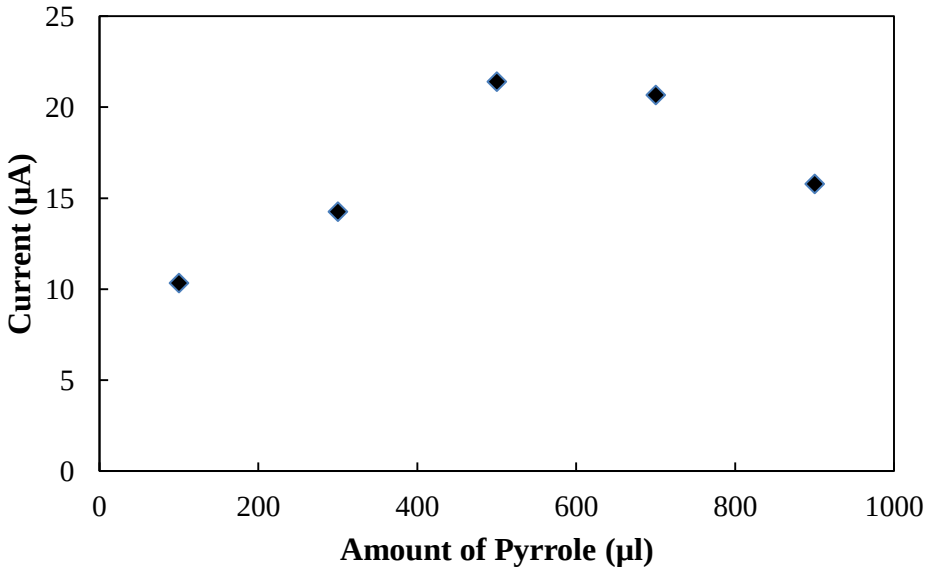

Figure 4.11: Effect of the pyrrole content on the current response of 3 mM H_2O_2 on the PPy-Co nanocomposites coated GCE in 0.2 M PBS (pH 7.0)

Influence of pH

The effect of the pH value of the phosphate buffer solution (PBS) on the oxidation current of H_2O_2 on PPy-Co nanocomposites coated GCE was investigated and the results are shown in Figure 4.12. It can be seen that the peak current of H_2O_2 oxidation is obviously influenced by the pH values. When pH is below 7.0, the peak current increase is associated with the increase in pH value. Then the peak current decreases when pH is more than 7.0. Over the pH ranges studied, the peak current achieved a maximum at pH 7.0. These results may be ascribed to the instability of H_2O_2 under both acidic and alkaline conditions. Besides, the decrease of the current value on alkaline conditions might be related to the self-degradation of H_2O_2 (Špalek et al., 1982). To minimise the loss of H_2O_2 in real sample during the detecting process, a neutral environment was required. Thus, pH 7 PBS was employed in all the subsequent experiments.

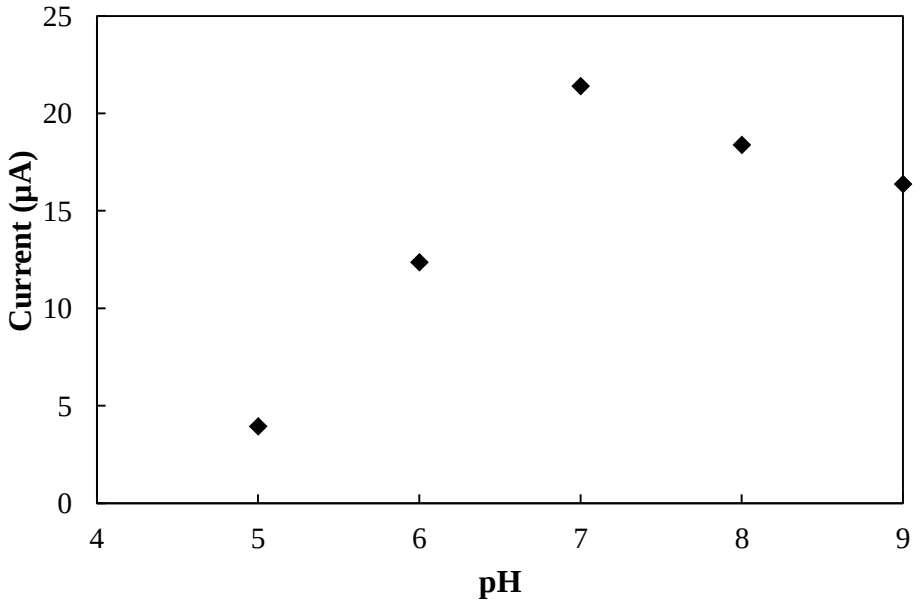

Figure 4.12: Effects of the pH of 0.2 M PBS on the current response of 3 mM H_2O_2 on the PPy-Co nanocomposites coated GCE

4.1.7 Chronoamperometric studies

The amperometry under stirred conditions is a more sensitive electroanalytical method than cyclic voltammetry and this method was employed in order to estimate the low detection limits. Figure 4.13 shows the amperometric response of PPy-Co nanocomposites coated GCE upon successive addition of H_2O_2 into the stirring (2000 rpm) of the PBS (pH 7.0) under the applied potential of 0.9 V. The oxidation current density reached a maximum steady-state value and achieved 95% of steady-state current density within 6 s, which was a clear indication of the rapid and sensitive H_2O_2 detection features shown by this electrode. It should be also mentioned that the currents increased linearly with the concentration of H_2O_2 between 20 μM and 80 mM. These responses demonstrated a stable and efficient catalytic property of PPy-Co nanocomposites coated on the GCE. There are two linear segments for the calibration curve of the current response to H_2O_2. The first linear segment (low concentration of H_2O_2) increases from 20 μM to 1 mM (Figure 4.13 B) with a linear regression equation

of I = 12.977 (μAmM^{-1}) + 3.27 (R^2 = 0.990), while, the second linear segment (high concentration of H_2O_2) increases up to 80 mM (Figure 4.13 C) with linear regression equation of I = 1.357 (μAmM^{-1}) + 27.24 (R^2 = 0.991).

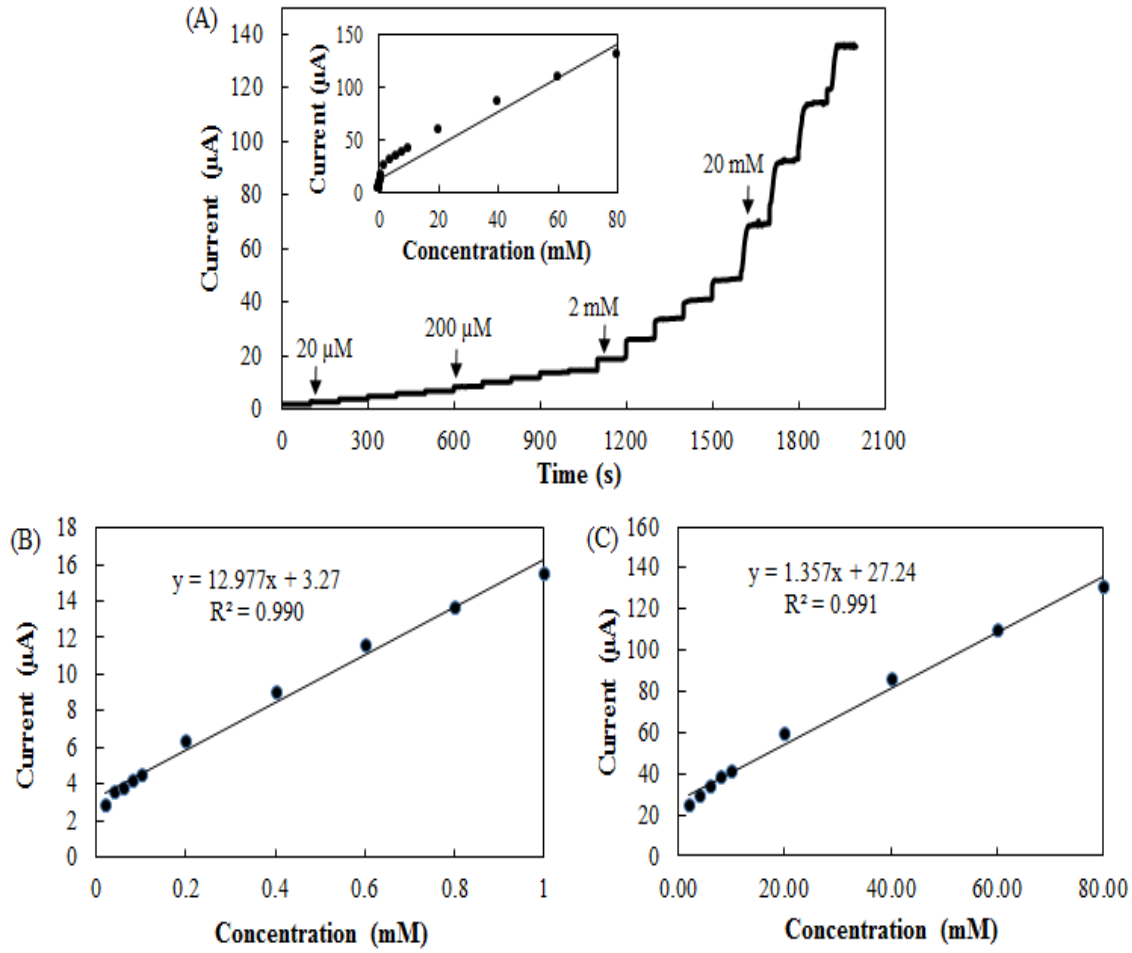

Figure 4.13: (A) Amperometric responses of PPy-Co nanocomposites coated GCE upon the successive addition of H_2O_2 into 0.2 M PBS (pH 7.0) with applied potential 0.9 V under stirring condition. Inert is the calibration curve. (B) The calibration curve at concentration range 20 μM – 1 mM and (C) The calibration curve at concentration range 1 – 80 mM

The limit of detection (LOD) and limit of quantification (LOQ) at a signal-to-noise of 3 are estimated to be 2.05 μM, 6.83 μM and 19.64 μM, 65.48 μM for two linear segments, respectively. The calculated sensitivity for H_2O_2 determination at these two linear segments is 12.997 μAmM^{-1} and 1.357 μAmM^{-1}. The obtained detection limits,

linear range and sensitivities of the PPy-Co nanocomposites modified GCE sensor are comparable to and even better than those recently developed modified electrode. For example, Mahmoudian et al. (2014) fabricated an electrochemical sensor based on the PPy/Fe_3O_4 nanostrip bundles/GCE for amperometric determination of H_2O_2, which showed that the detection limit for linear range of 0.1 – 60.0 mM is estimated to be 0.472 μM. Moreover, Lee et al. (2013) developed CoOOH nanosheet electrodes for non-enzymatic detection of H_2O_2 in alkaline solution and could detect H_2O_2 concentration up to 1.6 mM with detection limit of 40 μM and sensitivity of 99 $\mu AmM^{-1}cm^{-2}$. Han et al. (2013) developed a new sandwich structure nanocomposite of Ag nanoparticles supported on MnO_2 modified MWCNTs for fabricating a non-enzymatic H_2O_2 sensor. This fabricated sensor detected H_2O_2 in a linear range of 0.005 – 10.4 mM with sensitivity of 82.5 $\mu AmM^{-1}cm^{-2}$ and detection limit of 1.7 μM at a signal-to-noise ratio of 3. Whereas, the electrochemical H_2O_2 sensor based on the MWCNTs/$Ni(OH)_2$ modified GCE showed a significant linear dependence on the concentration of H_2O_2 up to 22 mM with detection limit of 66 μM (Zhang et al., 2012).

The overall H_2O_2 sensing performance of PPy-Co nanocomposite/GCE with rapid responses, high detection limit and wide linear range is competitive with the previous non-enzymatic H_2O_2 sensor as mentioned above. Herein, the wide linear range can be attributed to the previously mentioned morphological advantages of this nanocomposite, such as larger electroactive site due to the presence of smaller size PPy-Co nanocomposites and the superior electrocatalytic performance due to the effective electron transfer process between PPy-Co nanocomposites and GCE. Thus, by combining these properties with its high sensitivity and low detection limit, PPy-Co nanocomposite will be one of the major materials of preference for the next generation non-enzymatic H_2O_2 sensors that would be used for real samples.

4.1.8 Stability of PPy-Co nanocomposites modified GCE

In order to further explore and study, the stability, reproducibility and shelf-life of the developed sensor were investigated. These parameters are discussed in details in the following sections and are well known to play an important role in the development of a H_2O_2 sensor.

Stability and reproducibility

The stability and reproducibility of the developed sensor were investigated. The stability of the PPy-Co nanocomposites was determined by using cyclic voltammetric and the results are shown in Figure 4.14. As can be noticed, the nanocomposites showed a higher stability and the response remained stable even after 10 cycles (≈ 91%). These observations indicated that there is no inhibition effect of H_2O_2. On the other hand, the reproducibility of the PPy-Co nanocomposites in the detection of H_2O_2 was investigated by five independently prepared PPy-Co nanocomposites coated GCEs. The amperometric response upon the successive addition of 1 mM H_2O_2 into 0.2 M PBS (pH 7.0) were collected as shown in Figure 4.15. It is obvious from the results that the oxidation currents obtained for five different PPy-Co nanocomposites are very similar to each other and present a very good reproducibility. The relative standard deviation (RSD) was calculated to be 3.83%. This compares very favourably with other developed H_2O_2 sensors, such as Jia et al. (2014) calculated the RSD value of 3.94% for the current responses to 10 mM H_2O_2 on five independently prepared gold nanoparticles-graphene-chitosan modified electrode. Yan et al. (2013) also reported that the reproducibility of the gold electrode modified with granular cuprous oxide

nanowires has RSD of 4–5% for five electrodes, which been prepared under the same condition to detect H_2O_2.

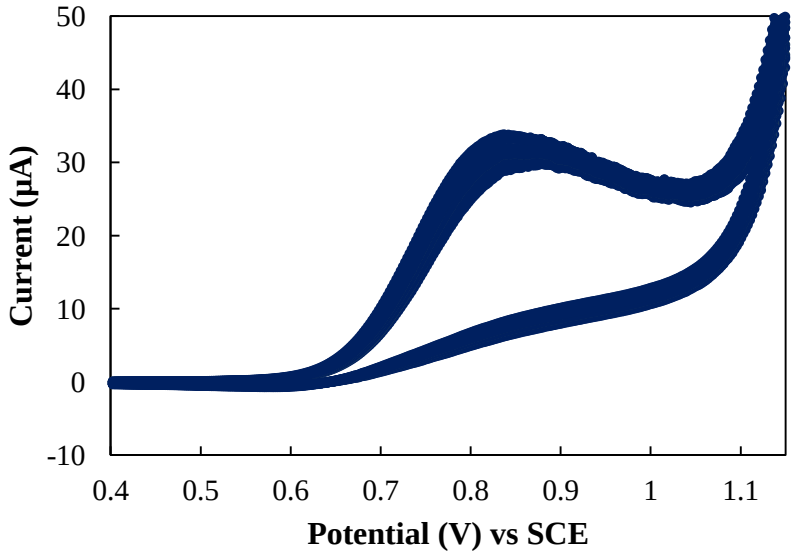

Figure 4.14: Repeated cyclic voltammograms of PPy-Co nanocomposites coated GCE in the presence of 3 mM H_2O_2 in PBS (pH 7.0) at scan rate 50 mVs^{-1}

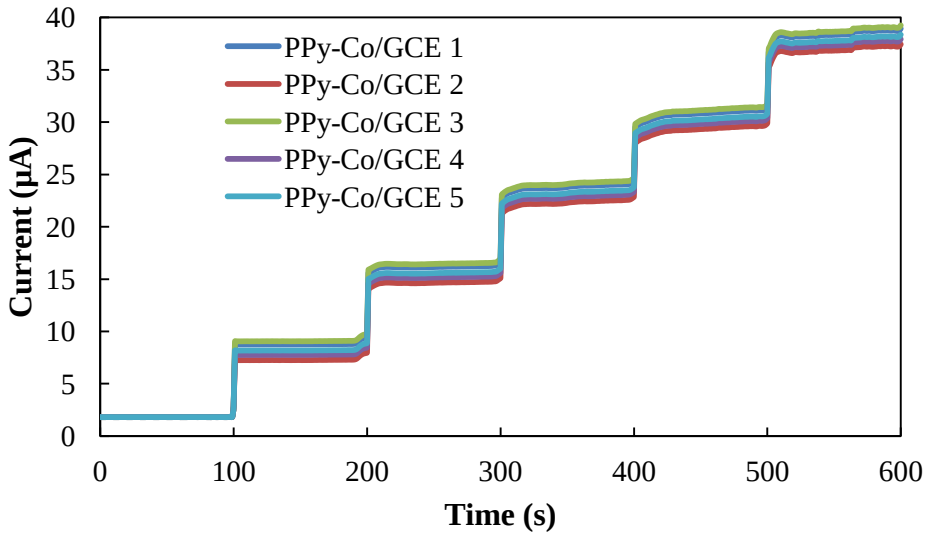

Figure 4.15: Amperometric response of five different PPy-Co nanocomposites/GCE upon successive addition of 1 mM H_2O_2 into 0.2 M PBS (pH 7.0) an applied potential 0.9 V under a stirring condition

Shelf-life

The shelf-life of the developed sensor was investigated by chronoamperometric detection upon the successive addition of 1 mM H_2O_2 into 0.2 M PBS (pH 7.0) and the results are shown in Figure 4.16. A PPy-Co nanocomposites/GCE was stored at 4 ºC in a refrigerator when it was not in use. After storage for 1 week, the response of the sensor was maintained about 98.6% of the initial values. The sensor still retained 95.3% of its original values after two weeks. The storage stability may be attributed to the stable film of the PPy-Co nanocomposite. This is comparable to the work done by Xu et al. (2013), who investigated the shelf-life of the CuO_2-rGO_{pa}/GCE which could retain 92% of the pristine current value after 14 days storage at 4 ºC. On the other hand, Kitte et al. (2013) reported that the current response of the Pd nanoparticles modified GCE declined about 29% for the determination made on the same electrode on the second day of the experiment and on the 10th day of the experiment, the current response decreased by 71%.

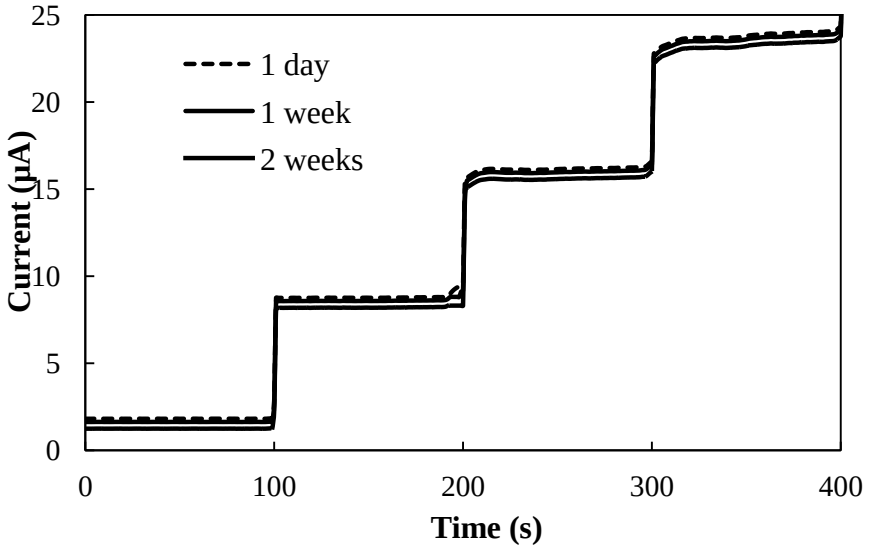

Figure 4.16: Shelf-life of PPy-Co nanocomposite/GCE in the presence of 3 mM H_2O_2 in PBS (pH 7.0) at 0.9 V

4.1.9 Investigation of the interfering compound and real sample analysis on the H_2O_2 detection

4.1.9.1 Effect of interference compounds

The possible interference from some co-existing electroactive compounds in real samples such as ascorbic acid, ethanol, glucose and glycine were assessed in order to investigate the selectivity of the developed non-enzymatic sensor. Figure 4.17 shows the amperometric response of the modified electrode upon successive addition of 3 mM of H_2O_2, ascorbic acid, ethanol, glucose and glycine into 0.2 M PBS (pH 7.0). As can be seen, two electrochemical signals resulting from H_2O_2 were basically identical and the responses made by ascorbic acid, ethanol, glucose and glycine are negligible. These observations indicate that the developed sensor can be employed in the selective detection of H_2O_2 in the presence of these common physiological materials.

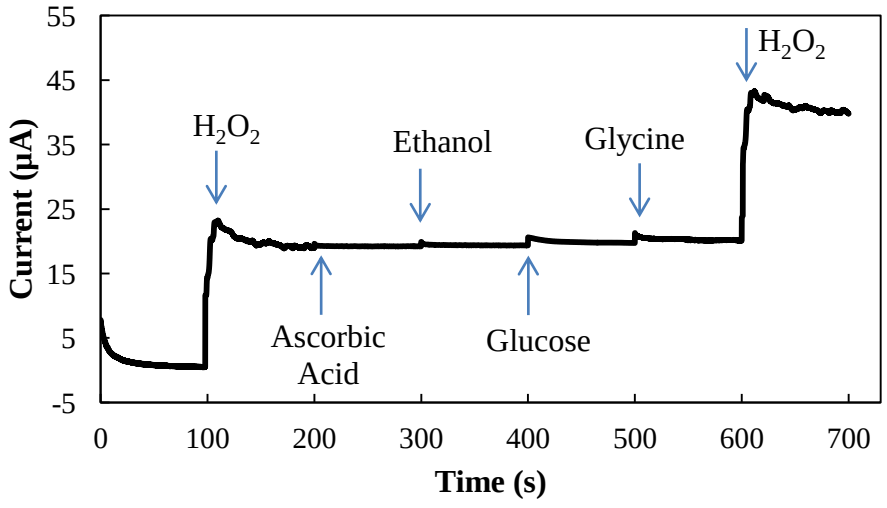

Figure 4.17: Amperometric responses of PPy-Co nanocomposites/GCE upon successive addition of 3 mM of H_2O_2, ascorbic acid, ethanol, glucose and glycine into 0.2 M PBS (pH 7.0) with an applied potential 0.9 V under a stirring condition

4.1.9.2 Application to lens cleaning solution and comparison with standard method

In order to verify the reliability of the sensor, the detection of H_2O_2 in the contact lens cleaning solution was carried out. The determination of H_2O_2 in contact lens cleaning solution samples was performed on the modified sensor using standard addition method as mentioned before in Chapter 3 section 3.6.1 and compared with standard titration method, section 3.6.2. All the measurements were performed four times and the concentration of H_2O_2 was calculated from calibration plots as shown in Figure 4.18. The calculated recovery and relative standard deviation (RSD) are listed in Table 4.2 and are in good agreement with those obtained by standard titration method. This suggests that the developed sensor has potential applications in the determination of certain concentration range of H_2O_2.

Table 4.2: Amperometric and titrimetric determination of H_2O_2 in contact lens cleaning solution

Standard concentration (mM)	**Amperometric measurements**		**Titrimetric measurements**	
	RSD (%)[a]	**Recovery (%)**	**RSD (%)[a]**	**Recovery (%)**
0.05	0.851	96.0	0.751	97.2
0.5	0.668	97.8	0.288	98.2
5	0.384	98.6	0.081	98.9
50	0.498	98.4	0.529	98.6

[a] RSD (%) calculated from four measurements

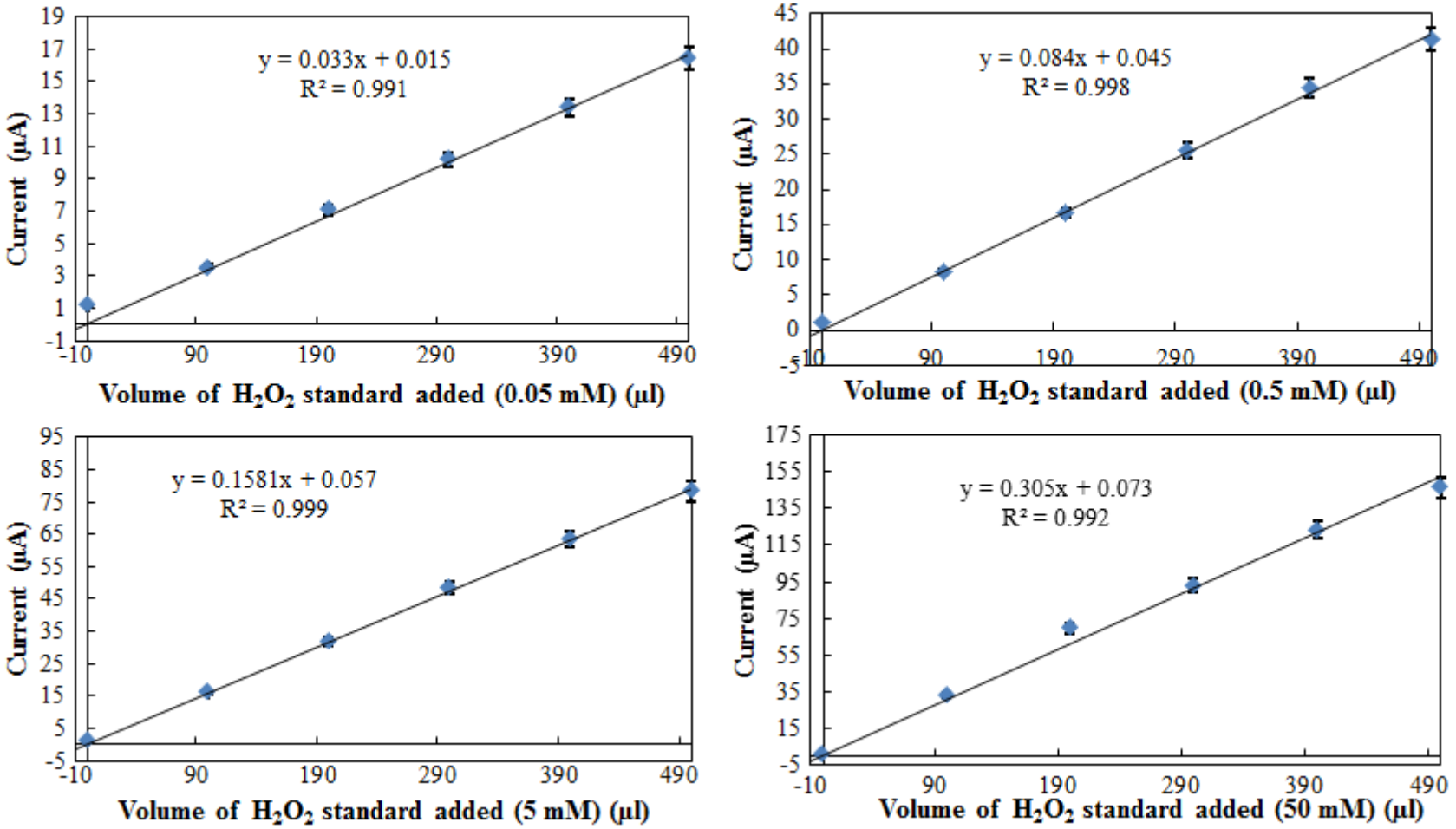

Figure 4.18: Calibration plots for determination of H_2O_2 in contact lens cleaning solution measured with different concentration of standard solution in 0.2 M PBS (pH 7.0) with an applied potential 0.9 V. Average values and error bars were calculated from four measurements

4.2 Polypyrrole coated nickel composites for glucose detection

In this section, the development and study of a new composite comprising of polypyrrole and nickel oxide for the enhanced detection of glucose are presented. Ni-based materials have been widely studied as electrode materials for fabricating non-enzymatic glucose sensors because they can function as efficient catalysts for electrocatalytic oxidation of glucose resulting from the redox couple of Ni^{3+}/Ni^{2+} in the alkaline medium (Luo et al., 2013; Tian et al., 2013; Danaee et al., 2012; Ding et al., 2011; Jiang & Zhang, 2010). So far, most Ni-based non-enzymatic glucose sensors are constructed by modifying substrates with Ni-based nanoparticle, Ni/carbon hybrids or porous nickel nanomaterials. Therefore, herein a simple non-enzymatic electrochemical sensor for glucose detection based on PPy-NiO composite modified GCE was demonstrated.

In this chapter, the synthesis of PPy-Ni composite by a facile and simplest method is presented. The synthesised composite were characterised using FTIR, TGA, FESEM-EDX and XRPD. In order to investigate the sensing properties towards glucose and the possible interaction involved, the PPy-NiO composite was fabricated with modified GCE to study their electrocatalytic capability. Several factors affecting the electrocatalytic performances of the proposed non-enzymatic sensor were further optimised. The linear range, detection limit, anti-interference performance, stability and reproducibility of the fabricated non-enzymatic glucose sensor were evaluated. Additionally, this PPy-NiO composite modified GCE was successfully applied to a commercial beverage green tea real sample.

4.2.1 Fourier Transform InfraRed

The molecular structure of samples was analysed by the Fourier Transform InfraRed (FTIR) spectroscopy. Figure 4.19 shows the FTIR spectra of the PPy-NiO composites, PPy and NiO particles. The bands detected in the 400 – 4000 cm^{-1} region are summarised in Table 4.3. The FTIR spectra of PPy shows characteristic peaks attributed to the C-H vibration at 2824.03 cm^{-1}, N-C stretching band at 1661.03 cm^{-1} and ring stretching mode of pyrrole ring at 1406.18 cm^{-1} (Nalage et al., 2013b). While, for NiO FTIR spectra, a strong peak is observed to be centred at 631.01 cm^{-1} corresponds to the stretching vibration of Ni-O. It was noticeable that the main absorption peaks in FTIR spectrum of PPy-NiO composites are affected by the presence of NiO in pure PPy and get shifted from 1400.18 cm^{-1} and 1661.03 cm^{-1} to 1381.06 cm^{-1} and 1670.11 cm^{-1}, respectively. This is due to the loss in conjugation and molecular order after modification of PPy with NiO. However, the shift of NiO stretching band at 633.21 cm^{-1} was observed in PPy-NiO composite due to binding of organic compound to the NiO (Chougule et al., 2012b). These results indicated a strong interaction between PPy and NiO particles.

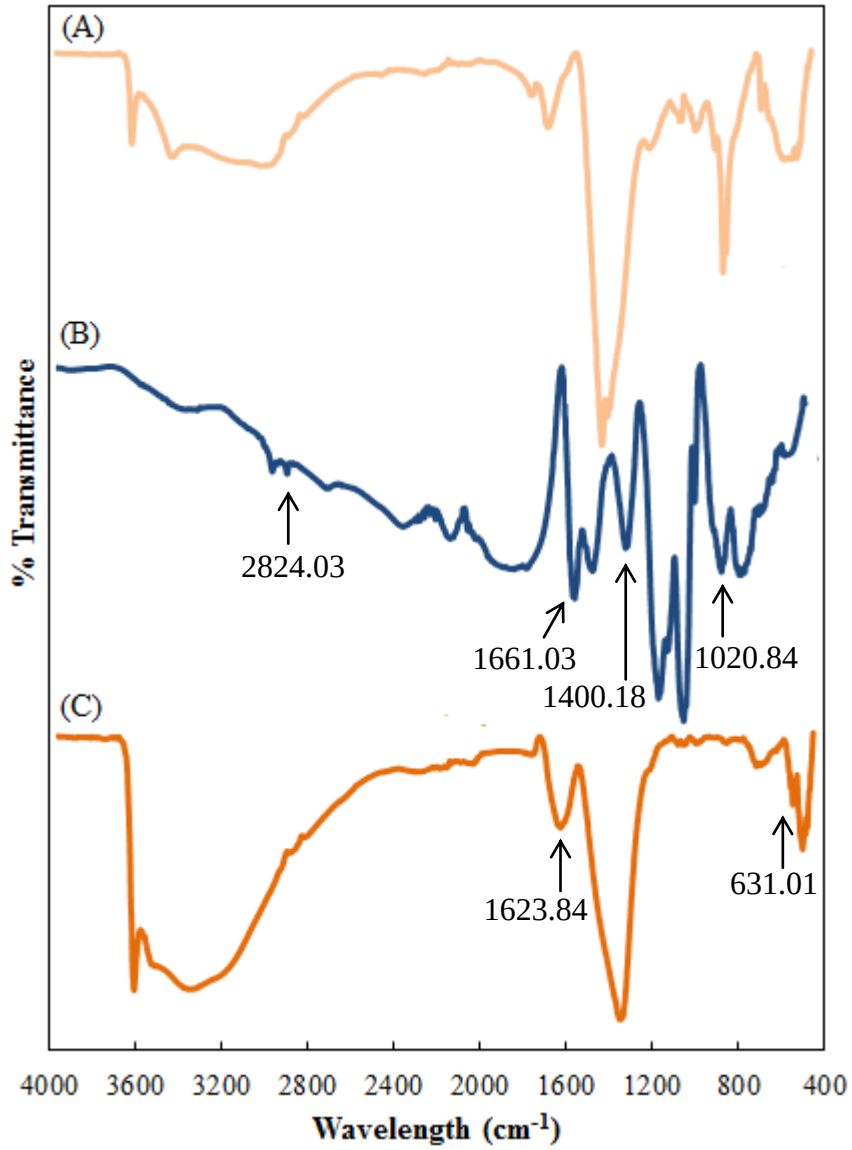

Figure 4.19: FTIR spectra of (A) PPy-NiO composites; (B) synthesised PPy in the absence of Ni^{2+} and (C) NiO particles synthesised in the absence of pyrrole monomer

Table 4.3: The maximum wavenumber of PPy-NiO composites, PPy and NiO particles

Mode	Wavenumber (cm^{-1})		
	PPy-NiO composite	**PPy**	**NiO particles**
(C-H)	2801.43	2824.03	-
(C-N=C)	1670.11	1661.03	-
PPy ring	1381.06	1400.18	-
=C-N	1013.28	1020.84	-
Ni-O	633.21	-	631.01
C=O	-	-	1623.84

4.2.2 Thermogravimetric analysis

The results of thermogravimetric analysis (TGA) of NiO particles synthesised in the absence of pyrrole monomer, pure PPy and PPy-NiO composite are shown in Figure 4.20. As seen in TGA spectra of pure PPy, the weight loss of 3.10% is observed at temperature 110 ºC, which is attributed to the removal of moisture in the PPy and the weight loss at the temperature higher than 200 ºC is due to degradation of PPy. The decomposition step initiates at 200 ºC and higher temperatures would then result in enhanced weight loss. A weight loss of 83.43% was observed up to 650 ºC due to the release of C, H and N moieties of PPy (Han, 2009; Tabassum et al., 2009). It is found that the TGA spectra of NiO particles synthesised in the absence of pyrrole monomer shows the first loss in weight near the temperature range 50 – 120 ºC, which could be due to the probable loss of water, volatile impurities and adsorbed surfactants present on NiO particles. Moreover, it was shown only 9.23% reduction in the weight until an operating temperature of 900 ºC, which clearly indicates that there is a formation of stable NiO material. As indicated in the TGA spectra of PPy-NiO composite, initially at the temperature range of 30 – 110 ºC, the weight loss is about 10%, which was attributed to the removal of water molecules/impurities associated with the polymer (Batool et al., 2012; Mavinakuli et al., 2010). There is a sharp decrease between 150 ºC and 250 ºC in the weight loss, which was due to the degradation of the polymer materials. At about 280 ºC, 30% weight loss is observed. The binding between the PPy and NiO shows a strong chemical interaction and hence, weight loss is found to be less as compared to that of the neat polymer over a similar temperature range (Guo et al., 2009). These results show that the PPy-NiO composites possess a better thermal stability as compared with pristine polypyrrole.

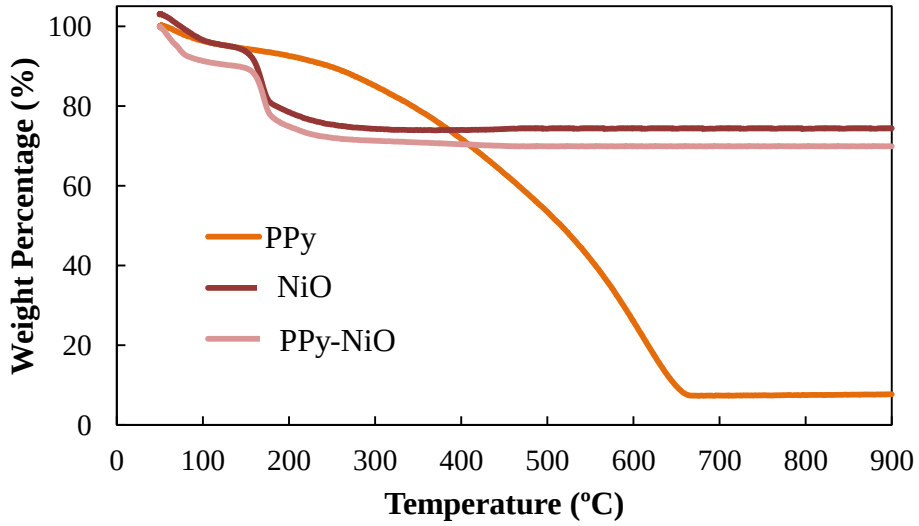

Figure 4.20: TGA spectra of NiO particles synthesised in the absence of pyrrole monomer, PPy in the absence of Ni^{2+} and PPy-NiO composite

4.2.3 Field emission scanning electron microscopy and energy dispersive x-ray analysis

The PPy-NiO composites and NiO particles in the absence of pyrrole monomer were examined by using field emission scanning electron microscopy (FESEM). Figure 4.21 (A) and (B) present the FESEM images captured for the PPy-NiO composites at magnification of 5 000 x and 10 000 x, respectively. While, the images obtained for NiO particles in the absence of pyrrole monomer are presented in Figure 4.21 (C) and (D) at magnification of 10 000 x and 25 000 x, respectively. These results clearly indicated the effect of pyrrole monomer on the morphology of the composite. The NiO particles in the absence of pyrrole monomer show granules structure and this morphology were changed after reacting with pyrrole monomer. The synthesised PPy-NiO composite shows needle-like structures with 330 ± 10 nm in width.

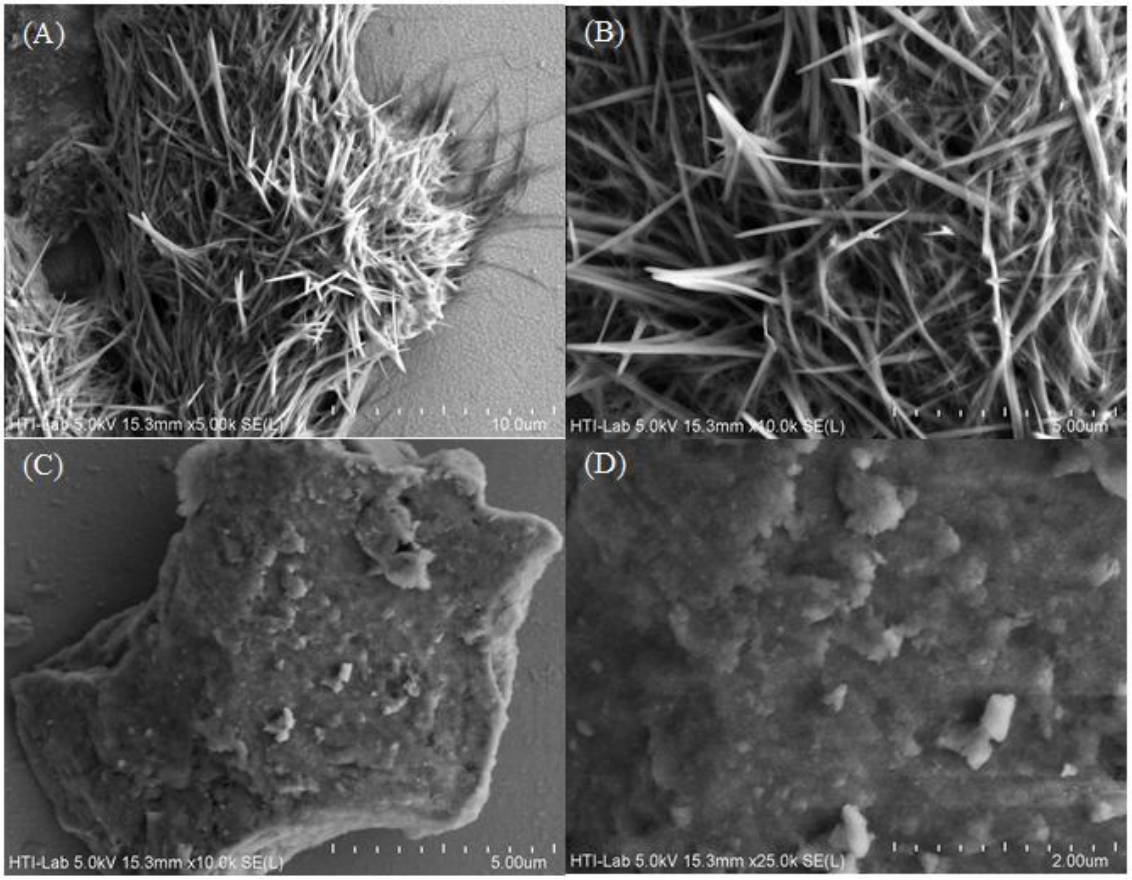

Figure 4.21: FESEM images of the PPy-NiO composites (A and B) and NiO particles in the absence of pyrrole monomer at lower and higher magnification

As mentioned before, the surface morphology of structure is strongly affected by the preparation conditions. So, the effect of PPy on NiO and the importance of the presence of PPy were demonstrated by investigating the surface morphology of PPy-NiO composites with different contents of pyrrole monomer using FESEM technique. Figure 4.22 shows the FESEM images of PPy-NiO composites with different contents of pyrrole monomer. An irregular morphology structure and some of the nickel surfaces, which remained uncovered, were observed for the pyrrole monomer content of 0.3 ml as shown in Figure 4.22 (A). This could be due to the smaller amount of pyrrole monomer in the reaction mixture during polymerisation. However, the PPy-NiO composites at 0.5 ml of pyrrole monomer content gave a clear and well-structured (needle-like) morphology as shown in Figure 4.22 (B). Moreover, it also indicates a greatly accessible surface area of PPy-NiO composites which adds an extra advantage

for sensor fabrication. When the content of pyrrole monomer increases to 0.7 ml, the morphology of PPy-NiO composites was shows that a thick coating of PPy onto nickel as shown in Figure 4.22 (C). This may be due to the existence of higher amount of pyrrole monomer during the polymerisation reaction which gives rise to clusters of pure PPy domains. It is understood that different contents of PPy offered surface property and reduction potential differences which leads to changes in the size and morphology of nickel particles.

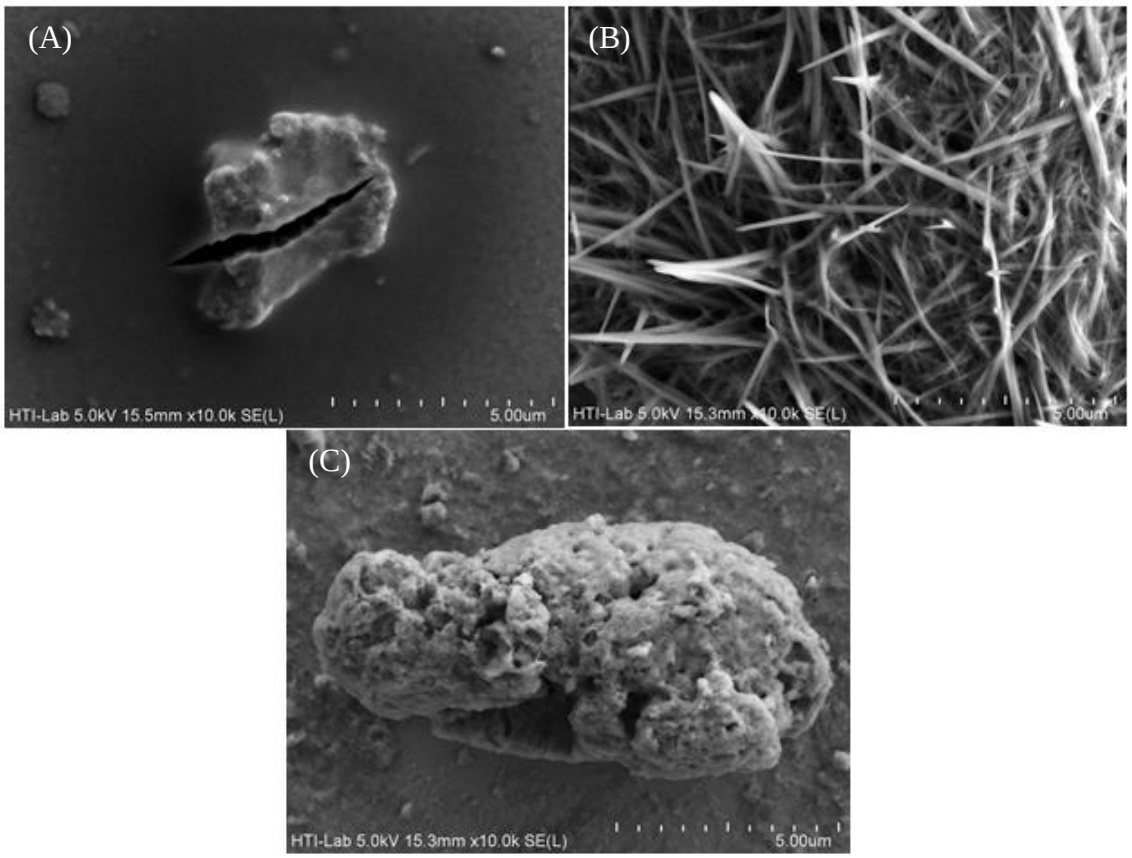

Figure 4.22: FESEM images of the PPy-Ni composites with different content of PPy: 0.3 ml (A) 0.5 ml (B) and 0.7 ml (C) with 10 kx

Energy dispersive x-ray (EDX) measurements were also performed on the PPy-NiO composites and the obtained results were shown in Figure 4.23. As can be seen, the signal of Carbon (C) at ~ 0.35 keV, Nitrogen (N) at ~ 0.25 keV, Oxygen (O) at ~ 1.95 keV and Nickel (Ni) at ~ 3.70 keV, which are found in the spot 1 indicated the

characteristic peaks of PPy-NiO composites. The signal of Indium (In) at ~ 0.40 keV and ~ 0.10 keV, which were found in the spot 2, indicated the ITO glass slide surface. However, the weak peak of Ni at ~ 2.55 keV in the spot 2 shows the unformed needle-like structure of the composite.

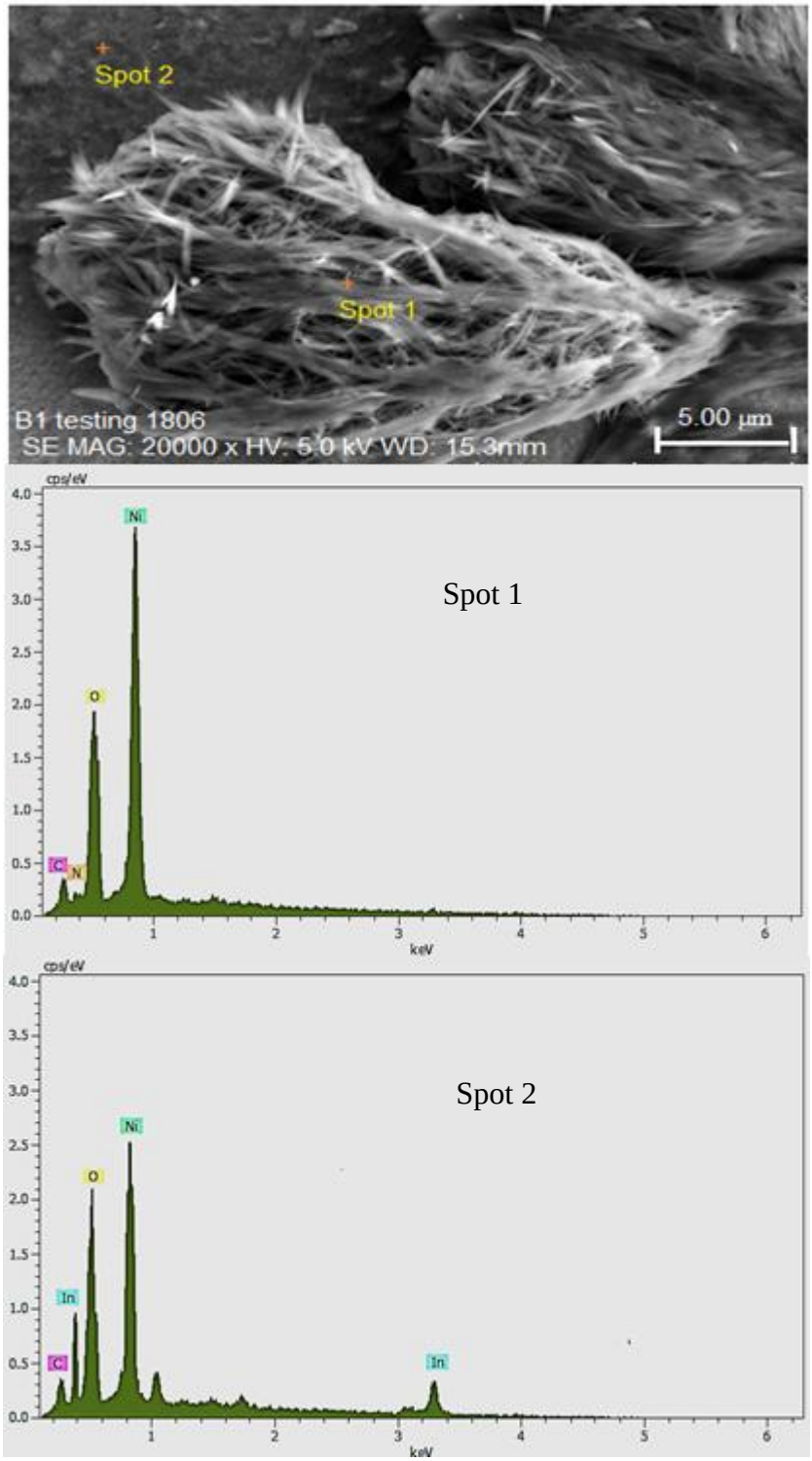

Figure 4.23: FESEM-EDX images of the PPy-NiO composites

4.2.4 X-ray powder diffraction

The x-ray powder diffraction (XRPD) patterns of PPy-NiO composites and NiO particles synthesised in the absence of pyrrole monomers are shown in Figure 4.24. The XRPD pattern of PPy-NiO composites (Figure 4.24 A) presents all the diffraction peaks of NiO and the broad peak of PPy at 10 – 30 º, indicating the characteristic peak of PPy. The XRPD pattern of NiO particles as shown in Figure 4.24 (B) revealed well-defined peaks having orientations in the (111), (200), (220), (311) and (222) planes. However, these diffraction peaks of NiO were found to shift to lower 2θ values in PPy-NiO composites compared to the XRPD patterns of NiO particles. The similar phenomenon was also observed by Nalage et al., (2013a). The decrease in the intensities of the NiO peaks in the PPy functionalised composites suggests that the NiO particles are uniformly and extensively dispersed in the PPy matrix and the broadness of the peaks remains the same, which further suggest a uniform dispersion of the particles.

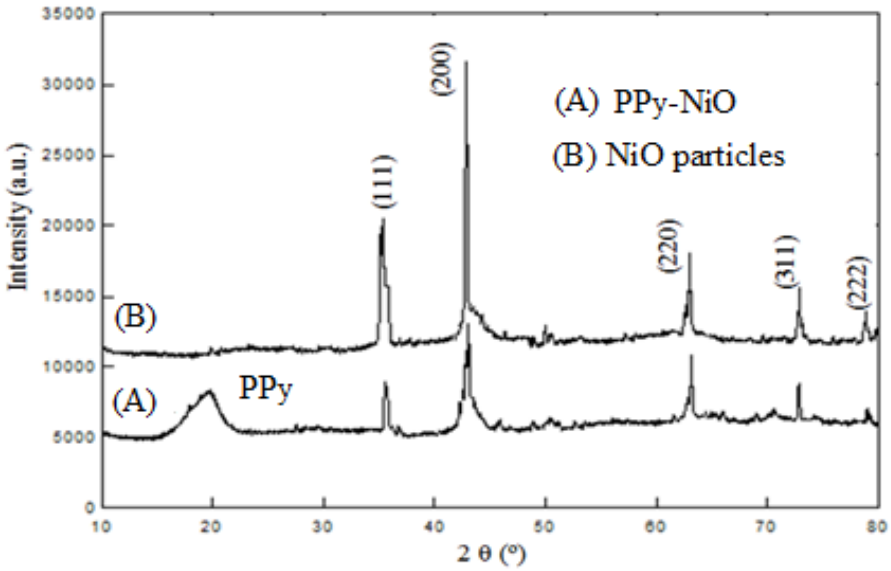

Figure 4.24: XRPD patterns of the (A) PPy-NiO composites and (B) NiO particles synthesised in the absence of pyrrole monomers

4.2.5 Electrochemical studies of the PPy-NiO composites for glucose detection

The electrocatalytic performance of the PPy-NiO coated GCE towards glucose oxidation in alkaline medium is shown in Figure 4.25. The bare GCE exhibited no electrochemical response in the absence of glucose (Figure 4.25 red-lined curve) and it still remained the same with no electrochemical response with the presence of glucose (Figure 4.25 green-lined curve). While, the addition of 0.1 mM glucose to PPy-NiO/GCE results in a significant increase of the oxidation current (Figure 4.25 grey-lined curve) and the reduction current are decreased, suggesting excellent electrocatalytic activity of PPy-NiO towards glucose oxidation. The oxidation of glucose to glucolactone was electro-catalysed by the PPy-NiOOH/PPy-NiO redox couple according to the following electrochemical reaction (Ci et al., 2014; Mu et al., 2011; Zhang et al., 2011; Zhu et al., 2011):

$$\mathrm{PPy-NiO} + (\mathrm{OH})^- \rightarrow \mathrm{PPy-NiOOH} + \mathrm{e}^- \quad \textbf{(4.3)}$$

$$\mathrm{PPy-NiOOH} + \mathrm{glucose} \rightarrow \mathrm{PPy-NiO} + \mathrm{glucolactone} \quad \textbf{(4.4)}$$

The increase of oxidation current is attributed to the electro-oxidation of glucose with PPy-NiO as an electro-catalyst which is accompanied by the oxidation of Ni^{2+} to Ni^{3+}. Besides that, the addition and oxidation of glucose would certainly induce adsorption of glucose and the oxidised intermediates on active site of Ni-based materials, which may slow down the kinetics of the corresponding reaction and thus give rise to a slight positive shift in the reduction peak (Ci et al., 2014). Therefore, it has been concluded that the PPy-NiO composites are suitable as mediators to shuttle the

electron between the glucose and working electrode and facilitate electrochemical regeneration following the electron exchange with glucose.

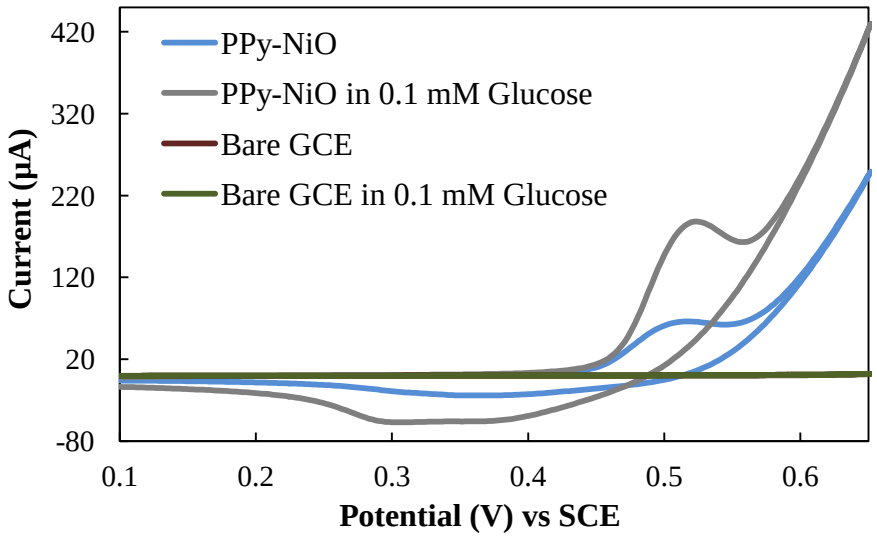

Figure 4.25: Cyclic voltammograms of the bare GCE and PPy-NiO composites coated GCE in the absence and presence of 0.1 mM glucose in NaOH (0.1 M) at scan rate 20 mVs^{-1}

Influence of the supporting materials

Indeed, in a control experiment using the electrocatalytic oxidation of each supporting materials including NiO particles, nafion and polypyrrole, towards 0.1 mM glucose in NaOH (0.1 M) was investigated with the cyclic voltammetry and the results are shown in Figure 4.26. No electrocatalytic oxidation current towards glucose for polypyrrole coated GCE without the presence of Ni^{2+} (Figure 4.26 orange-lined curve) was observed, underlining the importance of NiO. While, the effect of nafion on the electrochemical response (Figure 4.26 green-line curve) could be ignored since nafion was only employed as an adhesive to immobilise the composite on the surface of GCE. On the other hand, NiO particles coated GCE shows an obvious oxidation peak in Figure 4.26 (red-lined curve), which suggest the excellent catalytic activity of NiO

particles for oxidation of glucose. It was noticeable that the oxidation peak current of glucose on PPy-NiO composites coated GCE was significantly higher than that of NiO particles coated GCE. Thus, the increased current on PPy-NiO composites coated GCE obviously benefited from high specific area and good conductivity of PPy that could facilitate chemical deposition of NiO particles.

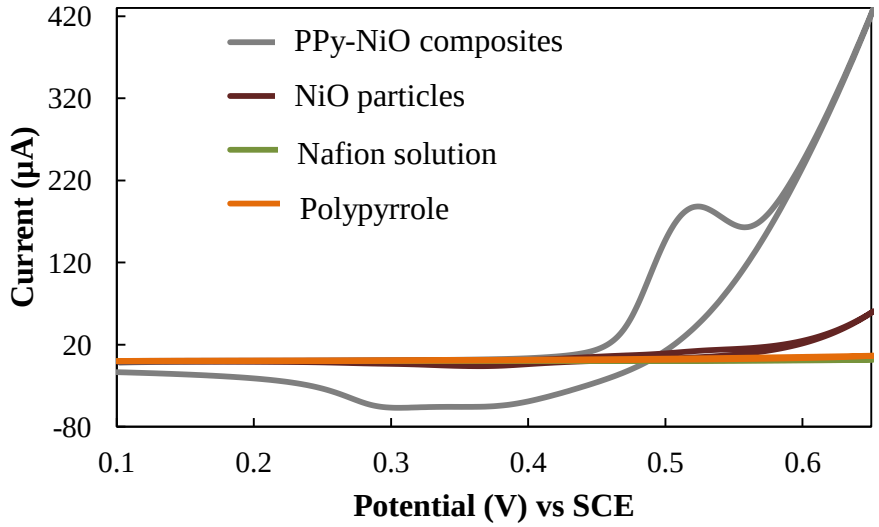

Figure 4.26: Cyclic voltammograms of the PPy-NiO composites, NiO particles, nafion and polypyrrole coated GCE in the presence of 0.1 mM glucose in NaOH (0.1 M) at scan rate 20 mVs^{-1}

Influence of scan rate

The effect of potential scan rate was also characterised in 0.1 M NaOH containing 0.1 mM glucose by cyclic voltammetry and the results are shown in Figure 4.27. It can be seen that the reduction and oxidation peak currents are both proportional to the scan rate in the range of 10 – 100 mVs^{-1}. As seen in Figure 4.28, the redox current observed on the PPy-NiO matrix scales linearly with the scan rate. This linearity might indicate a diffusion controlled process involving OH^- diffusion from the supporting

electrolyte to the electrode surface during the reduction step and from the electrode to the solution during the oxidation step (Subramanian et al., 2014).

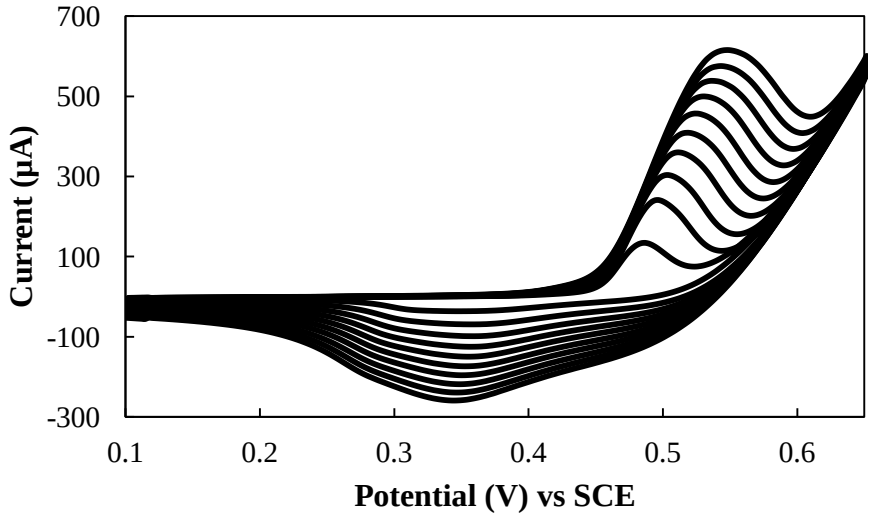

Figure 4.27: Cyclic voltammograms of the PPy-NiO composites coated GCE in the presence of 0.1 mM glucose in NaOH (0.1 M) at different scan rate; from inner to outer: 10, 20, 30, 40, 50, 60, 70, 80, 90 and 100 mVs^{-1}

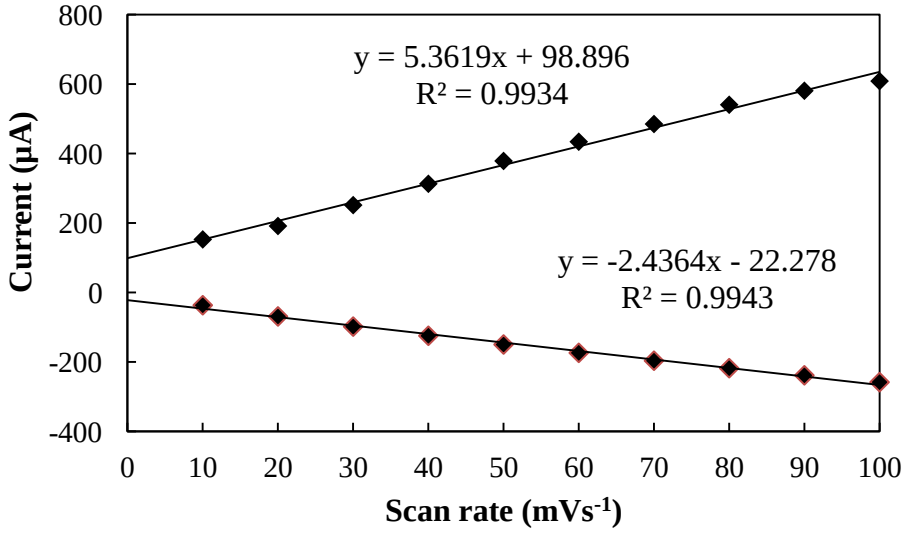

Figure 4.28: A linear plot of oxidation current vs. different scan rate from 10, 20, 30, 40, 50, 60, 70, 80, 90 and 100 mVs^{-1}

4.2.6 Optimisation of sensor

The above electrochemical studies demonstrated that the electrochemical oxidation of glucose could be accomplished in the vicinity of PPy-NiO composites on the GCE surface. With a specific end goal to enhance the execution of the sensor, the elements which may impact the reaction of the sensor, such as applied potential, pyrrole monomer content in the composites and sodium hydroxide concentration were considered and examined as follows:

Influence of applied potential

It is well known that the applied potential significantly affects the amperometric response of an electrochemical sensor. Therefore, the dependency of the amperometric response on the applied potential of the PPy-NiO composites coated GCE under the batch conditions were evaluated over the range of 0.7 V to 1.0 V; in this way, a suitable potential can be optimised for glucose detection. As shown in Figure 4.29, when a potential below 0.53 V (e.g. 0.45 – 0.50 V) was applied, a small current response was observed with each addition of glucose. However, an applied potential of 0.53, 0.55 or 0.57 V led to a remarkable enhancement in the current response upon each addition of glucose. Because of a relatively low potential of glucose detection, it is of great benefit to lower the background current and noise. Given the fact that gases will be produced on the surface of the electrode at a high potential (Ci et al., 2014), a potential of 0.53 V was selected as the optimum working potential for amperometric detection of glucose in the subsequent studies.

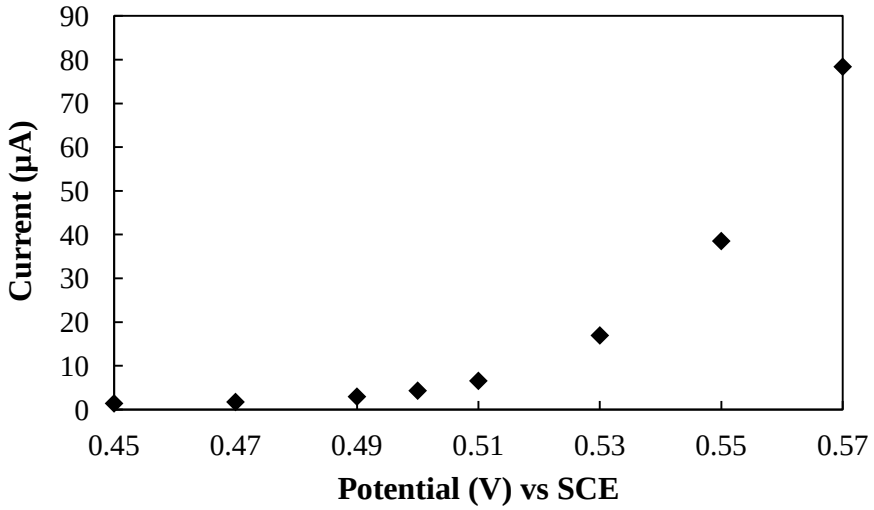

Figure 4.29: Effect of the applied potential on the current response of 0.1 mM glucose on the PPy-NiO composites coated GCE in 0.1 M NaOH

Influence of pyrrole content

The influence of the pyrrole content to the electrocatalytic oxidation of glucose was investigated and Figure 4.30 shows the chronoamperometry response for the composites of different pyrrole contents on the current response of 0.1 mM glucose in 0.1 M NaOH. It can be seen that the content of pyrrole monomer in the composite has a significant influence on the catalytic oxidation of glucose. The current response rapidly increased with the increase of the pyrrole content from 100 μl to 500 μl and the current response gradually decreased after 500 μl. This is because, if there is not enough monomer in solution, the composite will not form. Alternatively, if there is an excess of monomer in the solution, the polymer will form very quickly and may contain multiple defects or deformities, leading to a loss in sensing performance towards glucose (Ramanavicius et al., 2006; Sadki et al., 2000).

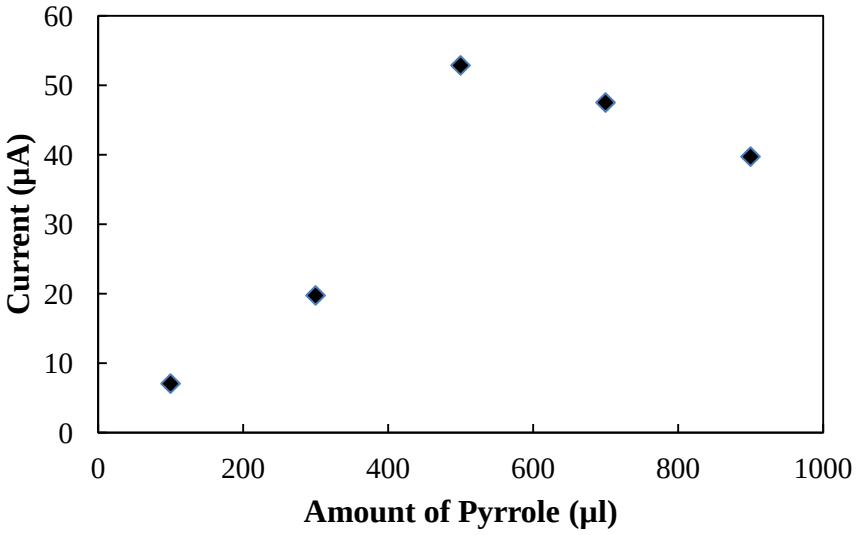

Figure 4.30: Effect of the pyrrole content on the current response of 0.1 mM glucose on the PPy-NiO composites coated GCE in 0.1 M NaOH

Influence of NaOH concentration

The influence of the NaOH concentration on the oxidation current of glucose on PPy-NiO composites coated GCE was investigated since an alkaline medium is required for enhancing the electrocatalytic activity of PPy-NiO for oxidation of carbohydrate compounds (Wang et al., 2010) and the results are shown in Figure 4.31. No response current of the oxidation of glucose is observed in the absence of NaOH. When the concentration of NaOH increases from 0.1 M to 0.5 M, the current increases due to the fact that glucose is more easily oxidised at higher pH. However, as the concentration of NaOH increases, the background signal increases and the response signal decreases. This is because the reference electrode is greatly affected by the high concentration of NaOH, which is consistent with the reported experimental phenomena that an increased background current was observed at high NaOH concentration (Mu et al., 2011). Thus, 0.1 M NaOH was chosen as the optimised medium for the subsequent experiments.

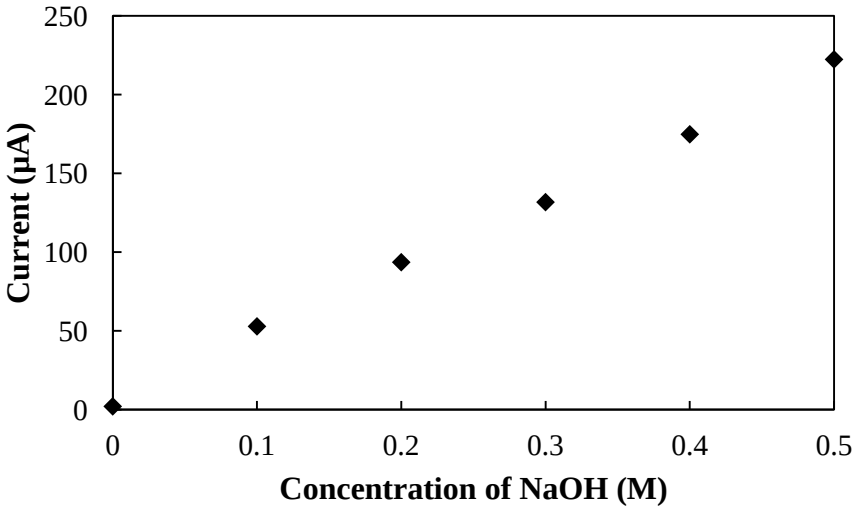

Figure 4.31: Effects of the concentration of NaOH on the current response of 0.1 mM glucose on the PPy-NiO composites coated GCE

4.2.7 Chronoamperometric studies

In the evaluation of an amperometric sensor, current responses are measured using different concentrations of the objective analyte at a fixed potential for a fixed time. The amperometric responses of the PPy-NiO composite/GCE to the successive addition of glucose into the stirring (2000 rpm) of the NaOH (0.1 M) under applied potential of 0.53 V was carried out and the results are shown in Figure 4.32. The amperometric response shows a staircase-like increase upon the addition of glucose with a very fast response time towards the oxidation of glucose. The PPy-NiO composite/GCE responses immediately upon glucose addition and reaches its steady-state level within 6 s; this is attributed to the good electrocatalytic properties of PPy-NiO. It can be seen that the currents increased linearly with the concentration of glucose between 0.01 mM and 20 mM and there are two calibration curves of the current response towards glucose. From the first calibration curve (Figure 4.32 B), an excellent linearity (R^2= 0.993) over a concentration range of 0.01 – 0.5 mM with a slope of 137.560 μAmM^{-1} was obtained. While, the second calibration curve (Figure 4.32 C)

over concentration range from 1 mM to 20 mM was obtained with R^2= 0.992 and a slope of 7.899 μAmM^{-1}. These responses demonstrate a stable and efficient catalytic property of PPy-NiO composites coated on the GCE.

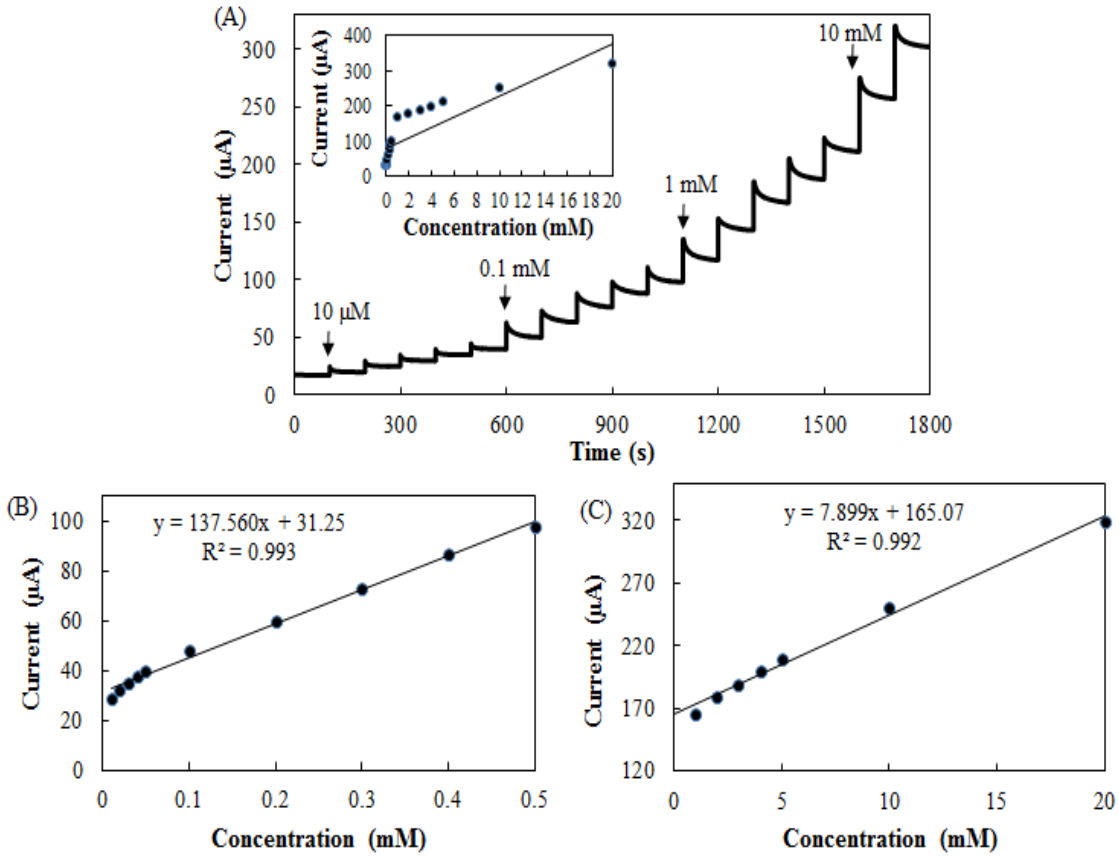

Figure 4.32: (A) Amperometric responses of PPy-NiO composites coated on GCE upon the successive addition of glucose into 0.1 M NaOH with an applied potential 0.53 V under stirring condition. Inert is the calibration curve; (B) The calibration curve at low concentration range of glucose; (C) the calibration curve at higher concentration range of glucose

The limit of detection (LOD) and limit of quantification (LOQ) were calculated by signal-to-noise ratio of 3 and were estimated to be 0.33 μM and 1.10 μM, respectively, for lower concentration range of glucose (0.01 – 0.5 mM). While, for the higher concentration range of glucose (1 – 20 mM), the LOD and LOQ were valued to be 5.77 μM and 19.24 μM, respectively. Besides, the sensitivity at these two concentration ranges for glucose determination is estimated to be 137.560 μAmM^{-1} and

7.899 μAmM^{-1}, respectively. The obtained sensitivity for the developed sensor is comparable with various non-enzymatic glucose sensors previously reported as shown in Table 4.4.

Table 4.4: Comparison of various non-enzymatic glucose sensors

Modified electrode	**Linear range (mM)**	**Sensitivity**	**LOD (μM)**	**Reference**
$Ni(OH)_2$ NF arrays	0.01 – 0.8	8500 $mAmM^{-1}cm^{-2}$	1.2	(Wang, G. et al., 2012)
Ni-rGO NBs	0.001 – 0.11	813 $\mu AmM^{-1}cm^{-2}$	-	(Wang, Z. et al., 2012)
sG-Ni/NiO	0.0001 – 0.005	48270 $\mu AmM^{-1}cm^{-2}$	0.28	(Kumary et al., 2013)
Ni-Co NSs-rGO	0.01 – 2.65	1773.61 $\mu AmM^{-1}cm^{-2}$	3.79	(Wang, L. et al., 2013)
NiO-HMS	0.00167 – 0.42	2.39 $mAmM^{-1}cm^{-2}$	0.53	(Ci et al., 2014)
$rGO/Ni(OH)_2$	0.015 – 30.0	11.40 $mAmM^{-1}cm^{-2}$	15	(Subramanian et al., 2014)
NiOHSs-rGO-NF	0.000625 – 0.2584 0.2584 – 10.50	3796 $\mu AmM^{-1}cm^{-2}$ 2721 $\mu AmM^{-1}cm^{-2}$	0.03	(Lu et al., 2014)
PPy-NiO	0.01 – 0.50 1.0 – 20.0	1094.80 $\mu AmM^{-1}cm^{-2}$ 62.87 $\mu AmM^{-1}cm^{-2}$	0.33 5.77	This work

4.2.8 Stability of PPy-NiO composites modified GCE

To further investigate and study, the stability, reproducibility and shelf-life of accurate usability of the fabricated sensor were examined, individually. These parameters are discussed in details in the subsequent segments and are known to be significant in the enhancement of a glucose sensor.

Stability and reproducibility

The stability and reproducibility of the developed sensor were investigated. The stability of the PPy-NiO composites was determined by using cyclic voltammetric technique and the results are shown in Figure 4.33. As noticed, the composites show a greater stability and the response remains stable even after 10 cycles (≈ 89%). This shows that there is a no inhibition effect during glucose determination. On the other hand, the reproducibility of the PPy-NiO composites for the detection of glucose was investigated by using five different PPy-NiO composites coated GCEs, prepared independently. The amperometric responses were collected upon the successive addition of 0.1 mM glucose into 0.1 M NaOH and the obtained results are shown in Figure 4.34. This developed sensor yielded a reasonable RSD value of 3.5% for the current determination of 0.1 mM glucose, which is comparable with other glucose sensors, such as those described by Ci et al. (2014) and also Wang, L. et al. (2013) who yielded an acceptable RSD of 3.7% and 5.6%, respectively, for the current determination in the presence of glucose, depending on the number of modified glucose sensor. Such good stability and reproducibility make the developed sensor attractive for real applications.

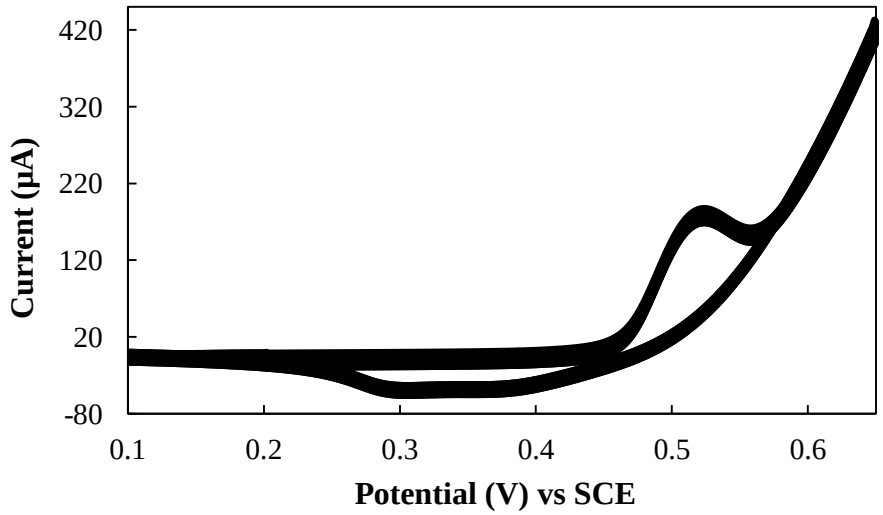

Figure 4.33: Repeated cyclic voltammograms of the PPy-NiO composites coated GCE in the presence of 0.1 mM glucose in NaOH (0.1 M) at scan rate 20 mVs^{-1}

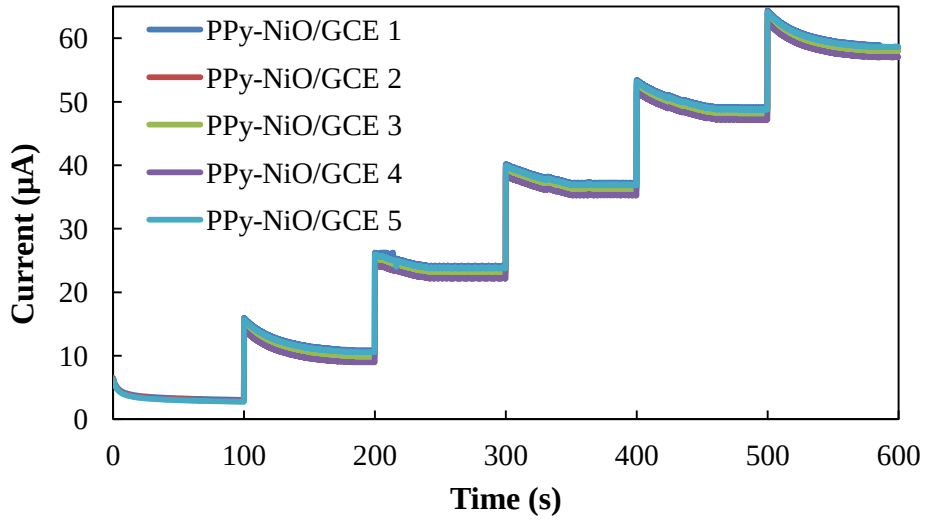

Figure 4.34: Amperometric responses of five different PPy-NiO composites coated GCEs upon successive addition of 0.1 mM glucose into NaOH (0.1 M) with an applied potential 0.53 V under stirring condition

Shelf-life

The shelf-life of the developed sensor was determined by investigating the current response of PPy-NiO composites coated GCE towards glucose with respect to storage time. The results are shown in Figure 4.35. After each investigation, the sensor

was washed with deionised water and stored at 4 ºC. Through this investigation, it was discovered that the modified GCE lost only 3.4% of its initial response over 1 week and it could keep up to 88.1% of the initial response to glucose after 2 weeks. This is comparable to the work done by Shahnavaz et al. (2014) as well as Shua et al. (2014) who investigated the shelf-life of different glucose sensors and found a range of shelf-life times from 1 to 15 days, subjected on the fabrication of glucose sensor.

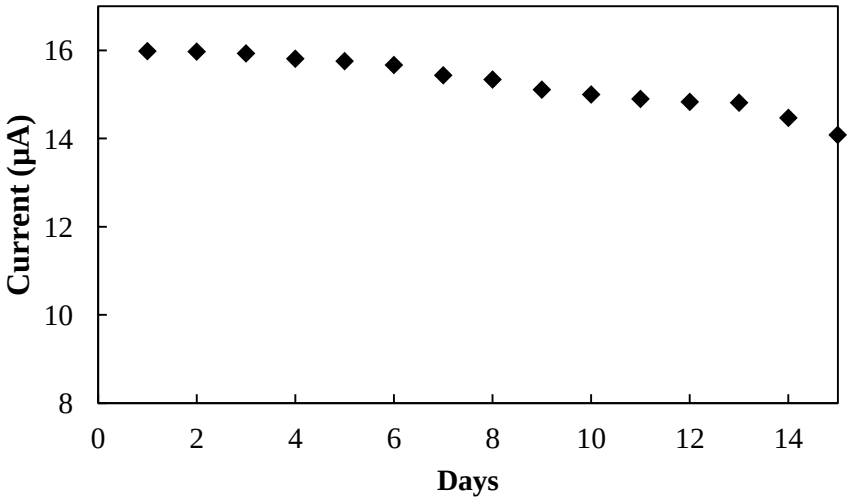

Figure 4.35: Shelf-life of PPy-NiO coated GCE in the presence of 0.1 mM glucose in NaOH (0.1 M) at 0.53 V

4.2.9 Investigation of the interfering compound and real sample analysis on the glucose detection

4.2.9.1 Effect of interference compounds

One challenge in non-enzymatic glucose detection is the specificity, as other organic substances could simultaneously oxidise at an applied potential of +0.53 V. In this study, possible interferences from some co-existing electroactive compounds in real samples such as ascorbic acid, fructose, sucrose and uric acid were chosen to evaluate

the selectivity of the sensor. Co-existing with glucose real samples, these substance concentrations are much lower than that of glucose. As shown in Figure 4.36, the interference studies were performed under optimum condition by comparing the current response to 0.1 mM glucose with 0.1 mM of each interfering substances. The substances did not interfere significantly to glucose detection which indicates a good selectivity. Thus, this developed sensor allows an accurate and selective non-enzymatic detection of glucose.

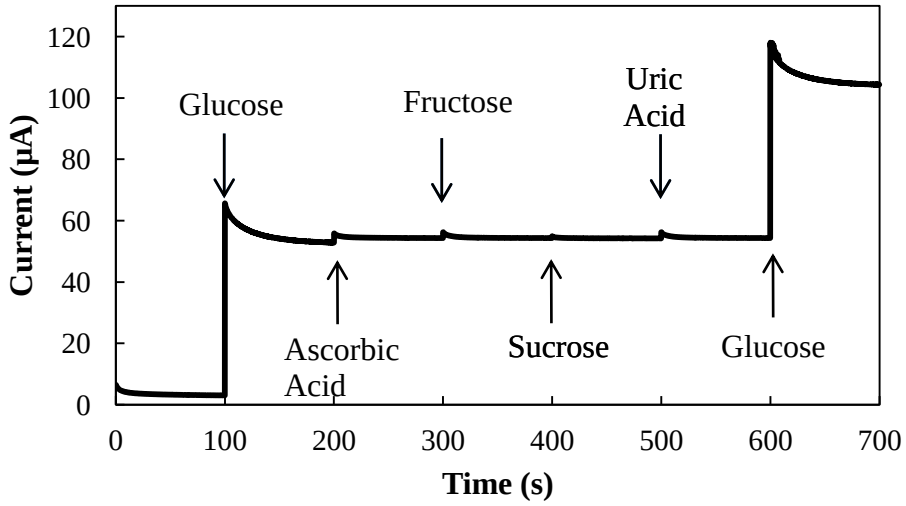

Figure 4.36: Amperometric responses of PPy-NiO composites coated GCE upon the successive addition of 0.1 mM glucose, ascorbic acid, fructose, sucrose and uric acid into NaOH (0.1 M) at 0.53 V under stirring condition

4.2.9.2 Application to commercial beverage and comparison with standard method

In order to evaluate the applicability and reliability of the proposed sensor, the detection of glucose in commercial beverage green tea was carried out and compared with the standard method UV-Vis spectroscopy (refer Chapter 3, Section 3.6.3). The real samples were purchased from market and the concentration of glucose was determined by using standard addition method (refer Chapter 3, Section 3.6.1). This was

achieved by adding NaOH (0.1 M) solution to a fixed volume of real sample (1 ml). All the measurements were performed four times. The content of glucose was calculated from the calibration plot shown in Figure 4.37. The obtained results are given in Table 4.5 which as can be seen are in good agreement with data obtained by the reference method (UV-Vis spectroscopy).

Table 4.5: Amperometric and UV-Vis spectrometric determination of glucose in commercial beverage green tea

Standard Concentration (mM)	**Amperometric measurements**		**UV-Vis spectrometric measurements**	
	RSD (%)[a]	**Recovery %**	**RSD (%)[a]**	**Recovery %**
0.05	0.869	96.75	0.118	97.90
0.1	0.933	98.62	0.704	99.58
0.15	0.915	98.47	0.586	99.13

[a] RSD (%) calculated from four measurements

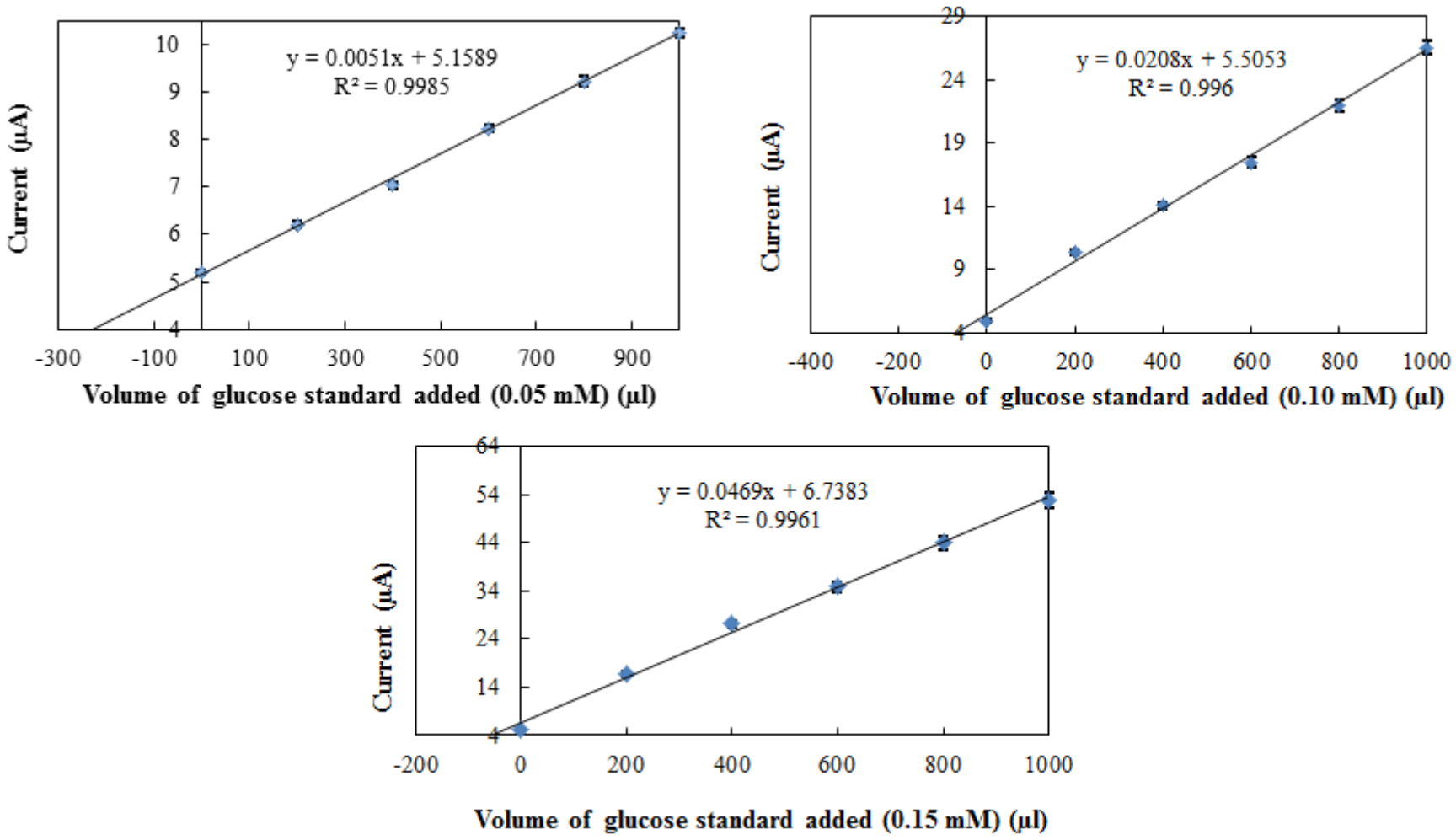

Figure 4.37: Calibration plots for determination of glucose in commercial beverage green tea measured with different concentration of standard solution of glucose in NaOH (0.1 M) with an applied potential 0.53 V. Average values and error bars were calculated from four measurements

4.3 Room temperature ionic liquid based silica-titania sol-gel matrix for hydrogen peroxide detection

The Si-Ti composites were synthesised by a sol-gel route in the presence of RTIL $[C_4MIm][NTf_2]$ as shown in Scheme 4.1, with the aim of obtaining microporous solids. The role of $[C_4MIm][NTf_2]$ content and their effect on the properties of these materials were evaluated. Subsequently, the development of Si-Ti/$[C_4MIm][NTf_2]$ sol to an enzymatic sensor for the enhanced detection of H_2O_2 is presented.

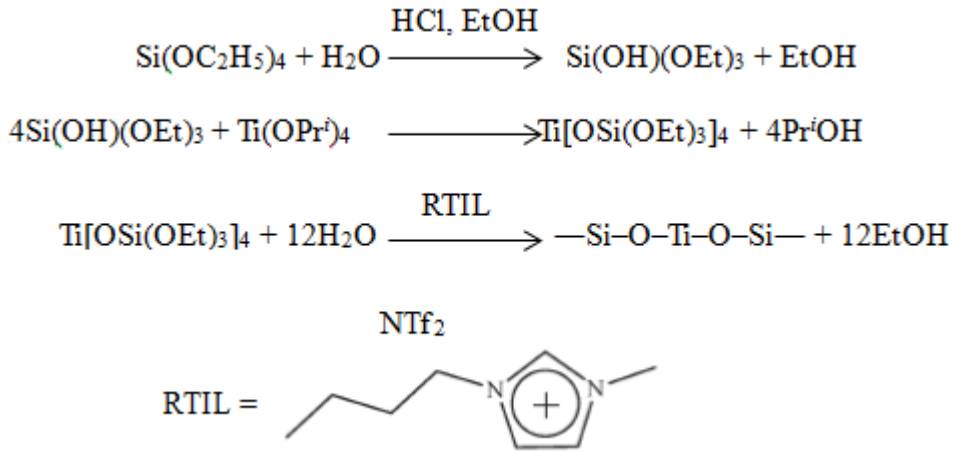

Scheme 4.1: Formation of Si-Ti gels using TEOS, TTIP and $[C_4MIm][NTf_2]$

It is very beneficial to fabricate a sensitive H_2O_2 sensor showing long-term stability since many biomolecules can be oxidised by oxidases to produce H_2O_2. The immobilisation of enzymes is one of the most important steps in the research of H_2O_2 electrochemical sensors. Recently, the introduction of sol-gel method to immobilise horseradish peroxidase (HRP) enzymes has been a trend in preparing H_2O_2 chemical sensors (Wang et al., 2000; Dõâaz et al., 1998). In this section, we tried to apply the synthesised composite for H_2O_2 sensor by immobilising horseradish peroxidase enzyme.

4.3.1 Characterisation of Si-Ti/[C_4IMm][NTf_2]

4.3.1.1 Fourier Transform Infrared

The Fourier Transform Infrared (FTIR) spectra of Si-Ti composite with and without RTIL [C_4MIm][NTf_2] are illustrated in Figure 4.38. In the FTIR spectrum of Si-Ti composite (0 wt%), the bands at 1059 cm^{-1} and 805 cm^{-1} correspond to asymmetric and symmetric stretching vibration of the Si-O-Si bonds (Mikushina et al., 2008; Murashkevich et al., 2008) and the band at 460 cm^{-1} correspond to bending vibration of Si-O-Si bonds (Shishmakov et al., 2012). While, the presence of shoulder band at 790 cm^{-1} is due to the symmetric stretching vibration of the Ti-O bonds of the TiO_4 tetrahedral (Murashkevich et al., 2008). The Si-O-Ti bond is characterised by the absorption band at 940 cm^{-1} and this band can also be attributed to the Si-OH bond (Vives & Meunier, 2008). The bending vibration of the trapped water molecules in the Si-Ti matrix was detected as a band at 3450 cm^{-1} and 1640 cm^{-1} (Chen, S. Y. et al., 2007; Zhang et al., 2005). These bands, especially band 1640 cm^{-1}, become weaker when the content of RTIL increases. The spectral characteristics of the Si-Ti composites with 10 to 90 wt% of [C_4MIm][NTf_2] as shown in Figure 4.38 are quite different from Si-Ti composite without [C_4MIm][NTf_2]. The new bands at 2900 cm^{-1} and 1576 cm^{-1} are corresponding to imidazolium cation alkyl groups and the in-plane C-C and C-N stretching vibration of the imidazolium ring, respectively (Shi & Deng, 2005). These bands exist in all Si-Ti composites in the presence of [C_4MIm][NTf_2] regardless of the amount of RTIL used and they become stronger as content of RTIL increases. Based on these results, it can be concluded that the vibrations of the [C_4MIm][NTf_2] molecular confined were severely affected due to the narrow space of pores in Si-Ti composite.

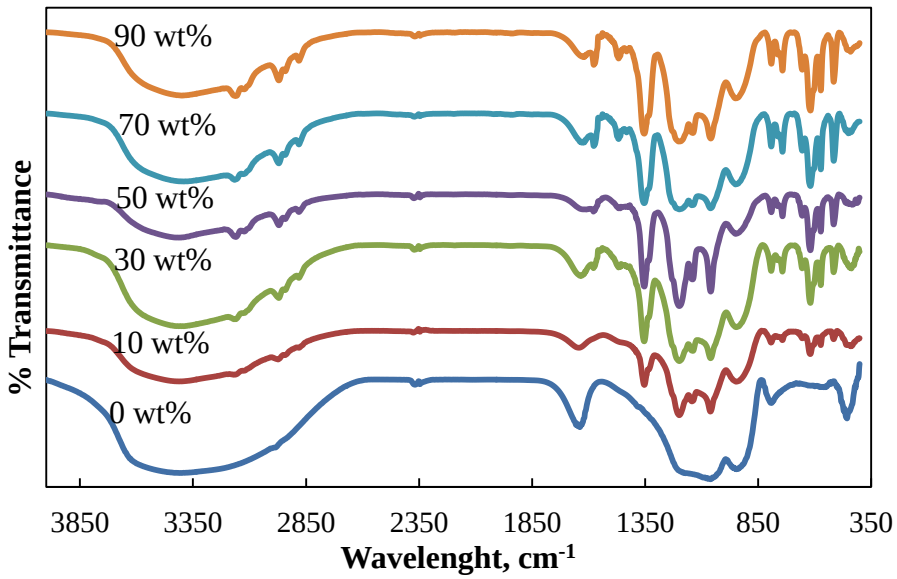

Figure 4.38: FTIR spectra of Si-Ti composite without and with different wt% of $[C_4MIm][NTf_2]$

4.3.1.2 Thermogravimetric analysis

Figure 4.39 represents thermogravimetric analysis (TGA) curve of Si-Ti composite with and without RTIL. In the first range of temperature at 50 – 140 ºC in TGA curves, the decomposition was observed for all the composites could be ascribed to the dehydration and evaporation of alcohol existing in the porous texture (Farag et al., 2008). While, the second range of temperature from 140 ºC to 340 ºC was attributed to the removal of the strongly bound water or the surface hydroxyl group in the composites. The combustion of the remaining alkoxy groups bind to silicon and titanium which results from the incomplete hydrolysis or condensation reactions can also contribute to these weight losses (Vives & Meunier, 2008). For Si-Ti composite (0 wt%) as shown in Figure 4.39, the weight loss occurred at 340 ºC indicating the decomposition of hydroxyl groups and organic molecules. Consequently, there is no weight loss for this composite and it can be concluded that the amorphous phase has changed to crystalline phase (Balachandran et al., 2010). The third range of temperature from 340 ºC to 470 ºC was observed for Si-Ti composite with 10 – 90 wt% RTIL.

These weight losses were assigned to the decomposition of $[C_4MIm][NTf_2]$ and the percentage of weight loss increased by increasing the content of RTIL. The forth range temperature (470 – 540 ºC) was also observed for Si-Ti composite with $[C_4MIm][NTf_2]$, which attributed to the oxidation of residue carbon. The Si-Ti composite without $[C_4MIm][NTf_2]$ starts to be decomposed at 150 ºC. On the other hand, Si-Ti composite with $[C_4MIm][NTf_2]$ starts to be decomposed at 180 ºC, which suggests that the composite with RTIL has increased the initial decomposition temperature and simultaneously, it also increased the final decomposition temperature from 390 ºC (without $[C_4MIm][NTf_2]$) to 430 ºC (with $[C_4MIm][NTf_2]$). This shows that the composite in the presence of RTIL is more stable than pure Si-Ti composite.

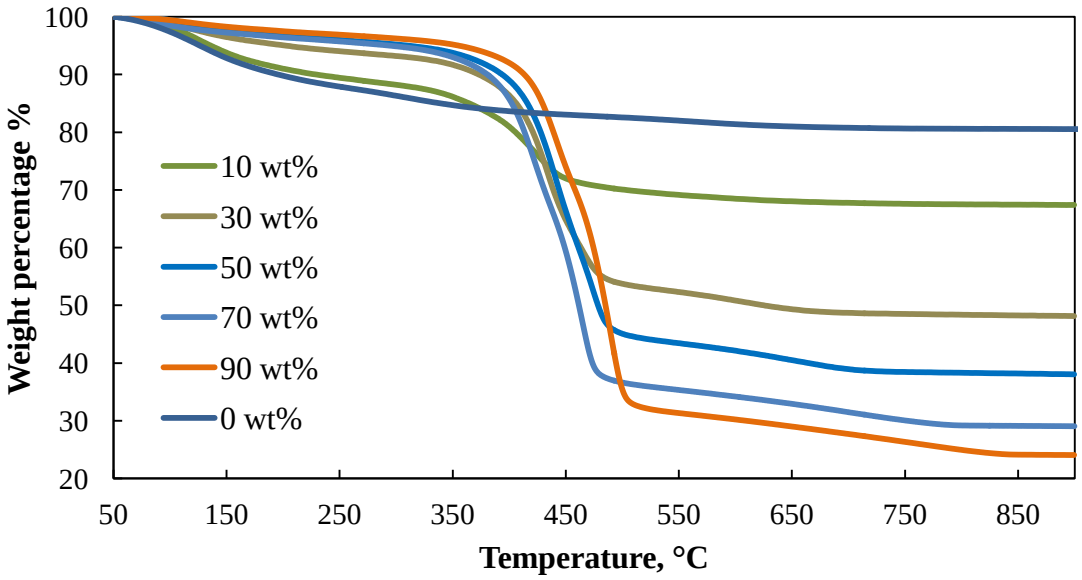

Figure 4.39: TGA curve of the Si-Ti composite without and with varied wt% $[C_4MIm][NTf_2]$

4.3.1.3 X-ray powder diffraction

The x-ray powder diffraction (XRPD) characterisation of Si-Ti composite with and without $[C_4MIm][NTf_2]$ was investigated and the results are presented in Figure

4.40. As can be seen, none of them shows any crystallites formation and the Si-Ti composites with various loading of $[C_4MIm][NTf_2]$ was amorphous after drying at 100 ºC. The Si-Ti composite with loading of 50 wt% $[C_4MIm][NTf_2]$ at different temperature was also studied. The XRPD patterns are shown in Figure 4.41 (A). It was observed that the crystallinity of TiO_2 increased with increasing temperature and in the range of temperature between 200 ºC and 800 ºC, the presence of TiO_2 anatase and rutile phase is observed while brookite phase was not detected. For the temperature lower than 200 ºC [Figure 4.41 (A iii-vi)], no diffraction peak is detected. This might indicate that the composites may contain very small amount of crystallites to the extent that within the resolution of XRPD device, no diffraction peaks could be obtained (Farag et al., 2008). However, these diffraction peaks were transformed to anatase phase after 200 ºC with increasing peak intensity. This suggests the progress of the crystallisation of TiO_2 (Gunji et al., 2005). The highest anatase crystallinity was observed at 600 ºC and then the crystalline phase started to be transformed to rutile at around 600 ºC and the rutile phase completely formed at 800 ºC. Whereas, Si-Ti composite without $[C_4MIm][NTf_2]$ shows a diffraction peak for anatase at lower temperature of 150 ºC [Figure 4.41 (B)] as compared Si-Ti composite with $[C_4MIm][NTf_2]$. It can be assumed that the presence of RTIL stabilises the anatase phase and elevates the temperature at which the phase transformation to rutile occurs. This might enhance the activity of the prepared composites as a catalyst.

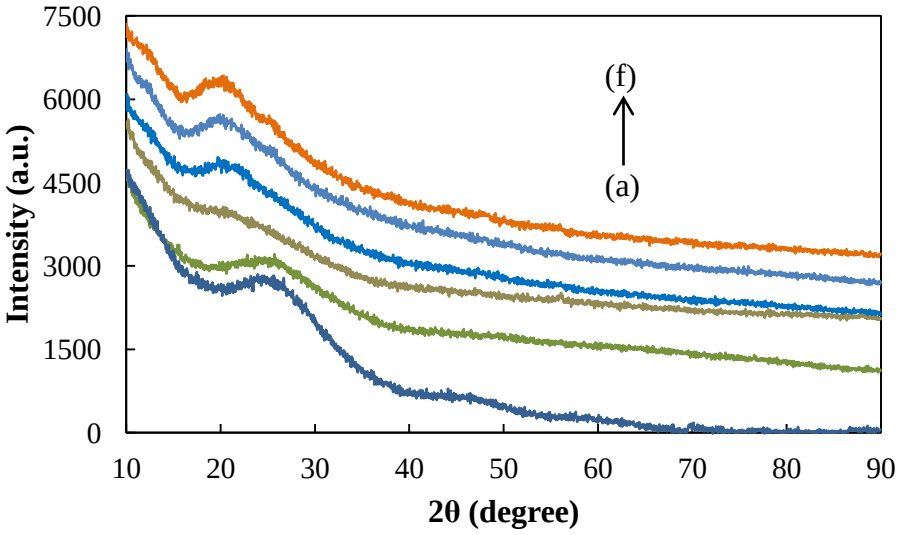

Figure 4.40: XRPD patterns of Si-Ti composite with $[C_4MIm][NTf_2]$ loading of: (a) 0 wt%, (b) 10 wt%, (c) 30 wt%, (d) 50 wt%, (e) 70 wt% and (f) 90 wt% after being dried at 100 ºC

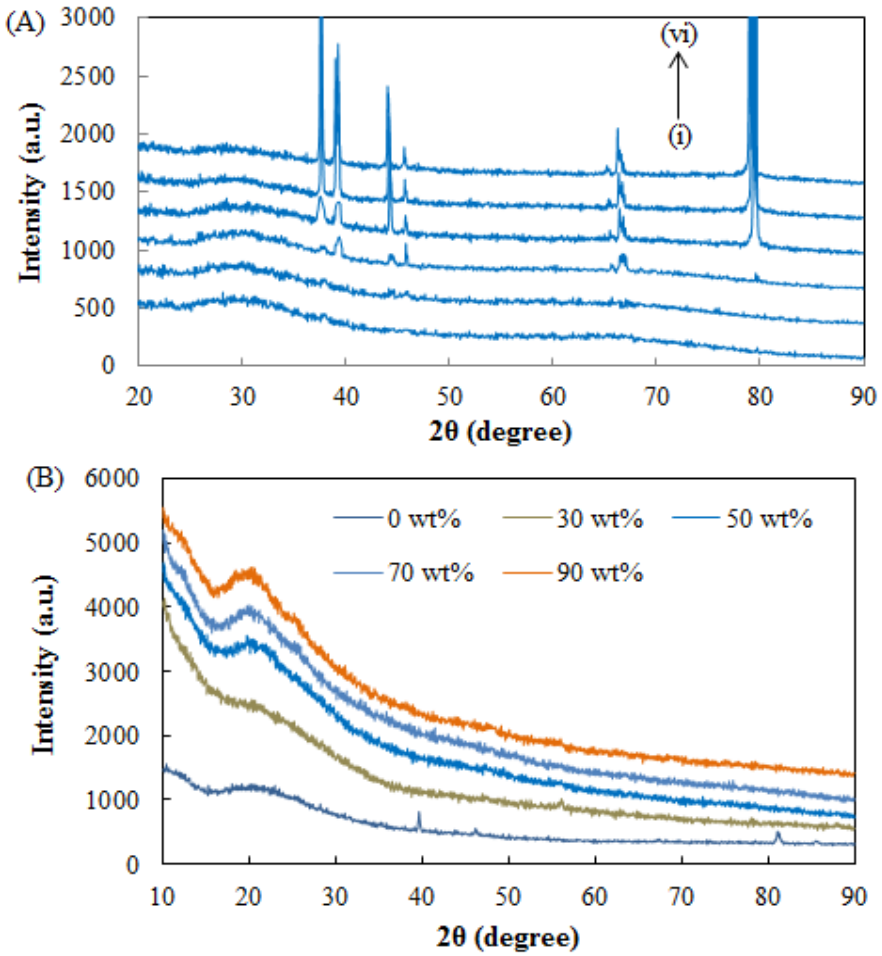

Figure 4.41: (A) XRPD patterns of Si-Ti composite with 50 wt% loading of $[C_4MIm][NTf_2]$ at different temperature (i) 80 ºC, (ii) 100 ºC, (iii) 200 ºC, (iv) 400 ºC, (v) 600 ºC and (vi) 800 ºC; (B) XRPD patterns of Si-Ti composite with different wt% loading of $[C_4MIm][NTf_2]$ at 150 ºC

4.3.1.4 Field emission scanning electron microscopy

Figure 4.42 shows the field emission scanning electron microscopy (FESEM) images of Si-Ti composites with and without various loadings of $[C_4MIm][NTf_2]$, in which particle/agglomerate morphology can be observed. The particle/agglomerate size of Si-Ti composites with $[C_4MIm][NTf_2]$ is a range from sub-micron particles to agglomerates of 3 – 10 μm. The pure Si-Ti composite shows that the sample exhibits an irregular morphology as seen in Figure 4.42 (A). The FESEM images of Si-Ti composites revealed a marked effect as the wt% loading of $[C_4MIm][NTf_2]$ increased. When the $[C_4MIm][NTf_2]$ was introduced, the irregular morphology changed to agglomeration structure, which conforming the presence RTIL on the Si-Ti composites. It was observed in Figure 4.43 (B – D) that Si-Ti composites aggregate together with $[C_4MIm][NTf_2]$ to form agglomerate particles and the number of agglomerate particles increases with the increase of the amount of the $[C_4MIm][NTf_2]$. The Si-Ti composites with lower loading of the RTIL were more opaque and white in appearance, while at higher loading, the composites become more transparent. Moreover, the gels were brittle when smaller volume of the RTIL were added and vice versa.

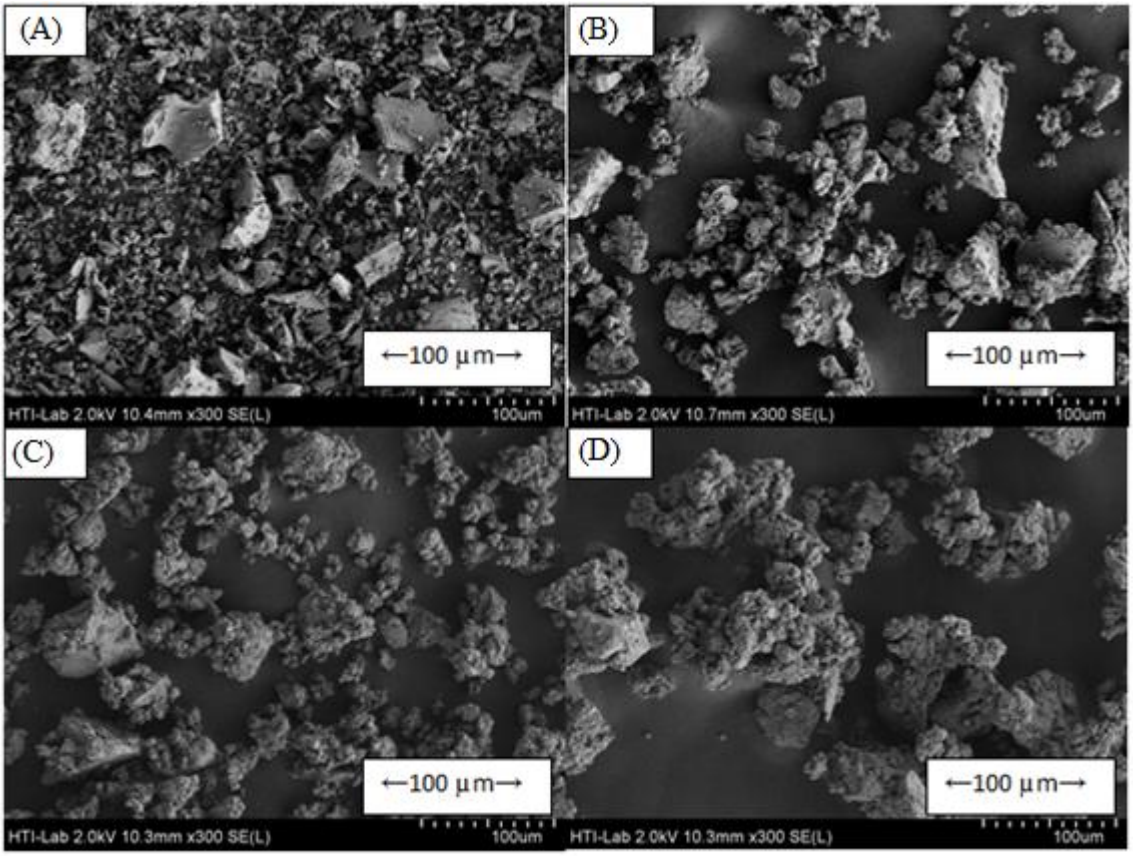

Figure 4.42: FESEM analysis of Si-Ti composites with (A) 0 wt%, (B) 30 wt%, (C) 50 wt% and (D) 90 wt% of $[C_4MIm][NTf_2]$

4.3.1.5 Elemental analysis

The elemental analysis was obtained by energy dispersive x-ray (EDX) analysis and CHN as listed in Table 4.6 and Table 4.7, respectively. The EDX analysis shows the existence of silicon, titania and oxygen in the Si-Ti composites with the presence and absence of $[C_4MIm][NTf_2]$. While, the presence of hydrogen, carbon and nitrogen in the refluxed Si-Ti/$[C_4MIm][NTf_2]$ composites was confirmed by CHN analysis. As can be seen in Table 4.6, the percentage of Si and Ti were found around 20 – 25% and 12 – 17%, respectively in Si-Ti composites with and without $[C_4MIm][NTf_2]$. Si-Ti composites with the RTIL show the presence of nitrogen composition indicating a successful encapsulation of imidazole on the Si-Ti matrix. The amounts of confined RTIL were determined by the presence of nitrogen in the composites through CHN

analysis (Table 4.7). The calculated confined RTIL for Si-Ti composites with various wt% of $[C_4MIm][NTf_2]$ was almost in the range of 0.032 – 0.034 $gmol^{-1}$.

Table 4.6: EDX analysis of Si-Ti composite with and without $[C_4MIm][NTf_2]$

$[C_4MIm][NTf_2]$ loading (wt%)	Si%	Ti%	O%	N%
0	25.2	12.6	62.2	-
10	25.4	12.9	59.6	2.2
30	24.8	13.8	49.8	11.6
50	21.7	10.3	49.5	18.6
70	22.9	13.5	43.9	19.7
90	20.1	17.1	43.5	19.5

Table 4.7: CHN analysis of Si-Ti composites with $[C_4MIM][NTf_2]$ after reflux

$[C_4MIm][NTf_2]$ loading (wt%)	C%	H%	N%
0	0.233	2.917	0.070
10	1.537	3.469	0.303
30	1.931	4.478	0.311
50	1.170	2.395	0.313
70	1.666	1.713	0.308
90	4.078	3.849	0.438

4.3.1.6 N_2 adsorption-desorption analysis

The surface analysis of Si-Ti composites with and without the RTIL was determined by the N_2 adsorption-desorption and BET analysis. N_2 adsorption-desorption isotherms of the refluxed Si-Ti composites with $[C_4MIm][NTf_2]$ loading from 10 wt% to 90 wt% shows a Type I isotherm, indicating a microporous or nano-porous structure as can be seen in Figure 4.43. Based on what can be observed in Table 4.8 and Figure 4.44, all the Si-Ti composites with different content of the RTIL showed the microporous characteristics with average pore diameter in the range of 0.0017 –

0.00205 μm and BET surface area of 190 – 283 m^2/g. The average pore diameter, pore volume and BET surface area for $[C_4MIm][NTf_2]$ loading of 10 wt% were 0.00171 μm, 0.08 cm^3/g and 190.51 m^2/g, respectively. By the way of $[C_4MIm][NTf_2]$ loading being increased to 30 wt% and 50 wt%, the average pore diameter correspondingly increased to 0.00182 μm and 0.00198 μm, respectively. The pore size of the Si-Ti composites considerably enlarged with $[C_4MIm][NTf_2]$ loading increasing from 10 wt% to 50 wt%. It was thought that the increased amount of the RTIL would induce the stacking arrangement of its cation and anion and results in the increase of pore diameter of the composite for the supramolecular structure of RTIL (Liu et al., 2005a). However, with further increasing of $[C_4MIm][NTf_2]$ loading to be 70 wt% and 90 wt%, the average pore diameter and BET surface area was almost the same with 50 wt% of $[C_4MIm][NTf_2]$ as noticed in Table 4.8. It can be said that the pore size and surface area of Si-Ti composites was not significantly affected by the variations of the RTIL content from 50 wt% to higher. Thus, the pore structure of the obtained microporous Si-Ti composites can be tuned by the variations of the RTIL content in the synthesis system, that is, the pore size increased with initial increasing of the RTIL content.

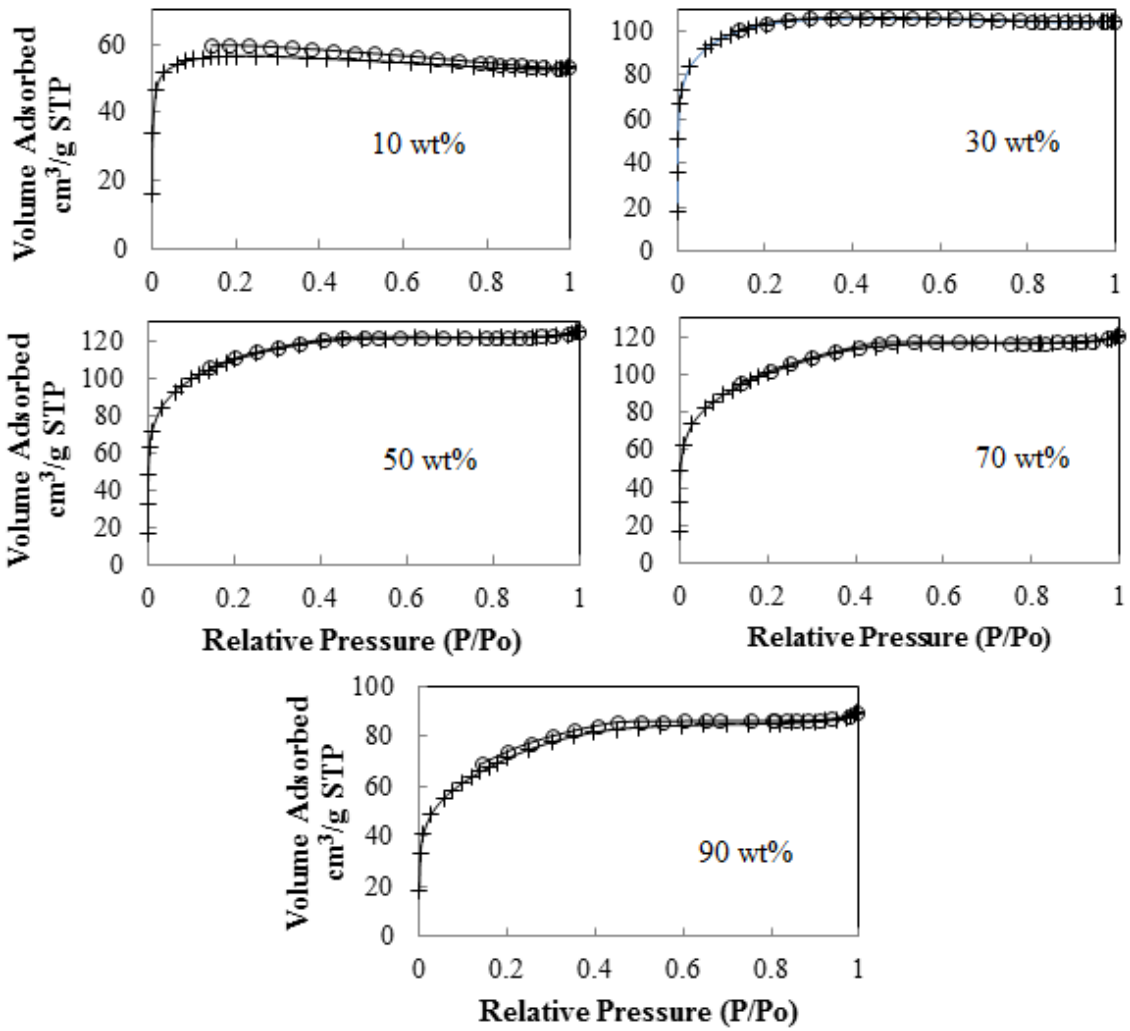

Figure 4.43: N_2 adsorption-desorption isotherms of Si-Ti composites with $[C_4MIm][NTf_2]$ loading from 10 to 90 wt%

Table 4.8: Pore structure of Si-Ti composites with various $[C_4MIm][NTf_2]$ loading

$[C_4MIm][NTf_2]$ loading wt%	Average pore diameter (nm)	Pore volume (cm^3/g)	BET surface area (m^2/g)
0	1.50	0.02	71.87
10	1.71	0.08	190.51
30	1.82	0.16	354.53
50	1.98	0.19	385.67
70	1.95	0.18	355.63
90	1.98	0.14	282.08

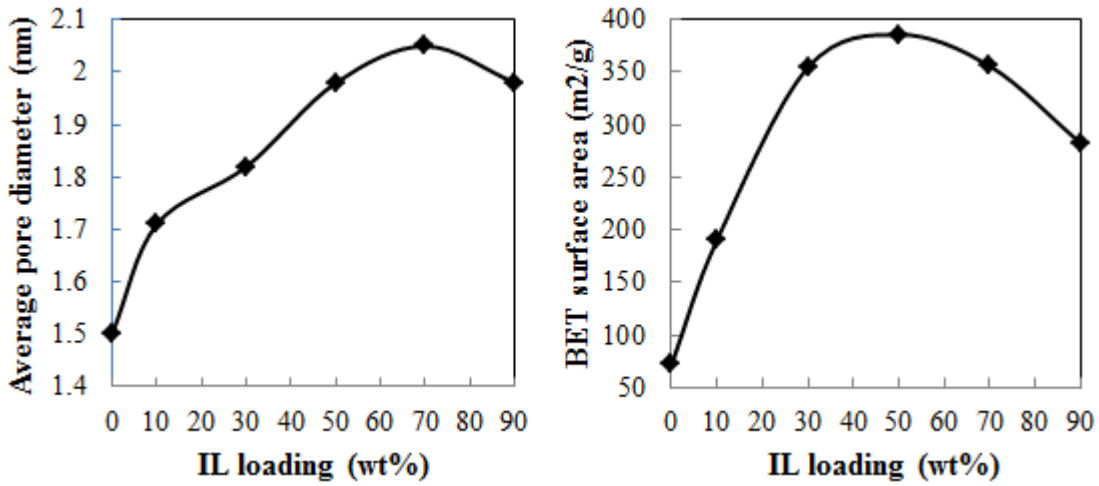

Figure 4.44: Effect of [C_4MIm][NTf_2] loading on the pore size and BET surface area of Si-Ti composite

4.3.2 Development of Si-Ti/[C_4MIm][NTf_2]-HRP/Fc modified GCE for the detection of H_2O_2

4.3.2.1 Electroactivity of Si-Ti/[C_4MIm][NTf_2]-HRP/Fc modified GCE

In this section, a simple and new enzymatic H_2O_2 sensor based on HRP encapsulated into Si-Ti/[C_4MIm][NTf_2] was attempted to be developed. Here, the "bilayer" configuration (ferrocene: HRP-sol-gel) was selected to fabricate enzymatic sensor. There was no obvious redox reaction between the HRP and the H_2O_2, if no electron mediators existed in the redox system. Among the various mediators, ferrocene (Fc) is a satisfactory candidate for the amperometric H_2O_2 sensor by measuring the reduction current. The one-electron oxidation of Fc to the stable ferrocenium cation is a simple electron transfer reaction, in which there are no difficulties arising from adsorption or associated chemical reaction (Wang et al., 2005). Therefore, Fc is employed as the mediator for determination of H_2O_2 in many studies (Fan et al., 2012; Luo et al., 2011; Şenel et al., 2010). In this study, Fc and HRP encapsulated in Si-Ti/[C_4MIm][NTf_2] were immobilised on the GCE surface in sequence. We expected

that the Si-Ti/[C_4MIm][NTf_2] matrix could improve the stability of ferrocene on the electrode and also probably, it could protect the encapsulated HRP from denature. As a mediator, Fc accelerated the redox reaction. The possible mechanism of the electron transfer is shown in Scheme 4.2.

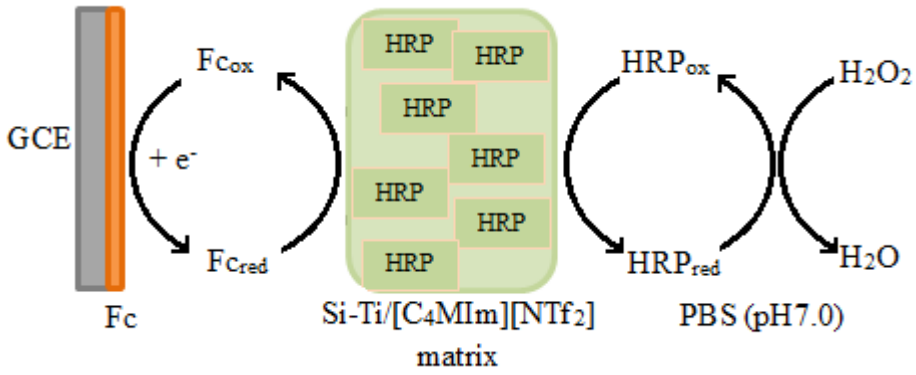

Scheme 4.2: The possible mechanism of the electroactivity of HRP-Si-Ti/[C_4MIm][NTf_2]/Fc modified GCE

The electrochemical behaviour of the enzyme electrode was studied using cyclic voltammetry. Figure 4.45 shows the cyclic voltammograms of the Fc modified GCE and Fc modified HRP-Si-Ti/[C_4MIm][NTf_2] GCE in 0.05 M PBS (pH 7.0). It can be seen that both electrodes have only one pair of quasi-reversible redox peaks of Fc and the peak current slightly increased in the presence of HRP. Thus, the presence of HRP is in favour of the electron transfer between Fc and GCE surface.

The cyclic voltammograms of the Fc modified GCE and Fc modified HRP-Si-Ti/[C_4MIm][NTf_2] GCE in 0.05 M PBS (pH 7.0) in the presence of H_2O_2 are shown in Figure 4.46. As can be seen, there is an obvious decrease of the cathodic and anodic peak currents which indicates that H_2O_2 did not oxidise Fc_{red} to Fc_{ox} in the presence of HRP and moreover, the Fc_{ox} is subsequently not reduced at the GCE surface. This might cause ferrocenium as the water-soluble oxidised form of Fc is easily leached out from

the electrode surface and leads to the instability of the enzyme electrode (Wang et al., 2005).

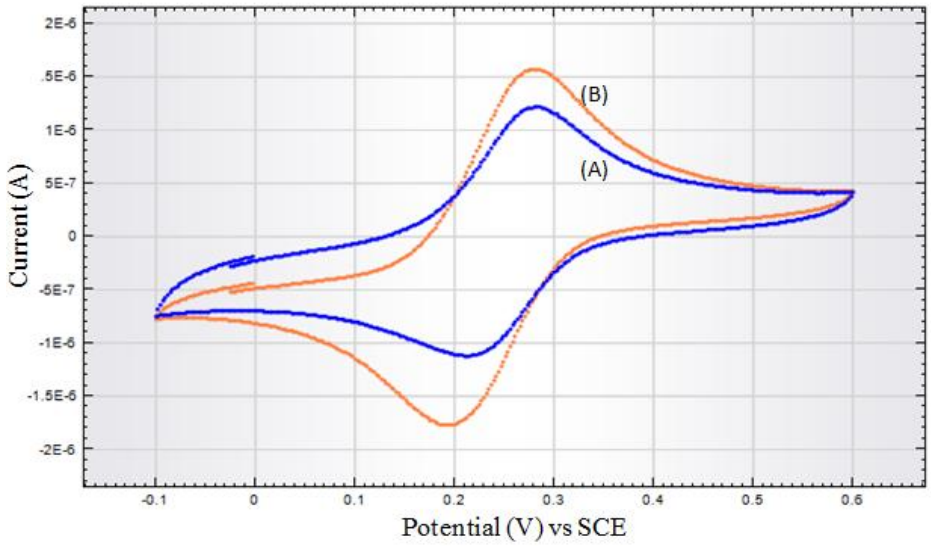

Figure 4.45: Cyclic voltammograms of (A) Fc mediated GCE and (B) Fc mediated HRP/Si-Ti/[C_4MIm][NTf_2] GCE in 0.05 M PBS (pH 7.0) at scan rate 50 mVs^{-1}

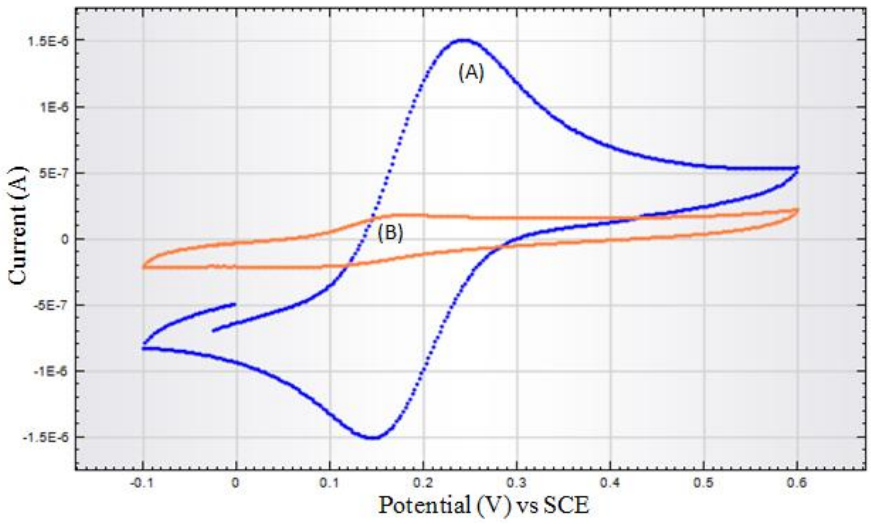

Figure 4.46: Cyclic voltammograms of Fc mediated HRP/Si-Ti/[C_4MIm][NTf_2] GCE in 0.05 M PBS (pH 7.0) in absence (A) and presence (B) of 0.2 mM H_2O_2 at scan rate 50 mVs^{-1}

Therefore, in a way to get the response, the Fc modified HRP/Si-Ti/[C_4MIm][NTf_2] GCE in 0.05 M PBS (pH 7.0) containing 0.2 mM H_2O_2 was

investigated with different ratio contents of Si and Ti in the sol-gel matrix. The results are presented in Figure 4.47. As noticed, the cyclic voltammogram shows a couple of well-defined oxidation and reduction peaks of Fc in the absence of H_2O_2 for all Si: Ti ratio. However, neither one gives a significant change in redox current after introducing H_2O_2 into 0.05 M PBS (pH 7.0). These results suggest that the presence of H_2O_2 does not favour the electron transfer between Fc and GCE surface. In addition, the repeatability and reproducibility of this modified electrode is very weak (produced the same results after several trials).

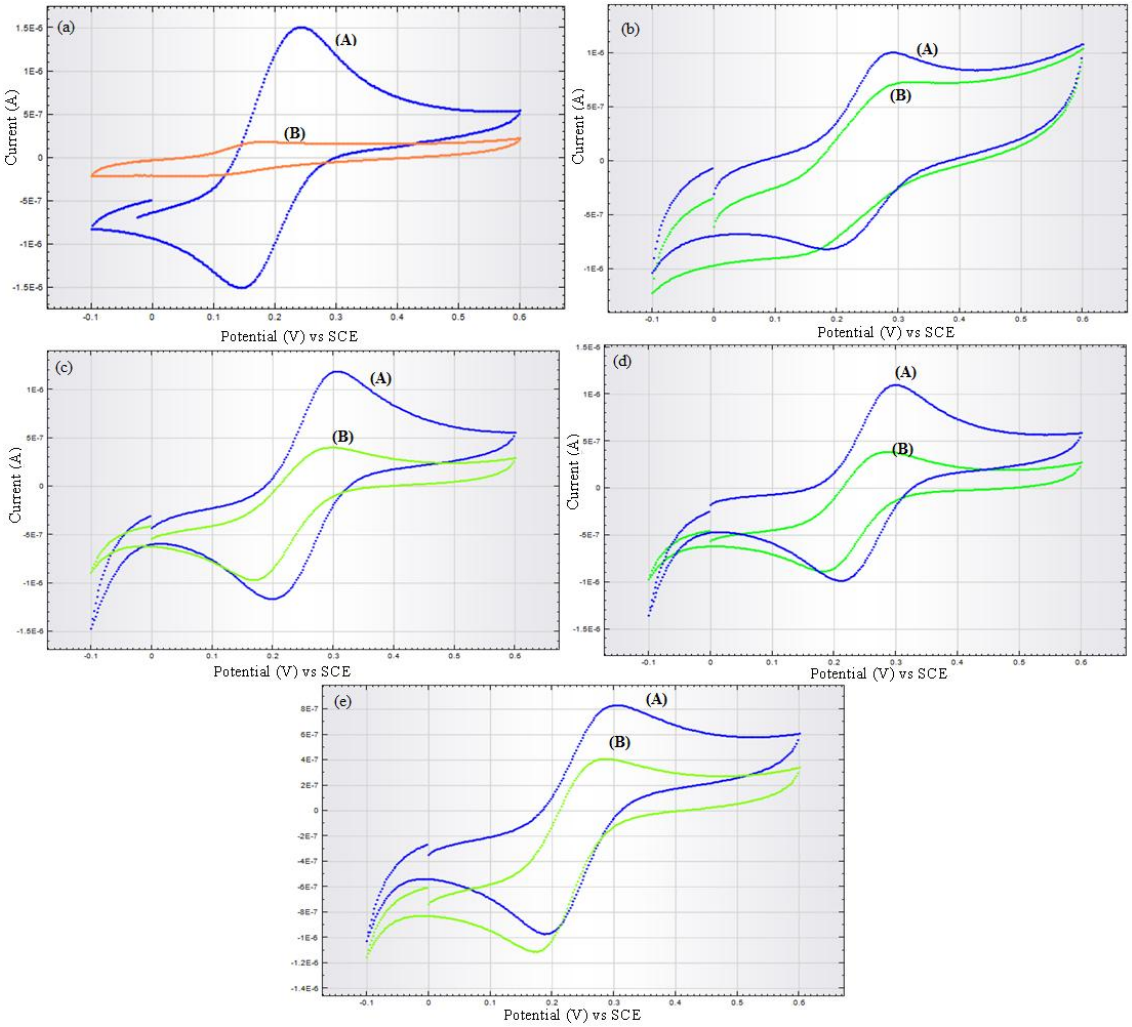

Figure 4.47: Cyclic voltammograms of Fc modified HRP-Si-Ti/$[C_4MIm][NTf_2]$ GCE with different Si: Ti ratio (a) 1:1; (b) 2:1; (c) 3:1; (d) 4:1 and (e) 5:1 at scan rate 50 mVs^{-1} in 0.05 M PBS (pH 7.0) containing (A) 0 and (B) 0.2 mM H_2O_2

Besides, film cracking is another problem encountered during fabrication of this sensor. This might be due to the fact that Fc-HRP-Si-Ti/[C_4MIm][NTf_2] film undergoes substantial changes in structure and solvent content during drying process, possibly leading to extensive cracking (Goring & Brennan, 2002). And, the film on the surface of GCE undergoes further cracking during cyclic voltammetry investigation (Figure 4.48), which caused leaching of HRP from the surface of electrode and could not produce a significant response.

Another possible reason of the failure is that the HRP might lose its activity during the encapsulation into Si-Ti/[C_4MIm][NTf_2]. This may be due to the preparation method of Fc modified HRP-Si-Ti/[C_4MIm][NTf_2] GCE. The sol-gel film was prepared from diluted stock standard sol-gel solution with a high volume of alcohol, which was not effective for enzyme encapsulation. This could lead to low enzyme loading or low film stability, which results in limited dynamic range and low sensitivity. Because of these drawbacks, the optimisation of this enzymatic sensor could not proceed further. Time is needed to solve these problems and fabricate H_2O_2 sensor based on Fc modified HRP-Si-Ti/[C_4MIm][NTf_2] GCE with more reliable properties.

Figure 4.48: Fc modified HRP-Si-Ti/[C_4MIm][NTf_2] after cyclic voltammetry investigation in 0.05 M PBS (pH 7.0) containing 0.2 mM H_2O_2

CHAPTER 5

CONCLUSION AND RECOMMENDATION

5.1 Conclusion

In this study, a systematic investigation has been conducted on the synthesis, characterisation, fabrication and chemical sensing property of the composite materials. The following outcomes have been achieved.

The new nanocomposite of PPy-Co was successfully synthesised and characterised using various tools and the results obtained were compared with polypyrrole and cobalt nanoparticles. The FTIR results confirmed the interaction between the polymer backbone and the cobalt nanoparticles of PPy-Co nanocomposites by showing the characteristics of the shifted peaks of pure polypyrrole. The TGA results showed that the PPy-Co nanocomposite has a better thermal stability compared to pristine polypyrrole. The FESEM images of this nanocomposite indicated a clear difference in the surface morphologies with high surface area. Meanwhile, the XRPD results confirmed that cobalt(II) is reduced to cobalt in the presence of pyrrole monomer and is protected by the polypyrrole. The electrochemical oxidation of H_2O_2 was achieved on the modified GCE coated with PPy-Co nanocomposites. The optimum response of this modified GCE towards H_2O_2 was observed at applied potential 0.9 V, 500 µl of pyrrole content and pH 7.0. The optimised modified sensor could detect H_2O_2 in a linear range of 20 µM to 80 mM with two linear segments (low and high concentrations of H_2O_2). The first linear segment ranges from 20 µM to 1 mM with a correlation coefficient (R^2) of 0.990 and sensitivity of 103.48 $\mu AmM^{-1}cm^{-2}$. While, the

second linear segment ranges up to 80 mM with a correlation coefficient (R^2) of 0.991 and sensitivity of 10.80 $\mu AmM^{-1}cm^{-2}$. The detection limit of both ranges is 2.05 μM and 19.64 μM, respectively. Besides, these nanocomposites modified GCE showed a good immunity from interference of electro-active materials towards the oxidation of H_2O_2 detection. Additionally, we proved that the modified electrode was successfully applied to contact lens cleaning solution real sample with recovery 96 – 98%.

Another composite comprising of polypyrrole and nickel oxide was successfully synthesised and characterised by various analytical techniques. The FTIR results indicated a strong interaction between polypyrrole and nickel oxide particles by showing their characteristic peaks in the spectrum. While, these composites proved to have a better thermal stability than pure polypyrrole. The FESEM results of PPy-NiO showed a needle-like structure with 330 ± 10 nm in width and also showed the effect of pyrrole monomers on the morphology of the composites. Meanwhile, the XRPD results confirmed that NiO particles are homogeneously and extensively dispersed in the PPy matrix. Then, the electrocatalytic performance of the PPy-NiO modified GCE towards oxidation of glucose was investigated by cyclic voltammograms and chronoamperometry method. The PPy-NiO composites modified GCE showed a suitable mediator to shuttle the electron between the glucose and GCE in alkaline medium and also facilitate electrochemical regeneration following the electron exchange with glucose at optimised condition (applied potential 0.53 V, 500 μl of pyrrole monomer content and 0.1 M NaOH). At this optimised condition, the modified GCE could detect glucose in a linear range of 0.01 – 0.50 mM and 1 – 20 mM with detection limit of 0.33 μM and 5.77 μM, respectively. While, the sensitivity of these two concentrations ranges are 1094.80 $\mu AmM^{-1}cm^{-2}$ and 62.87 $\mu AmM^{-1}cm^{-2}$, respectively. Moreover, this modified GCE indicated a good reproducibility with RSD 3.5% and also

showed a good selectivity in which co-existing substances in real samples such as ascorbic acid, fructose, sucrose and uric acid did not interfere significantly to glucose detection. Finally, we applied this PPy-NiO modified GCE to a commercial beverage green tea real sample.

Besides, Si-Ti composite in the presence of $[C_4MIm][NTf_2]$ was successfully synthesised as a microporous material via sol-gel method under room reaction conditions. The synthesised composite was characterised by various tools and the results obtained being compared with Si-Ti composite without RTIL. The FTIR results showed the presence of C-N groups, which indicated the presence of RTIL in the Si-Ti matrix. The FESEM results revealed that the presence of RTIL increased the pore size, while according to BET results the Si-Ti composite with RTIL had 191 – 386 m^2g^{-1} surface area. Moreover, the BJH pore size distribution revealed that the composite exhibited microporous with an average pore diameter of 1.70 – 2.12 nm. This composite was then fabricated as an enzymatic sensor using HRP to study catalytic activity towards H_2O_2 reduction. But, unfortunately this enzymatic sensor is failed to fabricated due to the film cracking and also the interaction between HRP/Si-Ti/$[C_4MIm][NTf_2]$ and H_2O_2/Si-Ti/$[C_4MIm][NTf_2]$ may lead to HRP denaturation and calibration drift.

5.2 Challenges and future perspectives

A wide range of new conducting polymer-metal nanocomposites is relied upon to enlarge the area of biosensors. Different techniques for the synthesis of one-dimensional conducting polymer-metal nanocomposites are liable to lead in new bio-sensing applications. The capability to functionalise the PPy-Co and PPy-NiO composites with the preferred groups to bind target biomolecules and doping these with

electronically active materials to achieve improved charge transfer, may prepare for new approaches for biosensor advancement. The synthesis of conducting polymer-metal nanocomposites with different morphologies at the nano level may offer a appropriate domain for obtaining the oriented immobilisation of desired biomolecules and consequently amplified signals. These conducting polymer-metal nanocomposites can be fabricated and tried in desired patterns such as sensor arrays, for the development of functional integrated devices. More studies on using this method to prepare the metal oxide nanostructures coated with conducting polymers for electrochemical sensing properties are being extended to other materials.

Sensor development is a difficult work and takes years of research. But, within the short period, it was really a tedious task to overcome the challenges related to fabrication of Si-Ti/[C_4MIm][NTf_2] composite based enzymatic sensor for H_2O_2. The work carried out for this material has opened several scopes of future researches based on proper selection of substances to form a better matrix for enzyme immobilisation for quality assessment of biosensor in particular. Thus, continued optimisation and improvement of the enzyme immobilisation and electrode fabrication process of Si-Ti/[C_4MIm][NTf_2] composite may be needed to fabricate H_2O_2 sensor with more reliable properties.

REFERENCES

Abo, M., Urano, Y., Hanaoka, K., Terai, T., Komatsu, T. & Nagano, T. (2011). Development of a Highly Sensitive Fluorescence Probe for Hydrogen Peroxide. *Journal of the American Chemical Society, 133*(27): 10629-10637.

Advani, S.G. (2007). *Processing and Properties of Nanocomposites*: World Scientific. pp. 450.

Ahmadalinezhad, A. (2011). *Nanomaterial-based Electrochemical Sensors for the Detection of Glucose and Cholesterol.* (Degree of Doctor of Philosophy in Biotechnology), Lakehead University.

Ajayan, P.M., Schadler, L.S. & Braun, P.V. (2003). *Nanocomposite Science and Technology*: Wiley, VCH Verlag GmbH Co. KGaA, Weinheim. pp. 10, 77-80, 111, 112.

Aldissi, M. (1992). *Intrinsically Conducting Polymers: An Emerging Technology*: Springer Science & Business Media, pp. 7.

Aleahmada, M., Taleghania, H.G. & Eisazadehb, H. (2011). Preparation and characterization of PAni/NiO nanocomposite using various surfactants. *Synthetic Metals, 161*: 990-995.

Ali, A., Israr-Qadir, M., Wazir, Z., Tufail, M., Ibupoto, Z.H., Jamil-Rana, S., . . . Willander, M. (2014). Cobalt oxide magnetic nanoparticles–chitosan nanocomposite based electrochemical urea biosensor. *Indian Journal of Physics*, DOI 10.1007/s12648-014-0594-3.

Antunes, F., Cadenas, E. & Brunk, U. (2001). Apoptosis induced by exposure to a low steady-state concentration of H_2O_2 is a consequence of lysosomal rupture. *Biochemical Journal, 356*: 549-555.

Atta, N.F. & El-Kady, M.F. (2010). Novel poly(3-methylthiophene)/Pd, Pt nanoparticle sensor: Synthesis, characterization and its application to the simultaneous analysis of dopamine and ascorbic acid in biological fluid. *Sensors and Actuators B: Chemical, 145*: 299–310.

Babonneau, F., Doeuff, S., Leaustic, A., Sanchez, C., Cartier, C. & Verdaguer, M. (1988). XANES and EXAFS Study of Titanium Alkoxides. *Inorganic Chemistry, 27*: 3166-3172.

Bai, H., Li, C., Chen, F. & Shi, G. (2007). Aligned three-dimensional microstructures of conducting polymer composites. *Polymer, 48*(18): 5259-5267.

Bai, J. & Zhou, B. (2014). Titanium dioxide nanomaterials for sensor applications. *Chemical Reviews, 114*(19): 10131-10176.

Balachandran, K., Venckatesh, R. & Rajeshwari, S. (2010). Synthesis of Nano TiO_2-SiO_2 Composite Using Sol-Gel Method: Effect on Size, Surface Morphology and Thermal Stability. *International Journal of Engineering Science and Technology, 2*: 3695-3700.

Bard, A.J. & Faulkner, L.R. (2000). *Electrochemical Methods: Fundamentals and Applications* (2 ed.): Wiley.

Batool, A., Kanwal, F., Imran, M., Jamil, T. & Siddiqi, S. (2012). Synthesis of polypyrrole/zinc oxide composites and study of their structural, thermal and electrical properties. *Synthetic Metals, 161*: 2753−2758.

Bavastrello, V., Stura, E., Carrara, S., Erokhin, V. & Nicolini, C. (2004). Poly(2,5-dimethylaniline)–MWNTs nanocomposite: a new material for conductometric acid vapours sensor. *Sensors and Actuators B: Chemical, 98*(2-3): 247-253.

BaytekİN, S. (2009). *Synthesis and Characterization of Polypyrrole Nanoparticles and Their Nanocomposites With Polypropylene.* (Master), Middle East Technical University.

Bencsik, G., Janáky, C., Endrődi, B. & Visy, C. (2012). Electrocatalytic properties of the polypyrrole/magnetite hybrid modified electrode towards the reduction of hydrogen peroxide in the presence of dissolved oxygen. *Electrochimica Acta, 73*: 53-58.

Bhattacharyya, S. & Snehesh, T.S. (2015). Effect of cobalt oxide additive on the fired properties of tri-axial ceramic. *Ceramics International, 41*(1): 61-67.

Bian, L.-J., Zhang, J.-H., Qi, J., Liu, X.-X., Dermot, D. & Lau, K.-T. (2010). Immobilization of molybdenum oxide in polyaniline and electro-catalytic properties of the composite modified electrode. *Sensors and Actuators B, 147*: 73-77.

Bian, X., Lu, X., Jin, E., Kong, L., Zhang, W. & Wang, C. (2010). Fabrication of Pt/polypyrrole hybrid hollow microspheres and their application in

electrochemical biosensing towards hydrogen peroxide. *Talanta, 81*(3): 813-818.

Bobacka, J., Ivaska, A. & Lewenstam, A. (2003). Potentiometric Ion Sensors Based on Conducting Polymers. *Electroanalysis,* 15: 366-374.

Bolto, B.A., Mcneill, R. & Weiss, D.E. (1963). Electronic Conduction in Polymers III: Electronic Properties of Polypyrrole. *Australian Journal of Chemistry, 16*: 1090–1103.

Bora, C., Kalita, A., Das, D., Dolui, S.K. & Mukhopadhyay, P.K. (2014). Preparation of polyaniline/nickel oxide nanocomposites by liquid/liquid interfacial polymerization and evaluation of their electrical, electrochemical and magnetic properties. *Polymer International, 63*: 445-452.

Branco, L.C., Rosa, J.N., Moura, R.J.J. & Afonso, C.a.M. (2002). Preparation and characterization of new room temperature ionic liquids. *Chemistry - A European Journal, 8*(16): 3671-3677.

Brinker, C.J. & Scherer, G.W. (1990). Sol-Gel Science: The Physics and Chemistry of Sol-gel Processing: Academic Press Inc., San Diego.

Butwong, N., Zhou, L., Ng-Eontae, W., Burakham, R., Moore, E., Srijaranai, S., . . . Glennon, J.D. (2014). A sensitive nonenzymatic hydrogen peroxide sensor using cadmium oxide nanoparticles/multiwall carbon nanotube modified glassy carbon electrode. *Journal of Electroanalytical Chemistry, 717-718*: 41-46.

Campos-Martin, J.M., Blanco-Brieva, G. & Fierro, J.L. (2006). Hydrogen peroxide synthesis: an outlook beyond the anthraquinone process. *Angew Chem Int Ed Engl, 45*(42): 6962-6984.

Çeken, B., Kandaz, M. & Koca, A. (2012). Electrochemical hydrogen peroxide sensor based on cobalt phthalocyanine captured in polyaniline film on a glassy carbon electrode. *Journal of Porphyrins and Phthalocyanines, 16*(04): 380-389.

Chaparro, D.L. (2007). *Novel Polymer-Metal Nanocomposites for Applications in Detection and Sensing.* (Master), University of South Florida, Graduate School Theses and Dissertations.

Chattopadhyay, S., Dash, S.K., Ghosh, T., Das, D., Pramanik, P. & Roy, S. (2013). Surface modification of cobalt oxide nanoparticles using phosphonomethyl

iminodiacetic acid followed by folic acid: a biocompatible vehicle for targeted anticancer drug delivery. *Cancer Nanotechnology, 4*(4-5): 103-116.

Chauhan, N. & Pundir, C.S. (2011). An amperometric biosensor based on acetylcholinesterase immobilized onto iron oxide nanoparticles/multi-walled carbon nanotubes modified gold electrode for measurement of organophosphorus insecticides. *Analytica Chimica Acta, 701*(1): 66-74.

Chen, C., Long, M., Zeng, H., Cai, W., Zhou, B., Zhang, J., . . . Wu, D. (2009). Preparation, characterization and visible-light activity of carbon modified TiO_2 with two kinds of carbonaceous species. *Journal of Molecular Catalysis A: Chemical, 314*, 35-41.

Chen, C., Xie, Q., Yang, D., Xiao, H., Fu, Y., Tan, Y. & Yao, S. (2013). Recent advances in electrochemical glucose biosensors: a review. *RSC Advances*, 3: 4473–4491.

Chen, S., Yuan, R., Chai, Y. & Hu, F. (2013). Electrochemical sensing of hydrogen peroxide using metal nanoparticles: a review. *Microchimica Acta, 180*(1-2): 15-32.

Chen, S., Yuan, R., Chai, Y., Zhang, L., Wang, N. & Li, X. (2007). Amperometric third-generation hydrogen peroxide biosensor based on the immobilization of hemoglobin on multiwall carbon nanotubes and gold colloidal nanoparticles. *Biosensors and Bioelectronics, 22*: 1268-1274.

Chen, S.Y., Han, C.C., Tsai, C.H., Huang, J. & Chen-Yang, Y.W. (2007). Effect of morphological properties of ionic liquid-templated mesoporous anatase TiO_2 on performance of PEMFC with Nafion/TiO_2 composite membrane at elevated temperature and low relative humidity. *Journal of Power Sources, 171*: 363-372.

Chen, W., Cai, S., Ren, Q.-Q., Wen, W. & Zhao, Y.-D. (2012). Recent advances in electrochemical sensing for hydrogen peroxide: a review. *The Analyst, 137*(1): 49-58.

Chen, Y., Li, Y., Wang, H. & Yang, M. (2007). Gas sensitivity of a composite of multi-walled carbon nanotubes and polypyrrole prepared by vapor phase polymerization. *Carbon, 45*: 357-363.

Chiang, C., Fincher, C., Park, Y., Heeger, A., Shirakawa, H., Louis, E., . . . Macdiarmid, A. (1977). Electrical Conductivity in Doped Polyacetylene. *Physical Review Letters, 39*(17): 1098-1101.

Chougule, M.A., Dalavi, D.S., Mali, S., Patil, P.S., Moholkar, A.V., Agawane, G.L., . . . Patil, V.B. (2012a). Novel method for fabrication of room temperature polypyrrole–ZnO nanocomposite NO_2 sensor. *Measurement, 45*(8): 1989-1996.

Chougule, M.A., Khuspe, G.D., Sen, S. & Patil, V.B. (2013). Polypyrrole–ZnO nanohybrids: effect of CSA doping on structure, morphology and optoelectronic properties. *Applied Nanoscience, 3*(5): 423-429.

Chougule, M.A., Sen, S. & Patil, V.B. (2012b). Facile and efficient route for preparation of polypyrrole-ZnO nanocomposites: Microstructural, optical, and charge transport properties. *Journal of Applied Polymer Science, 125*(S1): E541-E547.

Ci, S., Huang, T., Wen, Z., Cui, S., Mao, S., Steeber, D.A. & Chen, J. (2014). Nickel oxide hollow microsphere for non-enzyme glucose detection. *Biosensors and Bioelectronics, 54*: 251-257.

Ciftci, H., Oztekin, Y., Tamer, U., Ramanaviciene, A. & Ramanavicius, A. (2014). Electrochemical biosensor based on glucose oxidase encapsulated within enzymatically synthesized poly(1,10-phenanthroline-5,6-dione). *Colloids and Surfaces B: Biointerfaces, 123*: 685-691.

Colon, G., Hidalgo, M.C. & Navio, J.A. (2002). A novel preparation of high surface area TiO_2 nanoparticles from alkoxide precursor and using active carbon as additive. *Catalysis Today, 76*: 91-101.

Costa, D.a.S., Mambrini, R.V., Fernandez-Outon, L.E., Macedo, W.a.A. & Moura, F.C.C. (2013). Magnetic adsorbent based on cobalt core nanoparticles coated with carbon filaments and nanotubes produced by chemical vapor deposition with ethanol. *Chemical Engineering Journal, 229*: 35-41.

Danaee, I., Jafarian, M., Forouzandeh, F. & Gobal, F. (2012). Kinetic studies of glucose electrocatalytic oxidation on GC/Ni electrode. *International Journal of Chemical Kinetics, 44*: 712-721.

Das, D., Nath, B.C., Phukon, P., Saikia, B.J., Kamrupi, I.R. & Dolui, S.K. (2013). Nickel oxide/polypyrrole/silver nanocomposites with core/shell/shell structure: Synthesis, characterization and their electrochemical behaviour with antimicrobial activities. *Materials Chemistry and Physics, 142*(1): 61-69.

Dash, S. & Munichandraiah, N. (2013). Non-Enzymatic Electroanalysis of Glucose on Electrodeposited Au-PEDOT Dendrites. *ECS Electrochemistry Letters, 2*(9): B17-B20.

Devadathan, D. & Raveendran, R. (2014). Polyindole Based Nickel-Zinc Oxide Nanocomposite -Characterization and Antifungal Studies. *International Journal of Chemical Engineering and Applications, 5*(3): 240-243.

Devi, R., Thakur, M. & Pundir, C.S. (2011). Construction and application of an amperometric xanthine biosensor based on zinc oxide nanoparticles-polypyrrole composite film. *Biosensors and Bioelectronics, 26*(8): 3420-3426.

Diaz, A.F. & Hall., B. (1983). Mechanical-properties of electrochemically prepared polypyrrole films. *Ibm Journal of Research and Development, 27*: 342-347.

Diaz, A.F. & Kanazawa, K.K. (1983). Polypyrrole: An Electrochemical Approach to Conducting Polymers. In Miller, J.S. (Ed.), *Extended Linear Chain Compounds* (Vol. 3, pp. 417-441). New York and London: Plenum Press: Springer US.

Ding, K., Miao, Z., Liu, Z., Zhang, Z., Han, B., An, G., . . . Xie, Y. (2007). Facile Synthesis of High Quality TiO_2 Nanocrystals in Ionic Liquid via a Microwave-Assisted Process. *Journal of the American Chemical Society, 129*(20): 6362-6363.

Ding, Y., Liu, Y.X., Zhang, L.C., Wang, Y., Bellagamba, M., Parisi, J., . . . Lei, Y. (2011). Sensitive and selective nonenzymatic glucose detection using functional NiO–Pt hybrid nanofibers. *Electrochimica Acta, 58*: 209-214.

Dõâaz, A.N., Peinado, M.C.R. & Minguez, M.C.T. (1998). Sol-gel horseradish peroxidase biosensor for hydrogen peroxide detection by chemiluminescence. *Analytica Chimica Acta, 363*: 221-227.

Estepa, L. & Daudon, M. (1997). Contribution of Fourier Transform Infrared Spectroscopy to the Identification of Urinary Stones and Kidney Crystal Deposits. *3*(5): 347–369.

Faleni, N. & Moloto, M.J. (2013). Effect of Glucose as Stabilizer af ZnO And CdO Nanoparticles on The Morphology and Optical Properties. *International Journal of Research and Reviews in Applied Sciences, 14*(1): 127-135.

Fan, L., Zhang, Q., Wang, K., Li, F. & Niu, L. (2012). Ferrocene functionalized graphene: preparation, characterization and efficient electron transfer toward sensors of H_2O_2. *Journal of Materials Chemistry, 22*(13): 6165-6170.

Farag, H.K., Al Zoubi, M. & Endres, F. (2008). Sol-gel synthesis of alumina, titania and mixed alumina/titania in the ionic liquid 1-butyl-1-methylpyrrolidinium

bis(trifluoromethylsulphonyl) amide. *Journal of Materials Science, 44*(1): 122-128.

Geiser, T., Ishigaki, M., Leer, C.V., Matthay, M.A. & Broaddus, V.C. (2004). H_2O_2 inhibits alveolar epithelial wound repair in vitro by induction of apoptosis. *American Journal of Physiology Lung Cellular and Molecular Physiology, 287*: L448-L453.

Geng, L., Huang, X., Zhao, Y., Li, P., Wang, S., Zhang, S. & S. Wu. (2006). H_2S sensitivity study of polypyrrole/WO_3 materials. *Solid State Electronics, 50*: 723-726.

Gnanakan, S.R.P., Rajasekhar, M. & Subramania, A. (2009). Synthesis of Polythiophene Nanoparticles by Surfactant-Assisted Dilute Polymerization Method for High Performance Redox Supercapacitors. *International Journal of Electrochemal Science, 4*: 1289-1301.

Goring, G.L.G. & Brennan, J.D. (2002). Fluorescence and physical characterization of sol-gel-derived nanocomposite films suitable for the entrapment of biomolecules. *Journal of Materials Chemistry, 12*(12): 3400-3406.

Gunji, T., Yokogawa, M., Hongo, M. & Abe, Y. (2005). Synthesis, isolation, and characterization of polytitanasiloxanes and zirconasiloxanes by the hydrolytic cocondensation of tetraethoxysilane and titanium or zirconium tetraisopropoxide. *Journal of Polymer Science Part A: Polymer Chemistry, 43*(4): 763-772.

Guo, B., Kong, Q., Zhu, Y., Mao, Y., Wang, Z., Wan, M. & Chen, L. (2011). Electrochemically fabricated polypyrrole-cobalt-oxygen coordination complex as high-performance lithium-storage materials. *Chemistry, 17*(52): 14878-14884.

Guo, Z., Shin, K., Karki, A., Young, D. & Kaner, R. (2009). Fabrication and characterization of iron oxide nanoparticles filled polypyrrole nanocomposites. *Journal of Nanoparticle Research, 11*: 1441-1452.

Gyurcsanyi, R.E., Nyback, A.S., Toth, K., Nagy, G. & Ivaska, A. (1998). Novel polypyrrole based all-solid-state potassium-selective microelectrodes. *Analyst, 123*: 1339-1344.

Han, C.-C., Ho, S.-Y., Lin, Y.-P., Lai, Y.-C., Liang, W.-C. & Chen-Yang, Y.-W. (2010). Effect of π–π stacking of water miscible ionic liquid template with different cation chain length and content on morphology of mesoporous TiO_2

prepared via sol–gel method and the applications. *Microporous and Mesoporous Materials, 131*(1-3): 217-223.

Han, Y. (2009). Synthesis and characterization of montmorillonite/polypyrrole nanocomposite. *Polymer Composites, 30*: 66-69.

Han, Y., Zheng, J. & Dong, S. (2013). A novel nonenzymatic hydrogen peroxide sensor based on Ag–MnO_2–MWCNTs nanocomposites. *Electrochimica Acta, 90*, 35-43.

Hara, P., Hanefeld, U. & Kanerva, L.T. (2009). Immobilised Burkholderiacepacia lipase in dry organic solvents and ionic liquids: a comparison. *Green Chemistry, 11*: 250-256.

Heeger, A.J. (2001a). Nobel Lecture: Semiconducting and metallic polymers: The fourth generation of polymeric materials. *Reviews of Modern Physics, 73*: 681-700.

Heeger, A.J. (2001b). Semiconducting and metallic polymers: the fourth generation of polymeric materials. *Synthetic Metals, 125*(1): 23-42.

Helia, H. & Yadegari, H. (2010). Nanoflakes of the cobaltous oxide, CoO: Synthesis and characterization. *Electrochimica Acta, 55*: 2139-2148.

Hernandez, K. & Fernandez-Lafuente, R. (2011). Control of protein immobilization:coupling immobilization and site-directed mutagenesis to improve biocatalyst or biosensor performance. *Enzyme and Microbial Technology, 48*: 107-122.

Hosseini, H.S. & Entezami, A.A. (2003). Conducting polymer blends of polypyrrole with polyvinyl acetate, polystyrene, and polyvinyl chloride based toxic gas sensors. *Journal of Applied Polymer Science, 90*: 49-62.

Hou, Y., Ndamanisha, J.C., Guo, L.P., Peng, X.J. & Bai, J. (2009). Synthesis of ordered mesoporous carbon/cobalt oxide nanocomposite for determination of glutathione. *Electrochimica Acta, 54*: 6166-6171.

Hou, Y.D., Wang, X.C., Wu, L., Chen, X.F., Ding, Z.X., Wang, X.X. & X.Z. Fu. (2008). N-Doped SiO_2/TiO_2 mesoporous nanoparticles with enhanced photocatalytic activity under visible-light irradiation. *Chemosphere, 72*(3): 414-421.

Huang, J. & Yang, Z. (2014). Synthesis of ZnO/polypyrrole composites and an application in Zn/Ni rechargeable batteries. *RSC Advances, 4*(37): 19205.

Huang, Y., Jiang, R., Bao, S.J., Cao, Y. & Jia, D. (2009). $LiMn_2O_{4-y}$ Br_y Nanoparticles Synthesized by a Room Temperature Solid-State Coordination Method. *Nanoscale Research Letters, 4*: 353-358.

Hulanicki, A., Geab, S. & Ingman, F. (1991). Chemical Sensors Definitions and Classification. *Pure & Applied Chemistry, 63*(9): 1247-1250.

Husing, N., Launay, B., Doshi, D. & G. Kickelbick. (2002). Mesostructured Silica−Titania Mixed Oxide Thin Films. *Chemistry of Materials, 14*(6): 2429-2432.

Idris, N.H., Wang, J., Chou, S., Zhong, C., Rahman, M.M., Liu, H. (2011). Effects of polypyrrole on the performance of nickel oxide anode materials for rechargeable lithium-ion batteries. *Journal of Materials Research, 26*: 860-866.

Issac, S. (2011). *Fabrication of Electrochemical Sensors for the Determination of Pharmaceuticals.* (Doctor of Philosophy), Cochin University of Science and Technology.

Janáky, C. & Visy, C. (2013). Conducting polymer-based hybrid assemblies for electrochemical sensing: a materials science perspective. *Analytical and Bioanalytical Chemistry, 405*: 3489-3511.

Jia, D., Ren, Q., Sheng, L., Li, F., Xie, G. & Miao, Y. (2011). Preparation and characterization of multifunctional polypyrrole-Au coated NiO nanocomposites and study of their electrocatalysis toward several important bio-thiols. *Sensors and Actuators B, 160*(1): 168-173.

Jia, N., Huang, B., Chen, L., Tan, L. & Yao, S. (2014). A simple non-enzymatic hydrogen peroxide sensor using gold nanoparticles-graphene-chitosan modified electrode. *Sensors and Actuators B: Chemical, 195*: 165-170.

Jiang, L.-C. & Zhang, W.-D. (2010). A highly sensitive nonenzymatic glucose sensor based on CuO nanoparticles-modified carbon nanotube electrode. *Biosensors and Bioelectronics, 25*: 1402-1407.

Jin, C., Zheng, R.Y., Guo, Y., Xie, J.L., Zhu, Y.X. & Xie, Y.C. (2009). Hydrothermal synthesis and characterization of phosphorous-doped TiO_2 with high

photocatalytic activity for methylene blue degradation. *Journal of Molecular Catalysis A: Chemical, 313*: 44-48.

Jin, L., Shang, L., Guo, S., Fang, Y., Wen, D., Wang, L., . . . Dong, S. (2011). Biomolecule-stabilized Au nanoclusters as a fluorescence probe for sensitive detection of glucose. *Biosensors and Bioelectronics, 26*(5): 1965-1969.

Kadam, L.D. & Pati, P.S. (2001). Step potential analysis of cobalt oxide-based electrochromic devices. *Solar Energy Materials & Solar Cells, 70*: 15-23.

Kanchana, W.I., Sakai, T., Teshima, N., Katoh, S. & Grudpan, K. (2007). Successive determination of urinary protein and glucose using spectrophotometric sequential injection method. *Analytica Chimica Acta, 604*(2): 139-146.

Kaper, H., Sallard, S.B., Djerdj, I., Antonietti, M. & Smarsly, B.M. (2010). Toward a Low-Temperature Sol−Gel Synthesis of TiO2(B) Using Mixtures of Surfactants and Ionic Liquids. *Chemistry of Materials, 22*(11): 3502-3510.

Kelley, W.D., Ratliff, J., Thomas A., & Nenadic, C. (1992). Basic Statistics For Laboratories: A Primer for Laboratory Workers.

Kenkel, J. (2003). *Analytical Chemistry for Technicians* (Third ed. pp. 584). United States of America: CRC Press LLC. pp. 132 & 133.

Khuspe, G.D., Navale, S.T., Chougule, M.A. & Patil, V.B. (2013). Ammonia gas sensing properties of CSA doped PANi-SnO_2 nanohybrid thin film. *Synthetic Metals, 185-186*: 1-8.

Kim, S.-J., Hong, M.-K., Chung, J.-K. & Park, S.-Y. (2012). Electrochemical properties of Ni(OH)2/polypyrrole composite electrode prepared by electrodeposition for pseudo-capacitor. *Journal of Ceramic Processing Research, 13*: s274-s277.

Kitte, A., Assresahegn, D. & Soreta, R. (2013). Electrochemical determination of hydrogen peroxide at glassy carbon electrode modified with palladium nanoparticles. *Journal of the Serbian Chemical Society, 78*(5): 701-711.

Klingshirn, M.A., Spear, S.K., Holbrey, J.D. & Rogers, R.D. (2005). Ionic liquids as solvent and solvent additives for the synthesis of sol–gel materials. *Journal of Materials Chemistry, 15*: 5174-5180.

Kricheldorf, H.R., Nuyken, O. & Swift, G. (2005). *Handbook of Polymer Synthesis* (Dekker, M. Ed. pp. 12). USA. pp. 1,3,4.

Kumar, A., Singh, R.K., Singh, H.K., Srivastava, P. & Singh, R. (2013). Impact of p-Toluenesulfonate on Polypyrrole–Cobalt Catalyst for Oxygen Reduction Reaction. *Journal of Applied Polymer Science, 130*(4): 2645-2651.

Kumary, V.A., Nancy, T.E.M., Divya, J. & Sreevalsan, K. (2013). Nonenzymatic Glucose Sensor: Glassy Carbon Electrode Modified with Graphene-Nickel/Nickel Oxide Composite. *International Journal of Electrochemical Science, 8*: 2220-2228.

Kundu, S., Mukadam, M.D., Yusuf, S.M. & Jayachandran, M. (2013). Formation of shape-selective magnetic cobalt oxide nanowires: environmental application in catalysis studies. *CrystEngComm, 15*(3), 482.

Kung, C.W., Lin, C.Y., Lai, Y.H., Vittal, R. & Ho, K.C. (2011). Cobalt oxide acicular nanorods with high sensitivity for the non-enzymatic detection of glucose. *Biosensors and Bioelectronics, 27*: 125-131.

Lee, K.K., Loh, P.Y., Sow, C.H. & Chin, W.S. (2013). CoOOH nanosheet electrodes: Simple fabrication for sensitive electrochemical sensing of hydrogen peroxide and hydrazine. *Biosensors and Bioelectronics, 39*(1): 255-260.

Lee, S.H., Doan, T.T.N., Ha, S. & Koo, Y.-M. (2007a). Using ionic liquids to stabilize lipasewithin sol-gel derived silica. *Journal of Molecular Catalysis B: Enzymatic, 45*, 57-61.

Lee, S.H., Doan, T.T.N., Ha, S.H., Chang, W.-J. & Koo, Y.-M. (2007b). Influence of ionic liquids as additives on sol-gel immobilized lipase. *Journal of Molecular Catalysis B: Enzymatic, 47*: 129-134.

Lenz, J., Trieu, V., Hempelmann, R. & Kuhn, A. (2011). Ordered Macroporous Ruthenium Oxide Electrodes for Potentiometric and Amperometric Sensing Applications. *Electroanalysis, 23*(5), 1186-1192.

Li, C., Su, Y., Lv, X., Xia, H., Shi, H., Yang, X., . . . Wang, Y. (2012). Controllable anchoring of gold nanoparticles to polypyrrole nanofibers by hydrogen bonding and their application in nonenzymatic glucose sensors. *Biosensors and Bioelectronics, 38*: 402-406.

Li, D., Mathew, B. & Mao, C. (2012). Biotemplated synthesis of hollow double-layered core/shell titania/silica nanotubes under ambient conditions. *Small, 8*: 3691-3697.

Li, S.-J., Du, J.-M., Zhang, J.-P., Zhang, M.-J. & Chen, J. (2014). A glassy carbon electrode modifiedwith a filmcomposed of cobalt oxide nanoparticles and graphene for electrochemical sensing of H_2O_2. *Microchimica Acta, 181*: 631-638.

Li, W., Jung, H., Hoa, N.D., Kim, D., Hong, S.-K. & Kim, H. (2010). Nanocomposite of cobalt oxide nanocrystals and single-walled carbon nanotubes for a gas sensor application. *Sensors and Actuators B, 150*: 160-166.

Li, W.Y., Xu, L.N. & Chen, J. (2005). Co_3O_4 Nanomaterials in Lithium-Ion Batteries and Gas Sensors. *Advanced Functional Materials, 15*(5): 851- 857.

Li, X., He, G., Han, Y., Xue, Q., Wu, X. & Yang, S. (2012). Magnetic titania-silica composite-polypyrrole core-shell spheres and their high sensitivity toward hydrogen peroxide as electrochemical sensor. *Journal of Colloid and Interface Science, 387*(1): 39-46.

Li, X., Zhu, Q., Tong, S., Wang, W. & Song, W. (2009). Self-assembled microstructure of carbon nanotubes for enzymeless glucose sensor. *Sensors and Actuators B: Chemical, 136*(2): 444-450.

Liu, X., Niu, W., Li, H., Han, S., Hu, L. & Xu, G. (2008). Glucose biosensor based on gold nanoparticle-catalyzed luminol electrochemiluminescence on a three-dimensional sol–gel network. *Electrochemistry Communications, 10*(9): 1250-1253.

Liu, Y., Li, J., Wang, M., Li, Z., Liu, H., He, P., . . . Li, J. (2005a). Preparation and Properties of Nanostructure Anatase TiO_2 Monoliths Using 1-Butyl-3-methylimidazolium Tetrafluoroborate Room-Temperature Ionic Liquids as Template Solvents. *Crystal Growth Design, 5*(4): 1643-1649.

Liu, Y., Shi, L., Wang, M., Li, Z., Liu, H. & Li, J. (2005b). A novel room temperature ionic liquid sol-gel matrix for amperometric biosensor application. *Green Chemistry, 7*: 655-658.

Liu, Y., Wang, M., Li, J., Li, Z., He, P., Liu, H. & Li, J. (2005c). Highly active horseradish peroxidase immobilized in 1-butyl-3-methylimidazolium tetrafluoroborate room-temperature ionic liquid based sol-gel host materials. *Chemical Communications* (13): 1778-1780.

Liu, Z., Liu, Y., Zhang, L., Poyraz, S., Lu, N., Kim, M., . . . Zhang, X. (2012). Controlled synthesis of transition metal/conducting polymer nanocomposites. *Nanotechnology, 23*(33): 335603.

Liu, Z., Zhang, L., Poyraz, S. & Zhang, X. (2013). Conducting Polymer - Metal Nanocomposites Synthesis and Their Sensory Applications. *Current Organic Chemistry, 17*: 2256-2267.

Londeree, D.J. (2002). *Silica-Titania Composites For Water Treatment.* (Degree of Master), University of Florida.

Lu, P., Yu, J., Lei, Y., Lu, S., Wang, C., Liu, D. & Guo, Q. (2014). Synthesis and characterization of nickel oxide hollow spheres-reduced graphene oxide-nafion composite and its biosensing for glucose. *Sensors and Actuators B: Chemical,* http://dx.doi.org/10.1016/j.snb.2014.10.140.

Lu, X., Zhang, W., Wang, C., Wen, T.-C. & Wei, Y. (2011). One-dimensional conducting polymer nanocomposites: Synthesis, properties and applications. *Progress in Polymer Science, 36*: 671-712.

Luo, L., Li, F., Zhu, L., Ding, Y., Zhang, Z., Deng, D. & Lu, B. (2013). Nonenzymatic glucose sensor based on nickel(II)oxide/ordered mesoporous carbon modified glassy carbon electrode. *Colloids and Surfaces B: Biointerfaces, 102*: 307-311.

Luo, L., Zhu, L., Xu, Y., Shen, L., Wang, X., Ding, Y., . . . Deng, D. (2011). Hydrogen peroxide biosensor based on horseradish peroxidase immobilized on chitosan-wrapped $NiFe_2O_4$ nanoparticles. *Microchimica Acta, 174*(1-2): 55-61
.

Lupu, S., Lete, C., Marin, M., Totir, N. & Balaure, P.C. (2009). Electrochemical sensors based on platinum electrodes modified with hybrid inorganic-organic coatings for determination of 4-nitrophenol and dopamine. *Electrochimica Acta, 54*: 1932-1938.

Ma, C., Sun, Z., Chen, C., Zhang, L. & Zhu, S. (2014). Simultaneous separation and determination of fructose, sorbitol, glucose and sucrose in fruits by HPLC-ELSD. *Food Chem, 145*: 784-788.

Ma, H., Shi, T. & Song, Q. (2014). Synthesis and Characterization of Novel PVA/SiO_2-TiO_2 Hybrid Fibers. *Fibers, 2*: 275-284.

Macdiarmid, A.G. (2001). "Synthetic metals": a novel role for organic polymers. *Current Applied Physics, 1*(4-5): 269-279.

Mahmoudian, M.R., Alias, Y., Basirun, W.J., Golsheikh, A.M. & Jamali-Sheini, F. (2013a). Synthesis of polypyrrole coated manganese nanowires and their application in hydrogen peroxide detection. *Materials Chemistry and Physics, 141*(1): 298-303.

Mahmoudian, M.R., Alias, Y., Basirun, W.J., Woi, P.M., Baradaran, S. & Sookhakian, M. (2014). Synthesis, characterization, and sensing applications of polypyrrole coated Fe_3O_4 nanostrip bundles. *Ceramics International, 40*: 9265-9272.

Mahmoudian, M.R., Alias, Y., Basirun, W.J. & Yousefi, R. (2013b). Synthesis and Characterization of Zinc/Polypyrrole Nanotube as a Protective Pigment in Organic Coatings. *Metallurgical and Materials Transactions a-Physical Metallurgy and Materials Science, 44A*(7): 3353-3363.

Mahulikar, P.P., Jadhav, R.S., Hundiwale,D.G. (2011). Performance of Polyaniline/TiO_2 Nanocomposites in Epoxy for Corrosion Resistant Coatings. *Iranian Polymer Journal, 20*(5): 367-376.

Mahyar, A., Behnajady, M.A. & Modirshahla, N. (2010). Characterization and photocatalytic activity of SiO_2-TiO_2 mixed oxide nanoparticles prepared by sol-gel method. *Indian Journal of Chemistry, 49A*: 1593-1600.

Makhlouf, S.A., Parker, F.T., Spada, F.E. & Berkowitz, A.E. (1997). Magnetic anomalies in NiO nanoparticles *Journal of Applied Physics, 81*: 5561-5563.

Malinauskas, A., Malinauskiene, J. & Ramanavicius, A. (2005). Conducting polymer-based nanostructurized materials: electrochemical aspects. *Nanotechnology, 16*(10): R51-R62.

Mao, H., Li, Y., Liu, X., Zhang, W., Wang, C., Al-Deyab, S.S. & El-Newehy, M. (2011). The application of novel spindle-like polypyrrole hollow nanocapsules containing Pt nanoparticles in electrocatalysis oxidation of nicotinamide adenine dinucleotide (NADH). *J Colloid Interface Sci, 356*(2): 757-762.

Martínez, M.W., Thompson, T.T. & Smit, M.A. (2010). Characterization and Electrocatalytic Activity of Carbon-supported Polypyrrole-Cobalt-Platinum Compounds. *International Journal of Electrochemical Science, 5*: 931 - 943.

Mavinakuli, P. (2010). *Multifunctional Conducitve Polypyrrole Nanocomposites.* (Degree Master of Engineering Science), Lamar University.

Mavinakuli, P., Wei, S.Y., Wang, Q., Karki, A.B., Dhage, S., Wang, Z., . . . Guo, Z.H. (2010). Polypyrrole/Silicon Carbide Nanocomposites with Tunable Electrical Conductivity. *Journal of Physical Chemistry C, 114*(9): 3874-3882.

Meng, F., Shi, W., Sun, Y., Zhu, X., Wu, G., Ruan, C., . . . Ge, D. (2013). Nonenzymatic biosensor based on CuxO nanoparticles deposited on polypyrrole nanowires for improving detection range. *Biosensors and Bioelectronics, 42*: 141-147.

Meng, Z., Liu, B., Zheng, J., Sheng, Q. & Zhang, H. (2011). Electrodeposition of cobalt oxide nanoparticles on carbon nanotubes, and their electro-catalytic properties for nitrite electrooxidation. *Microchimica Acta, 175*: 251-257.

Mikushina, Y.V., Shishmakov, A.B., Matskevich, V.V., Zhuravlev, N.A., Koryakova, O.V., Kharchuk, V.G. & Petrov, L.A. (2008). TiO_2–SiO_2 binary xerogels: synthesis and characterization. *Russian Journal of Inorganic Chemistry, 53*: 1557-1560.

Mu, Y., Jia, D., He, Y., Miao, Y. & Wu, H.L. (2011). Nano nickel oxide modified non-enzymatic glucose sensors with enhanced sensitivity through an electrochemical process strategy at high potential. *Biosensors and Bioelectronics, 26*(6): 2948-2952.

Murashkevich, A.N., Lavitskaya, A.S., Barannikova, T.I. & Zharskii, I.M. (2008). Infrared absorption spectra and structure of TiO_2-SiO_2 composites. *Journal of Applied Spectroscopy, 75*(5): 730-734.

Nagashree, K. & Ahmed, M. (2010). Electrocatalytic oxidation of methanol on Ni modified polyaniline electrode in alkaline medium. *Journal of Solid State Electrochemistry, 14*: 2307-2320.

Nalage, S.R., Chougule, M.A., Shashvati Sen & Patil, V.B. (2013a). Novel method for fabrication of NiO sensor for NO_2 monitoring. *Journal of Materials Science: Materials in Electronics, 24*: 368-375.

Nalage, S.R., Mane, A.T., Pawar, R.C., Lee, C.S. & Patil, V.B. (2014). Polypyrrole–NiO hybrid nanocomposite films: highly selective, sensitive, and reproducible NO_2 sensors. *Ionics, 20*: 1607-1616.

Nalage, S.R., Navale, S.T. & Patil, V.B. (2013b). Polypyrrole-NiO hybrid nanocomposite: Structural, morphological, optical and electrical transport studies. *Measurement, 46*(9): 3268-3275.

Nancy, T.E.M. & Kumary, V.A. (2014). Synergistic electrocatalytic effect of graphene/nickel hydroxide composite for the simultaneous electrochemical determination of ascorbic acid, dopamine and uric acid. *Electrochimica Acta, 133*: 233-240.

Nandapure, B.I., Kondawar, S.B., Salunkhe, M.Y. & Nandapure, A.I. (2013). Magnetic and transport properties of conducting polyaniline/nickel oxide nanocomposites. *Advanced Materials Letters, 4*(2): 134-140.

Navale, S.T., Khuspe, G.D., Chougule, M.A. & Patil, V.B. (2014a). Polypyrrole, α-Fe_2O_3 and their hybrid nanocomposite sensor: An impedance spectroscopy study. *Organic Electronics, 15*(10): 2159-2167.

Navale, S.T., Khuspe, G.D., Chougule, M.A. & Patil, V.B. (2014b). Synthesis and characterization of hybrid nanocomposites of polypyrrole filled with iron oxide nanoparticles. *Journal of Physics and Chemistry of Solids, 75*(2): 236-243.

Nogueira, R.F., Oliveira, M.C. & Paterlini, W.C. (2005). Simple and fast spectrophotometric determination of H_2O_2 in photo-Fenton reactions using metavanadate. *Talanta, 66*: 86-91.

Ogura, K. & Shiigi, H. (1999). A CO_2 Sensing Composite Film Consisting of Base-Type Polyaniline and Poly(vinyl alcohol). *Electrochemical and Solid-State Letters, 2*: 478-480.

Ohlan, A., Singh, K., Chandra, A. & Dhawan, S.K. (2010). Microwave Absorption Behavior of Core−Shell Structured Poly (3,4-Ethylenedioxy Thiophene)−Barium Ferrite Nanocomposites. *ACS Applied Materials & Interfaces, 2*(3): 927-933.

Olson, T.S., Pylypenko, S., Atanassov, P., Asazawa, K., Yamada, K., Tanaka, H. (2010). Anion-Exchange Membrane Fuel Cells: Dual-Site Mechanism of Oxygen Reduction Reaction in Alkaline Media on Cobalt-Polypyrrole Electrocatalysts. *Journal of Physical Chemistry C, 114*: 5049-5059.

Orináková, R. & Filkusová, M. (2010). Hydrogen evolution on microstructured polypyrrole films modified with nickel. *Synthetic Metals, 160*: 927-931.

Pang, H., Shi, Y., Du, J., Ma, Y., Li, G., Chen, J., . . . Yuan, B. (2012). Porous nickel oxide microflowers synthesized by calcination of coordination microflowers and their applications as glutathione electrochemical sensor and supercapacitors. *Electrochimica Acta, 85*: 256-262.

Pastor, I., Salinas-Castillo, A., Esquembre, R., Mallavia, R. & Mateo, C.R. (2010). Multienzymatic system immobilization in sol-gel slides: Fluorescent superoxide biosensors development. *Biosensors and Bioelectronics, 25*: 1526-1529.

Patil, D., Kolhe, K., Potdar, H.S. & Patil, P. (2011). Investigation of poly(o-anisidine)-SnO_2 nanocomposites for fabrication of low temperature operative liquefied petroleum gas sensor. *Journal of Applied Physics, 110*: 124501.

Patil, D., Patil, P., Seo, Y.-K. & Hwang, Y.K. (2010). Poly(o-anisidine)–tin oxide nanocomposite: Synthesis, characterization and application to humidity sensing. *Sensors and Actuators B: Chemical, 148*: 41-48.

Patois, T., Sanchez, J.-B., Berger, F., Fievet, P., Segut, O., Moutarlier, V., . . . Lakard, B. (2013). Elaboration of ammonia gas sensors based on electrodeposited polypyrrole-Cobalt phthalocyanine hybrid films. *Talanta, 117*: 45-54.

Pionteck, J., Omastová, M., Pötschke, P., Simon, F. & Chodák, I. (1999). Morphology, conductivity, and mechanical properties of polypyrrole-containing composites. *Journal of Macromolecular Science, Part B, 38*(5): 737-748.

Poyraz, S., Liu, Z., Liu, Y., Lu, N., Kim, M.J. & Zhang, X. (2014). One-step synthesis and characterization of poly(o-toluidine) nanofiber/metal nanoparticle composite networks as non-enzymatic glucose sensors. *Sensors and Actuators B: Chemical, 201*: 65-74.

Qin, X., Lu, W., Luo, Y., Chang, G. & Sun, X. (2011). Preparation of Ag nanoparticle-decorated polypyrrole colloids and their application for H_2O_2 detection. *Electrochemistry Communications, 13*(8): 785-787.

Radhakrishnan, S. & Paul, S. (2007). Conducting polypyrrole modified with ferrocene for applications in carbon monoxide sensors. *Sensors and Actuators B: Chemical, 125*: 60-65.

Radhakrishnan, S., Prakash, S., Rao, C.R.K. & Vijayan, M. (2009). Organically soluble bifunctional polyaniline-magnetite composites for sensing and supercapacitor applications. *Electrochemical and Solid-State Letters, 12*(4): A84-A87.

Ram, M.K., Yavuz, O. & Aldissi, M. (2005). NO_2 gas sensing based on ordered ultrathin films of conducting polymer and its nanocomposite. *Synthetic Metals, 151*: 77-84.

Ramanavicius, A., Ramanaviciene, A. & Malinauskas, A. (2006). Electrochemical sensors based on conducting polymer-polypyrrole. *Electrochimica Acta, 51*(27): 6025-6037.

Ren, J., Li, Z., Liu, S., Xing, Y. & Xie, K. (2008). Silica–Titania mixed Oxides: Si–O–Ti Connectivity, Coordination of Titanium, and Surface Acidic Properties. *Catalysis Letters, 124*(3-4): 185-194.

Roninson, I.B. (2003). Tumor cell senescence in cancer treatment. *Cancer Research, 63*: 2705-2715.

Sadki, S., Schottland, P., Brodie, N. & Sabouraud, G. (2000). The mechanisms of pyrrole electropolymerization. *Chemistry Society Reviews, 29*: 283-293.

Safarnavadeh, V., Zare, K. & Fakhari, A.R. (2013). Capability of parasulfonato calix[6]arene, as an anion dopant, and organic solvents in enhancing the sensitivity and loading of glucose oxidase (GOx) on polypyrrole film in a biosensor: a comparative study. *Biosensors and Bioelectronics, 49*: 159-163.

Salimi, A., Hallaj, R., Soltanian, S. & Mamkhezri, H. (2007). Nanomolar detection of hydrogen peroxide on glassy carbon electrode modified with electrodeposited cobalt oxide nanoparticles. *Analytica Chimica Acta, 594*(1): 24-31.

Salimi, A., Mamkhezri, H., Hallaj, R. & Soltanian, S. (2008). Electrochemical detection of trace amount of arsenic (III) at glassy carbon electrode modified with cobalt oxide nanoparticles. *Sensors and Actuators B: Chemical, 129*: 246-254.

Seema, S. & Prasad, M.V.N.A. (2014). Dielectric Spectroscopy of Nanostructured Polypyrrole-NiO Composites. *Journal of Polymers,* http://dx.doi.org/10.1155/2014/950304, 1-5.

Şenel, M., Çevik, E. & Abasıyanık, M.F. (2010). Amperometric hydrogen peroxide biosensor based on covalent immobilization of horseradish peroxidase on ferrocene containing polymeric mediator. *Sensors and Actuators B: Chemical, 145*(1): 444-450.

Seo, I., Pyo, M. & Cho, G. (2002). Micrometer to Nanometer Patterns of Polypyrrole Thin Films via Microphase Separation and Molecular Mask. *Langmuir, 18*: 7253-7257.

Shahnavaz, Z., Lorestani, F., Alias, Y. & Woi, P.M. (2014). Polypyrrole–$ZnFe_2O_4$ magnetic nano-composite with core–shell structure for glucose sensing. *Applied Surface Science, 317*: 622-629.

Shi, F. & Deng, Y. (2005). Abnormal FT-IR and FTRaman spectra of ionic liquids confined in nano-porous silica gel. *Spectrochimica Acta Part A, 62*: 239-244.

Shi, J., Ci, P., Wang, F., Peng, H., Yang, P., Wang, L., . . . Chu, P.K. (2011). Nonenzymatic glucose sensor based on over-oxidized polypyrrole modified Pd/Si microchannel plate electrode. *Biosensors and Bioelectronics*, *26*(5): 2579-2584.

Shiddiky, M.J. & Torriero, A.A. (2011). Application of ionic liquids in electrochemical sensing systems. *Biosensors and Bioelectronics, 26*(5): 1775-1787.

Shim, J.H., Kang, M., Lee, Y. & Lee, C. (2012). A nanoporous ruthenium oxide framework for amperometric sensing of glucose and potentiometric sensing of pH. *Microchimica Acta, 177*(1-2): 211-219.

Shirakawa, H. (2001). Nobel Lecture: The discovery of polyacetylene film—the dawning of an era of conducting polymers. *Reviews of Modern Physics, 73*: 713-718.

Shirakawa, H., Louis, E.J., Macdiarmid, A.G., Chiang, C.K. & Heeger, A.J. (1977). Synthesis of Electrically Conducting Organic Polymers: Halogen Derivatives of Polyacetylene, (CH)x. *Journal of the Chemical Society, Chemical Communications*, 578-580.

Shishmakov, A.B., Mikushina, Y.V., Koryakova, O.V., Valova, M.S., Petrov, L.A. & Melkozerov, S.A. (2012). Synthesis of TiO_2-SiO_2 xerogels via the hydrolysis of a tetrabutoxytitanium-tetraethoxysilane mixture in aqueous ammonia and hydrochloric acid atmospheres. *Russian Journal of Inorganic Chemistry*, *57*: 787-793.

Shrivastava, A. & Gupta, V. (2011). Methods for the determination of limit of detection and limit of quantitation of the analytical methods. *Chronicles of Young Scientists, 2*(1): 21.

Shu, X., Chen, Y., Yuan, H., Gao, S. & Xiao, D. (2007). H_2O_2 Sensor Based on the Room-Temperature Phosphorescence of Nano TiO_2/SiO_2 Composite. *Analytical Chemistry*, *79*: 3695-3702.

Shua, H., Caoa, L., Changa, G., Heb, H., Zhanga, Y. & Hea, Y. (2014). Direct Electrodeposition of Gold Nanostructures onto Glassy Carbon Electrodes for Non-enzymatic Detection of Glucose. *Electrochimica Acta, 132*: 524-532.

Shuklaa, S.K., Singh, N.B. & Rastogi, R.P. (2013). Efficient ammonia sensing over zinc oxide/polyaniline nanocomposite. *Indian Journal of Engineering & Materials Sciences, 20*: 319-324.

Si, P., Huang, Y., Wang, T. & Ma, J. (2013). Nanomaterials for electrochemical non-enzymatic glucose biosensors. *RSC Advances, 3*(11): 3487-3502.

Siwinska-Stefanska, K., Ciesielczyk, F., Kolodziejczak-Radzimska, A., Paukszta, D., Sojka-Ledakowicz, J. & Jesionowski, T. (2012). TiO_2-SiO_2 inorganic barrier composites: from synthesis to application. *Pigment & Resin Technology, 41*: 139-148.

Skotheim, T.A. & Az, J.R. (2006). *Conjugated polymers: Theory, synthesis, properties, and characterization* (3 ed.). USA: CRC Press, Tayor & Francis Group.

Sonavane, A.C., Inamdar, A.I., Dalavi, D.S., Deshmukh, H.P. & Patil, P.S. (2010). Simple and rapid synthesis of NiO/PPy thin films with improved electrochromic performance. *Electrochimica Acta, 55*: 2344-2351.

Souza, R.L.D., Faria, E.L.P.D., Figueiredo, R.T., Freitas, L.D.S., Iglesias, M., Mattedi, S., . . . Soares, C.M.F. (2013). Protic ionic liquid as additive on lipase immobilization using silica sol-gel. *Enzyme and Microbial Technology, 52*: 141-150.

Špalek, O., Balej, J. & Paseka, I. (1982). Kinetics of the decomposition of hydrogen peroxide in alkaline solutions. *Journal of the Chemical Society, Faraday Transactions 1, 78*: 2349-2359.

Srivastava, M., Srivastava, S.K., Nirala, N.R. & Prakash, R. (2014). A chitosan-based polyaniline-Au nanocomposite biosensor for determination of cholesterol. *Analytical Methods, 6*: 817-824.

Subramanian, P., Niedziolka-Jonsson, J., Lesniewski, A., Wang, Q., Li, M., Boukherroub, R. & Szunerits, S. (2014). Preparation of reduced graphene oxide–$Ni(OH)_2$ composites by electrophoretic deposition: application for non-enzymatic glucose sensing. *Journal of Materials Chemistry A, 2*(15): 5525.

Sun, L., Ding, K., Shi, Y., He, Z., Li, X. & Li, B. (2014). Synthesis and Characterization of SnO_2/polypyrrole Nanocomposites by Hydrothermal

Reverse Microemulsion. *Journal of Inorganic and Organometallic Polymers, 24*: 395-400.

Szeifert, J.M. (2011). *Mesoporous Titania Materials- Tuning and Optimizing Nanostructures and Porous Morphologies.*

Tabassum, M.R., Shah, A.F., Ahmad, S. & Singla, M.L. (2009). Comparative Study of synthesis, characterization and electric properties of polypyrrole and polythiophene composites with tellurium oxide. *Journal of Materials Science: Materials in Electronics, 20*: 958-966.

Tai, H., Jiang, Y., Xie, G., Yu, J. & Chen, X. (2007). Fabrication and gas sensitivity of polyaniline–titanium dioxide nanocomposite thin film. *Sensors and Actuators B: Chemical, 125*: 644-650.

Tandon, R.P., Tripathy, M.R., Arora, A.K. & Hotchandani, S. (2006). Gas and humidity response of iron oxide-Polypyrrole nanocomposites. *Sensors and Actuators B: Chemical, 114*: 768-773.

Tian, H., Jia, M., Zhang, M. & Hu, J. (2013). Nonenzymatic glucose sensor based on nickel ion implanted-modified indium tin oxide electrode. *Electrochimica Acta, 96*: 285-290.

Tian, K., Alex, S., Siegel, G. & Tiwari, A. (2015). Enzymatic glucose sensor based on Au nanoparticle and plant-like ZnO film modified electrode. *Materials Science and Engineering: C, 46*: 548-552.

Ting, Z., Syed, M., Elena, B., Bong, Y.Y., Robert, C.H., Nosang, V.M. & Marc, A.D. (2007). Poly(m-aminobenzene sulfonic acid) functionalized single-walled carbon nanotubes based gas sensor. *Nanotechnology, 18*(16): 165504.

Torsi, L., Pezzuto, M., Siciliano, P., Rella, R., Sabbatini, L., Valli, L. & Zambonin, P.G. (1998). Conducting polymers doped with metallic inclusions: New materials for gas sensors. *Sensors and Actuators B: Chemical, 48*(1-3): 362-367.

Toyo'oka, T., Kashiwazaki, T. & Kato, M. (2003). On-line screening methods for antioxidants scavenging superoxide anion radical and hydrogen peroxide by liquid chromatography with indirect chemiluminescence detection. *Talanta, 60*: 467-475.

Turner, M.B., Spear, S.K., Holbrey, J.D. & Rogers, R.D. (2004). Production of Bioactive Cellulose Films Reconstituted from Ionic Liquids. *Biomacromolecules, 5*(4): 1379-1384.

Valko, M., Izakovic, M., Mazur, M., Rhodes, C.J. & Telser, J. (2004). Role of oxygen radicals in DNA damage and cancer incidence. *Molecular and Cellular Biochemistry, 266*: 37-56.

Varshney, S., Singh, K., Ohlan, A., Jain, V.K., Dutta, V.P. & Dhawan, S.K. (2012). Synthesis, characterization and surface properties of Fe_2O_3 decorated ferromagnetic polypyrrole nanocomposites. *Journal of Alloys and Compounds, 538*: 107-114.

Vibha, S., Aswal, D.K., Manmeet, K., Koiry, S.P., Gupta, S.K., Yakhmi, J.V., . . . Deshpande, S.K. (2007). Enhanced NO_2 selectivity of hybrid poly(3-hexylthiophene): ZnO-nanowire thin films. *Applied Physics Letters, 90*: 043516.

Vives, S. & Meunier, C. (2008). Influence of the synthesis route on sol-gel SiO_2–TiO_2 (1:1) xerogels and powders. *Ceramics International, 34*: 37-44.

Wang, G., He, X., Wang, L., Gu, A., Huang, Y., Fang, B., . . . Zhang, X. (2013). Non-enzymatic electrochemical sensing of glucose. *Microchimica Acta, 180*(3-4): 161-186.

Wang, G., Lu, X., Zhai, T., Ling, Y., Wang, H., Tong, Y. & Li, Y. (2012). Free-standing nickel oxide nanoflake arrays: synthesis and application for highly sensitive non-enzymatic glucose sensors. *Nanoscale, 4*(10): 3123-3127.

Wang, H.-S., Pan, Q.-X. & Wang, G.-X. (2005). A Biosensor Based on Immobilization of Horseradish Peroxidase in Chitosan Matrix Cross-linked with Glyoxal for Amperometric Determination of Hydrogen Peroxide. *Sensors, 5*: 266-276.

Wang, H., Ma, N., Yan, Z., Deng, L., He, J., Hou, Y., . . . Yu, G. (2015). Cobalt/polypyrrole nanocomposites with controllable electromagnetic properties. *Nanoscale,* DOI: 10.1039/c4nr06978a.

Wang, K.-M., Li, J., Yang, X.-H., Shen, F.-L. & Wang, X. (2000). A chemiluminescent H_2O_2 sensor based on horseradish peroxidase immobilized by sol–gel method. *Sensors and Actuators B: Chemical, 65*: 239-240.

Wang, L., Lou, Z., Fei, T. & Zhang, T. (2012). Ring-like PdO-decorated NiO with lamellar structures and their application in gas sensor. *Sensors and Actuators B: Chemical Reviews, 1180*: 171-172.

Wang, L., Lu, X., Ye, Y., Sun, L. & Song, Y. (2013). Nickel-cobalt nanostructures coated reduced graphene oxide nanocomposite electrode for nonenzymatic glucose biosensing. *Electrochimica Acta, 114*: 484-493.

Wang, L. & Wang, E. (2004). A novel hydrogen peroxide sensor based on horseradish peroxidase immobilized on colloidal Au modified ITO electrode. *Electrochemistry Communications, 6*: 225-229.

Wang, Y., Xu, Y., Luo, L., Ding, Y., Liu, X. & Huang, A. (2010). A novel sensitive nonenzymatic glucose sensor based on perovskite $LaNi_{0.5}Ti_{0.5}O_3$-modified carbon paste electrode. *Sensors and Actuators B: Chemical, 151*(1): 65-70.

Wang, Z., Hu, Y., Yang, W., Zhou, M. & Hu, X. (2012). Facile One-Step Microwave-Assisted Route towards Ni Nanospheres/Reduced Graphene Oxide Hybrids for Non-Enzymatic Glucose Sensing. *Sensors, 12*(12): 4860-4869.

Wei, J., Xing, G., Gao, L., Suo, H., He, X., Zhao, C., . . . Xing, S. (2013). Nickel foam based polypyrrole–Ag composite film: a new route toward stable electrodes for supercapacitors. *New Journal of Chemistry, 37*(2): 337-341.

Xu, F.G., Deng, M., Li, G.Y., Chen, S.H. & Wang, L. (2013). Electrochemical behavior of cuprous oxide-reduced graphene oxide nanocomposites and their application in nonenzymatic hydrogen peroxide sensing. *Electrochimica Acta, 88*: 59-65.

Xu, P., Han, X., Zhang, B., Du, Y. & Wang, H.-L. (2014). Multifunctional polymer–metal nanocomposites via direct chemical reduction by conjugated polymers. *Chemical Society Reviews, 43*: 1349-1360.

Xu, Q., Ji, X., Li, H., Liu, J. & He, Z. (2010). An on-column fracture/end-column reaction interface for chemiluminescence detection in capillary electrophoresis. *Journal of Chromatography A, 1217*: 5628-5634.

Yan, Z., Zhao, J., Qin, L., Mu, F., Wang, P. & Feng, X. (2013). Non-enzymatic hydrogen peroxide sensor based on a gold electrode modified with granular cuprous oxide nanowires. *Microchimica Acta, 180*(1-2): 145-150.

Yang, F., Jiao, L., Shen, Y., Xu, X., Zhang, Y. & Niu, L. (2007). Enhanced response induced by polyelectrolyte-functionalized ionic liquid in glucose biosensor based sol-gel organic-inorganic hybrid material. *Journal of Electroanalytical Chemistry, 608*: 78-83.

Yang, W., Li, Y., Bai, Y. & Sun, C. (2006). Hydrogen peroxide biosensor based on myoglobin/colloidal gold nanoparticles immobilized on glassy carbon electrode by a Nafion film. *Sensors and Actuators B: Chemical, 115*: 42-48.

Yu, H., Jin, J., Jian, X., Wang, Y. & Qi, G.-C. (2013). Preparation of Cobalt Oxide Nanoclusters/Overoxidized Polypyrrole Composite Film Modified Electrode and Its Application in Nonenzymatic Glucose Sensing. *Electroanalysis, 25*(7): 1665-1674.

Yuan, X., Hu, X.-X., Ding, X.-L., Kong, H.-C., Sha, H.-D., Lin, H., Wen, W., Shen, G., Guo, Z., Ma, Z.-F., Yang, Y. (2013). Effects of cobalt precursor on pyrolyzed carbon-supported cobalt-polypyrrole as electrocatalyst toward oxygen reduction reaction. *Nanoscale Research Letters, 8*: 478.

Zhang, T.T., Yuan, R., Chai, Y.Q., Li, W.J. & Ling, S.J. (2008). A novel nonenzymatic hydrogen peroxide sensor based on a polypyrrole nanowire-copper nanocomposite modified gold electrode. *Sensors, 8*(8): 5141-5152.

Zhang, W., Zhang, X., Zhang, L. & Chen, G. (2014). Fabrication of carbon nanotube-nickel nanoparticle hybrid pasteelectrodes for electrochemical sensing of carbohydrates. *Sensors and Actuators B: Chemical, 192*: 459-466.

Zhang, X., Huang, Y., Gu, A., Wang, G., Fang, B. & Wu, H. (2012). Hydrogen Peroxide Sensor Based on Carbon Nanotubes/β-$Ni(OH)_2$ Nanocomposites. *Chinese Journal of Chemistry, 30*(3): 501-506.

Zhang, Y., Li, G., Wu, Y., Luo, Y. & Zhang, L. (2005). The Formation of Mesoporous TiO_2 Spheres via a Facile Chemical Process. *The Journal of Physical Chemistry B, 109*: 5478-5481.

Zhang, Y., Xu, F., Sun, Y., Shi, Y., Wen, Z. & Li, Z. (2011). Assembly of $Ni(OH)_2$ nanoplates on reduced graphene oxide: a two dimensional nanocomposite for enzyme-free glucose sensing. *Journal of Materials Chemistry, 21*(42): 16949-16954.

Zhao, F., Wu, X., Wang, M., Liu, Y., Gao, L. & Dong, S. (2004). Electrochemical and Bioelectrochemistry Properties of Room-Temperature Ionic Liquids and Carbon Composite Materials. *Analytical Chemistry, 76*: 4960-4967.

Zhao, H. (2010). Methods for stabilizing and activating enzymes in ionic liquids- a review. *Journal of Chemical Technology and Biotechnology, 85*: 891-907.

Zhao, Y.-P., Cai, Z.-S., Zhou, Z.-Y. & Fu, X.-L. (2011). Fabrication of conductive network formed by polyaniline–ZnO composite on fabric surfaces. *Thin Solid Films, 519*(18): 5887-5891.

Zhi, F., Lu, X., Yang, J., Wang, X., Shang, H., Zhang, S. & Xue, Z. (2009). Selective Anion Sensing through a Self-Assembled Monolayer of Thiol-End-Functionalized Porphyrin. *Journal of Physical Chemistry C, 113*: 13166-13172.

Zhu, J., Jiang, J., Liu, J., Ding, R., Li, Y., Ding, H., . . . Huang, X. (2011). CNT-network modified Ni nanostructured arrays for high performance non-enzymatic glucose sensors. *RSC Advances, 1*(6): 1020-1025.

Zou, B.X., Bian, L.-J., Wang, Y., Li, X.J. & Liu, X.X. (2011). Electrocatalytic reduction of bromate, chlorate, nitrite and 4-nitrophenol at WO_3/PANI modified electrode. *Acta Chimica Sinica, 69*: 1575-1581.

Zou, B.X., Liu, X.X., Diamond, D. & Lau, K.T. (2010). Electrochemical synthesis of WO_3/PANI composite for electrocatalytic reduction of iodate. *Electrochimica Acta, 55*: 3915-3920.

SUPPLEMENTARY

LIST OF PUBLICATIONS

Tilagam Marimuthu, M. R. Mahmoudian, Sharifah Mohamad, Yatimah Alias. Characterization of non-enzymatic hydrogen peroxide sensor of polypyrrole coated cobalt nanocomposites. Sensor and Actuator B, 2014, 202, 1037-1043 (ISI-Cited Publication) (Q1- 3.840)

Tilagam Marimuthu, Sharifah Mohamad, Yatimah Alias. Needle-like polypyrrole-NiO composite for non-enzymatic detection of glucose. Synthetic Metals, 2015, 207, 35-41 (ISI-Cited Publication) (Q2- 2.222)

Tilagam Marimuthu, Sharifah Mohamad, Yatimah Alias. Characterization of new silica titania mixed oxide in the presence of 1-butyl-3 methylimidazolium bis(trifluoromethylsulfonyl) imide by sol gel technique. Journal of Sol-Gel Science and Technology, 2014, 70, 104-110 (ISI-Cited Publication) (Q1- 1.547)

Sharifah Mohamad, Hemavathy Surikumaran, Muggundha Raoov, **Tilagam Marimuthu**, Kumuthini Chandrasekaram and Puvaneswary Subramaniam Article: Conventional Study on Novel Dicationic Ionic Liquid Inclusion with β-Cyclodextrin. Int. J. Mol. Sci. 2011, 12(9), 6329-6345 (ISI-Cited Publication) (Q2- 2.339)

LIST OF PAPERS PRESENTED

Tilagam Marimuthu, M.R. Mahmoudian, Sharifah Mohamad, Yatimah Alias. Synthesis of polypyrrole coated cobalt nanowires and their application in hydrogen peroxide detection. AsiaSense the 6th International Conference on Sensors 2013, 27-29 August 2013, Melaka

Tilagam Marimuthu, Sharifah Mohamad, Yatimah Alias. Synthesis and characterization of new silica-titania mixed oxide in the presence of ionic liquid by sol-gel technique, International Conference on Ionic Liquids 2013 (ICIL 2013), 10-14 December 2013, Langkawi, Kedah

Tilagam Marimuthu, Sharifah Mohamad, Yatimah Alias. Synthesis and characterization of inorganic/organic hybrid nanocomposites of polypyrrole, 18th Malaysian International Chemical Congress 2014 (18th MICC 2014), 3-5 November 2014, Putra World Trace Centre, Kuala Lumpur

Tilagam Marimuthu, Sharifah Mohamad, Yatimah Alias. Polypyrrole coated nickel composites for glucose sensor, The 6th International Conference on Postgraduate Education (ICPE-6 2014), 17-18 December 2014, Main Hall Universiti Teknikal Malaysia, Melaka

Tilagam Marimuthu, Sharifah Mohamad, Yatimah Alias. Polypyrrole coated cobalt nanocomposites for hydrogen peroxide detection, The Seoul International Conference on Engineering and Applied Science (SICEAS 2015), 08-10 January 2015, Courtyard by Marriott Seoul Times Square, South Korea